UFL/COEL-89/015

EFFECTS OF SEAWALLS ON THE ADJACENT BEACH

by

Takao Toue
and
Hsiang Wang

Sea Grant Project No. R/C-S-26
Grant No. NA86AA-D-SG068

1989

UFL/COEL-89/015

EFFECTS OF SEAWALLS ON THE ADJACENT BEACH

Takao Toue
and
Hsiang Wang

Coastal and Oceanographic Engineering Department
College of Engineering
University of Florida
Gainesville, Florida 32611

Sea Grant Project No. R/C-S-26
Grant No. NA86AA-D-SG068

1989

TABLE OF CONTENTS

LIST OF FIGURES

LIST OF TABLES

EFFECTS OF SEAWALLS ON THE ADJACENT BEACH

by

TAKAO TOUE and HSIANG WANG

Abstract

This study was carried out to examine the effects of seawalls on the adjacent beach by three dimensional model test. The results obtained from model test were analyzed in terms of volumetric changes and shoreline and hydrographic change to quantify the effects of seawalls.

The experiments were carried out in the wave basin of Coastal and Oceanographic Engineering department, University of Florida. A model seawall was installed on the test beach (19m×14m) which was initially molded into equilibrium shapes. During the test, hydrographic surveys were conducted at regular time intervals. The main variable in the experiment is the wave angle. Cases both with and without seawall were tested.

Before examining the effects of seawalls, the problems inherent to model test were examined. First, assessment of equilibrium beach profile concept, flow regime and modes of sediment transport were examined. The experimental set up is found to be reasonably representative of prototype phenomena, for the erosive conditions but not for the recovery conditions. Second, using equilibrium beach profile as a prototype template, several modeling laws were examined. Again, it was found that modeling law for erosion is far more firmly established than for that of accretion. From this analysis, it was also confirmed that the physical meanings of scale parameter "A" of the equilibrium profile is the settling velocity scale parameter.

The effects of seawalls were examined in terms of volumetric changes and shoreline changes. In the volumetric change analysis, three types of volumetric changes were defined and examined. Especially, the volume change in a control area surrounding seawall showed that the erosion rate in front of and adjacent the seawall

was larger than that without seawall for oblique incident waves, but is smaller for normal incident waves. Although the rate of erosion was larger with seawall, the analysis also showed that the influence of seawall was localized.

In the shoreline and hydrographic change analysis, first of all, the dominant modes of shoreline movement were examined using empirical eigenfunction. The dominant mode of eigenfunction of shoreline was represented by the simple retreat mode and the rhythmic feature mode. These dominant modes did not differ between cases with and without seawall. Moreover, the temporal eigenfunction without seawall is very similar to that with seawall. The most obvious effect of seawall which appeared in the first spatial eigenfunction mode was the groin effect at the downdrift side. The hydrographic change analysis revealed that the first spatial eigenfunction was much more irregular and the contribution of the first eigenfunction was smaller than that of the shoreline.

Based on the empirical solution of one-line theory, alongshore diffusivity was calculated. The calculated value was compared with the existing formula and was found to be reasonable for natural beach.

CHAPTER 1
INTRODUCTION

1.1 Statement of the Problem

Beach erosion is found along many portions of the coast of the world. The causes of the erosion could be sea level rise, reduction in sediment supply, interruption of the littoral drift by structures. There are several conventional engineering solutions to combat such erosion. Those are (1) coastal structures such as groins, seawalls, breakwaters and coastal dikes, and (2) non-structural solutions, such as beach nourishments. Among them, seawalls might be the most efficient and direct method to protect the up-land property provided that they are designed adequately.

Recently, the adverse effects of seawalls on their fronting and adjacent beaches have gained great attention and raised criticism about the use of seawalls in the coastal area. The most often alleged effects are (1) offshore profile slope steepening, (2) intensified local scour, (3) transport of sand to a substantial distance offshore, (4) adverse down drift erosion and (5) delay post-storm recovery (Dean, 1986). Although numerous example can be found from articles in newspaper or popular magazine reporting the adverse effects of seawalls, reliable and scientific based document is actually scarce. Moreover, the conclusion derived from the few technical reports on the adverse effects of seawalls remain controversial. Considering the merits of seawall as the reliable structure to protect upland erosion,abandoning or prohibiting seawalls altogether as means of coastal protection without firmly establishing their effects might be irrational. Therefore, there is a need to examine the effects of seawalls carefully and to quantify them if possible. Also, to examine the causes and effects of seawalls might lead to more rational design in the future.

1.2 Effects of Seawalls -Literature Review

A summary of an evaluation on the coastal armoring effects was given by Dean (1986). Subsequently, Kraus (1987) also presented a general review. Although Kraus titled his paper as the review of effects of seawall, the subject was extended to revetments, breakwaters and dikes. In the present study, the terminology of seawall is defined as the vertical structure with backfills and is normally located onshore from the shoreline. Based on this definition, the literatures concerning effects of seawalls are reviewed.

1.2.1 Model Test

There were many two dimensional model tests related to seawall, but most studies paid attention to the local scour and the stability of seawall. Hattori and Kawamata's (1977) and Barnett's (1987) two dimensional wave tank studies were the few dealing with beach evolution in front of seawalls. Hattori and Kawamata concluded that except in the immediate vicinity of seawall, the erosional and recovery process of beaches with or without the presence of seawall was similar. Barnett (1987) also carried out two dimensional model test, and concluded that the major transport process was not significantly influenced by the presence of seawall. Furthermore, he examined the volume change of beach profile, and found that the volume of sand retained upland of the structure which would be eroded under identical wave condition without seawall was found to be greater than the additional volume eroded at the toe of the structures . The ratio of sand volume saved versus additional volume eroded was found to be approximately 2 to 1.

Three dimensional experiment for seawall effects was carried out by McDougal, Sturtevant and Kommer (1987) in a relatively small basin ($7m \times 7m$). Only flanking effects were examined. Combining with field survey results, they established an empirical relation between flanking and the length of seawall as

$$s = 0.101 \times L_s \tag{1.1}$$

where s is the flanking erosion, and L_s is the length of the seawall.

Equation (1.1) does not include the forcing factor such as the wave height, period and so on. Besides, the data, upon which the equation was based, was considerably scattered.

1.2.2 Field Survey

Field observations of beach changes under the influence of seawall were conducted by only a few. Based on aerial-photograph, Birkemeier (1980) estimated the bluff and shore erosion along a stretch of beach in the southeastern section of Lake Michigan from 1970 to 1974. To compare erosion rate of both protected and unprotected shorelines, he selected five reaches along the beach, each approximately 1.6 km long and each with different characteristics; one of which contained a section of seawall 579 meter long. Erosion due to flanking at both downdrift and updrift of the seawall were evident. These erosions appeared to be localized as all the five reaches sustained approximately the same rate of shoreline and bluff recession. Since his study is based on interpretation of aerial-photos the beach changes in front of a seawall cannot be evaluated.

Berigan's (1985) study was based on beach surveys from the water line to the seawall front. The Traval Seawall is located in San Francisco. It was built to protect a 220m long badly eroding beach front. The toe of structure is above the highest astronomical tide. By analyzing beach profiles taken over a seven year period and relation of beach changes to wave energy, Berigan found that: low wave energy has little effect; intermediate wave energy built up the beach and high wave energy removed sand in front of seawall. He also concluded that while beach rebuilding is a slow process, the existence of the seawall accelerated the rebuilding process considerably compared with a beach with no seawall, which is quite contrary to common belief.

Kana and Svetichny (1982) monitored the beach profile change in South Car-

olina coast where the beach nourishment projects were carried out. They compared the sculptured beach to the seawall backed beach, and concluded the seawall backed beach results the more significant erosion than the sculptured beach but flawed.

Kriebel, Dally and Dean (1986) also monitored the beach profile at Clearwater in Florida after hurricane Elena. They examined the recovery process at down-drift side of seawall, in front of seawall and the up-drift side of seawall. After comparing the profiles, they made the general remark that the toe scouring at the base of a seawall associated with a storm event was clearly evident but also suggested that the presence of seawall did not considerably alter the beach recovery. The same amount of sand that would have supplied to beach through upland was probably deprived from the beach in the form toe scouring.

Walton and Sensabaugh (1985) investigated the flanking effects in Florida coast, and suggested the suitable return wall length.

Dette and Gartner (1987) presented the time history of the island of Sylt/North Sea and also by examining the changes in the beach topography which were measured in 1869, 1953 and 1967; the long term resonance of the coastal structures on the foreshore bed features were estimated. They obtained the following conclusion:
(1) The characteristic feature of the foreshore consisting of longshore bars and troughs has not been "destroyed" due to the presence of coastal structures.
(2) In the vicinity of the coastal structures, it is obvious that the trough has deepened with time and also seems to be shifted landward.
(3) With respect to a final judgement about the interaction of structure and foreshore topography probably the considered time space is not yet sufficient.

1.2.3 Numerical Simulation

The models developed by Ozasa and Brampton (1980) and Hanson and Kraus (1980) have been applied on seawall-backed beaches. The authors made the simplified assumption in their model that the beach profile simply moves seaward or

shoreward in parallel to itself without changing form. Hanson and Kraus (1986) in their shoreline evolution model incorporated a seawall as a solid boundary to compute plan form changes. Local effects such as sea bottom scouring and flanking were not modeled. As Kraus (1987) observed, the simulation does not follow the real sediment transport.

Kraus and Larson (1988) and Larson (1988) incorporated in their beach profile model a two dimensional longshore bar configuration and allowed the bar to move and to change shape and volume based on wave properties. A seawall is permitted in the model as a solid boundary. Again, similar to Hanson and Kraus's approach, local scour and wave reflection effects are not modelled.

1.3 Possible Mechanisms of Seawall's Effects

The effects of seawall are not well understood, but several possible mechanisms can be deduced from our general knowledge in coastal engineering. These are illustrated in Fig. 1.1 and are also described below:

(1) flanking effects: Flanking due to wave refraction and diffraction is expected to occur on the corners of the seawall to cause local erosion.

(2) cross wave effects: During storm surge period, the water depth in front of seawall is likely to be larger than that along the beach and wave reflection will occur as shown in Fig. 1.1 b. Consequently, the longshore current together with more reflected wave energy trapped in the trough will remove sand in front of seawall and transport them to down drift location.

(3) groin effects: If the shoreline retreats due to littoral drift, the seawall will eventually protrude seaward and act like a groin. Although this groin effect does not remove sand from the system it increases downdrift erosion pressure.

(4) sand supply cut off: Seawall prevents sand from being added to the littoral system, which again adds erosional stress downdrift and could result in lower bar profile in front of seawall during the storm surge period.

1.4 Objectives and Procedure

The main objective of the present study was to attempt to quantify the three dimensional effects of seawall on beach changes described in previous section. In order to gain a fundamental understanding it was decided to conduct three dimensional model tests in the laboratory environment. In analyzing the model test results, the following problems have been addressed.

(1) Effects of seawall on the volumetric changes in the system

(2) Effects of seawall on the shoreline and hydrography

Furthermore, the inherent problems associated with model testing such as scale effects, modeling law and so on are also examined to insure the adequacy of the model test results.

This report consists of seven chapters. After introduction, model test procedure is described in chapter 2. In chapter 3, the problem inherently related to the model test is examined carefully including modeling laws. The effects of seawall on volumetric changes and shoreline changes are examined in chapter 4 and 5, respectively. In analyzing the shoreline changes, both empirical eigenfunction analysis and a one-line concept are employed. Then, in chapter 6, based on the modeling law established in the present study, model test results are translated into prototype. Finally, in chapter 7, conclusions and recommendations for future studies are given.

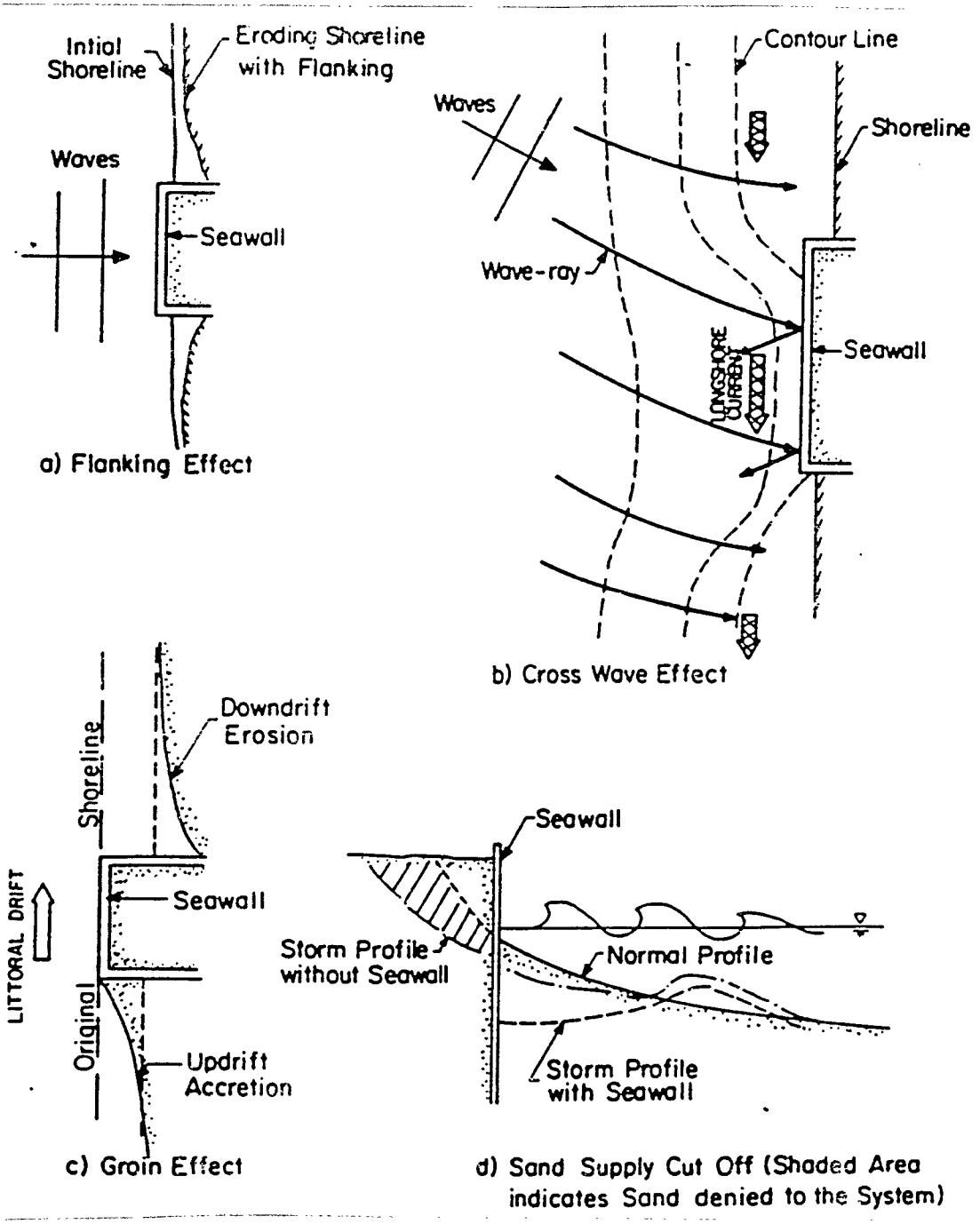

Figure 1.1: Erosion Mechanisms in the Presence of Seawall

CHAPTER 2
MODEL TEST APPARATUS, PROCEDURE AND CONDITION

2.1 Model Test Apparatus

2.1.1 Wave Basin

The model test is carried out in the wave basin of the Coastal and Oceanographic Engineering Department, University of Florida. The dimension of the basin is approximately 28 m x 28 m and 1 meter deep. It is equipped with a snake-type wave maker which consists of 88 paddles of 24 cm width each. By adjusting the phase of each individual paddle, waves of various oblique angles can be generated. The wave maker is capable of generating waves of wave heights ranging from 1 cm to 12 cm and wave periods from 0.89 to 1.89 sec.

2.1.2 The Beach and Seawall Model

The beach and seawall system used in the experiments is shown in Fig.2.1 The beach is composed of 125 tons of well sorted fine quartz sand. The total length of the beach is about 19 m and the distance from the back shore to the toe of the beach is 14 m. The orientation of the shoreline is 10 degree to the wave maker. The back shore of the beach is supported by a block wall of 81 cm high.

Both sides of the beach are constrained by wooden templates cut into a design beach profile shape. This design allows wave induced long-shore current to circulate unimpeded through the backside of the beach.

The beach profile is shaped in accordance with the concept of equilibrium beach profile (Dean, 1977). Based upon a fall velocity of Ws = 1.7 cm/sec, which corresponds to the median size of the beach sand used in the model, the geometry of the

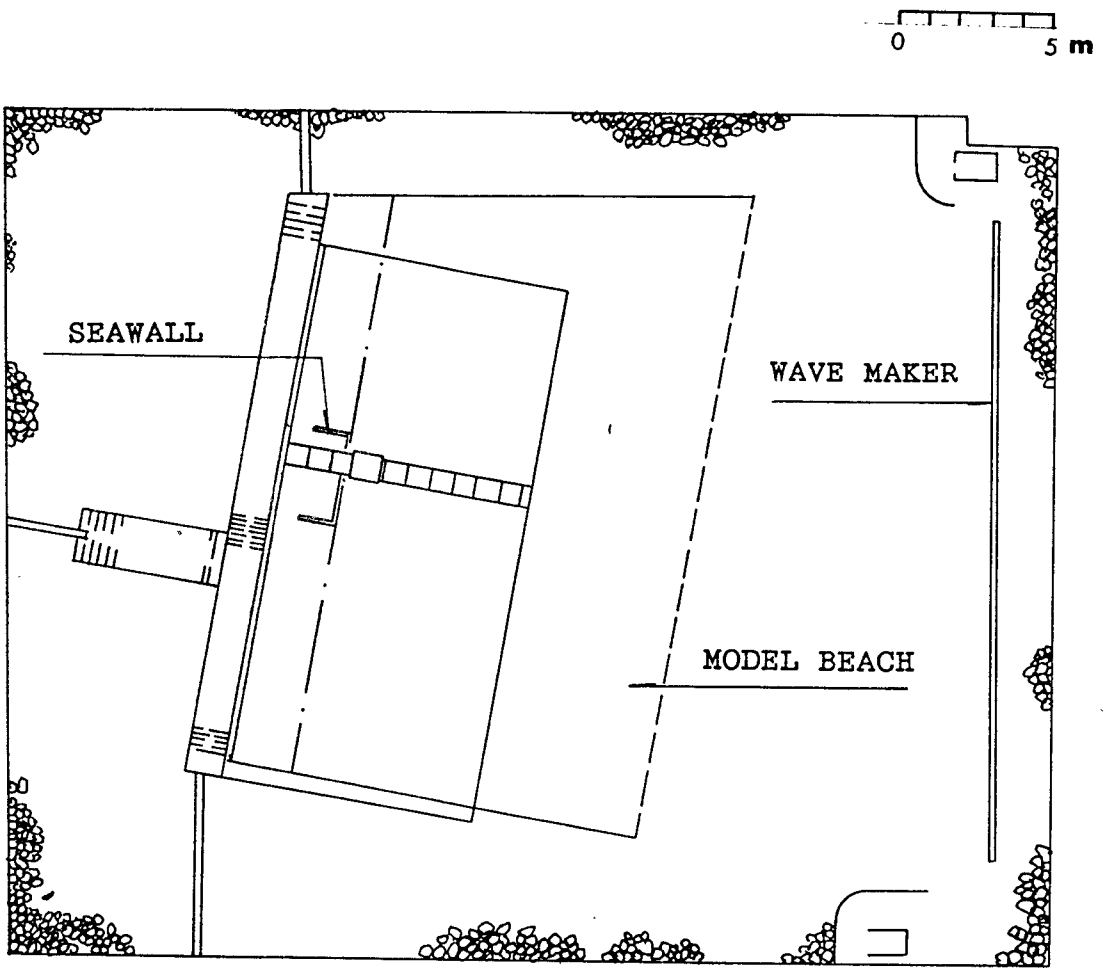

Figure 2.1: Beach and Seawall System in the Experiment

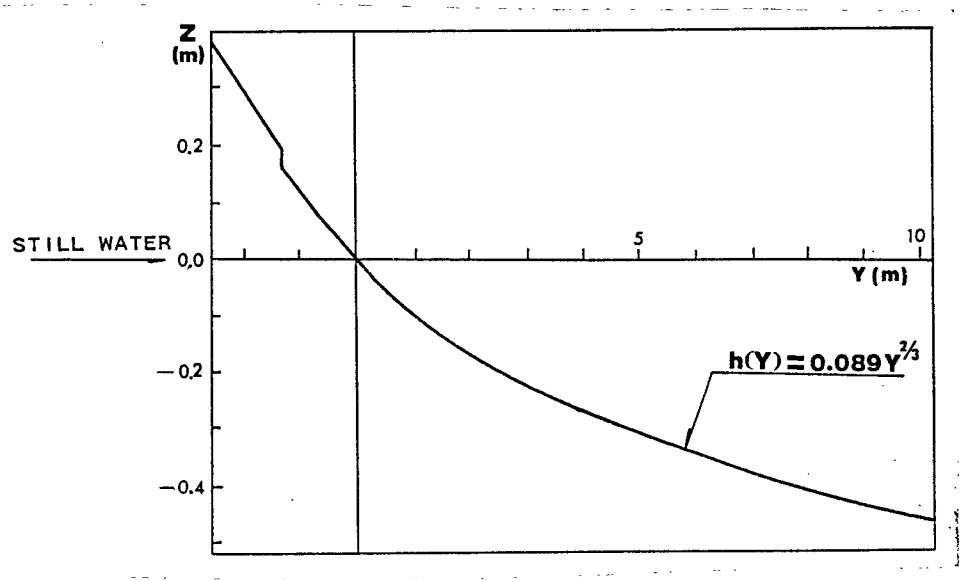

Figure 2.2: Geometry of the Initial Profile in the Model Test

profile is given by

$$h(y) = \begin{pmatrix} -0.152y & -2.50m < y < -1.22m \\ -0.135y & -1.22m < y < -0.61m \\ -0.130y & -0.61m < y < 0.095m \\ -0.089y^{2/3} & 0.095m < y \end{pmatrix} \tag{2.1}$$

Figure 2.2 shows the geometry of the profile according the above equation. The details concerning the model beach design and the physical parameters involved can be found in Bodge (1986). Table 2.1 summarizes the physical parameters related to model design.

The model seawall is made of sheet metal. It is installed parallel to the beach near its center. The length of the seawall is 3.0 m and with 1.0 m return walls on each side to prevent flanking. The height of the seawall is 45 cm which is sufficient to prevent wave over toppings. The toe of the seawall is located at 45 cm above the basin bottom which corresponds to the mean water level of storm conditions in the present test configurations. Details of test conditions will be discussed later.

Table 2.1: Physical Parameters of the Model

Median Sediment Size	$D_{50} = 0.16$ mm
Sorting Coefficient	$S_o = 1.27$
Median Fall Velocity	$W_s = 1.7$ cm/sec
Shoreline Length	19 m
Back-shore to Toe Length	14 m
Time Scale	$N_t \approx 6$
Vertical Length Scale	$N_v \approx 9$
Horizontal Length Scale	$N_h = 18$
Distortion ($N_v : N_h$)	2 : 1
Design Water depth	45 cm and 35 cm
Design Submerged Profile	$h(x) = A\ x^{2/3}$
Design " A " Parameter	$A = 0.089\ m^{1/3}$

2.1.3 Measurement Apparatus

There are three basic quantities to be measured: the beach profile and hydrographic changes, the input wave conditions and the near shore current.

The measurement of beach profile and nearshore contour was carried out by means of an automated profile measurement system designed by the Coastal and Oceanographic Engineering Laboratory (COEL). The assembly, as shown in Fig. 2.3, consists of four major components: the supporting platform, the wheeled truss, the profiler carriage and the profiler.

The supporting platform is a rectangular steel frame spans the entire area to be surveyed. The wheeled truss, as the name implies, is a steel truss structure with guided wheels.The truss is placed on the pair of shore-parallel rails of the supporting platform and is free to traverse from one end of the beach to the other. The cross-shore movement is facilitated by the motorized profiler carriage mounted on the truss. The profiler, which is the heart of the system, is a pivoting arm mounted on the carriage. At the lower end of the arm, a freely rotating PVC wheel is attached. As the carriage moves forward, the profiling arm swings behind and below the carriage following the beach face as the bottom wheel rolls along the

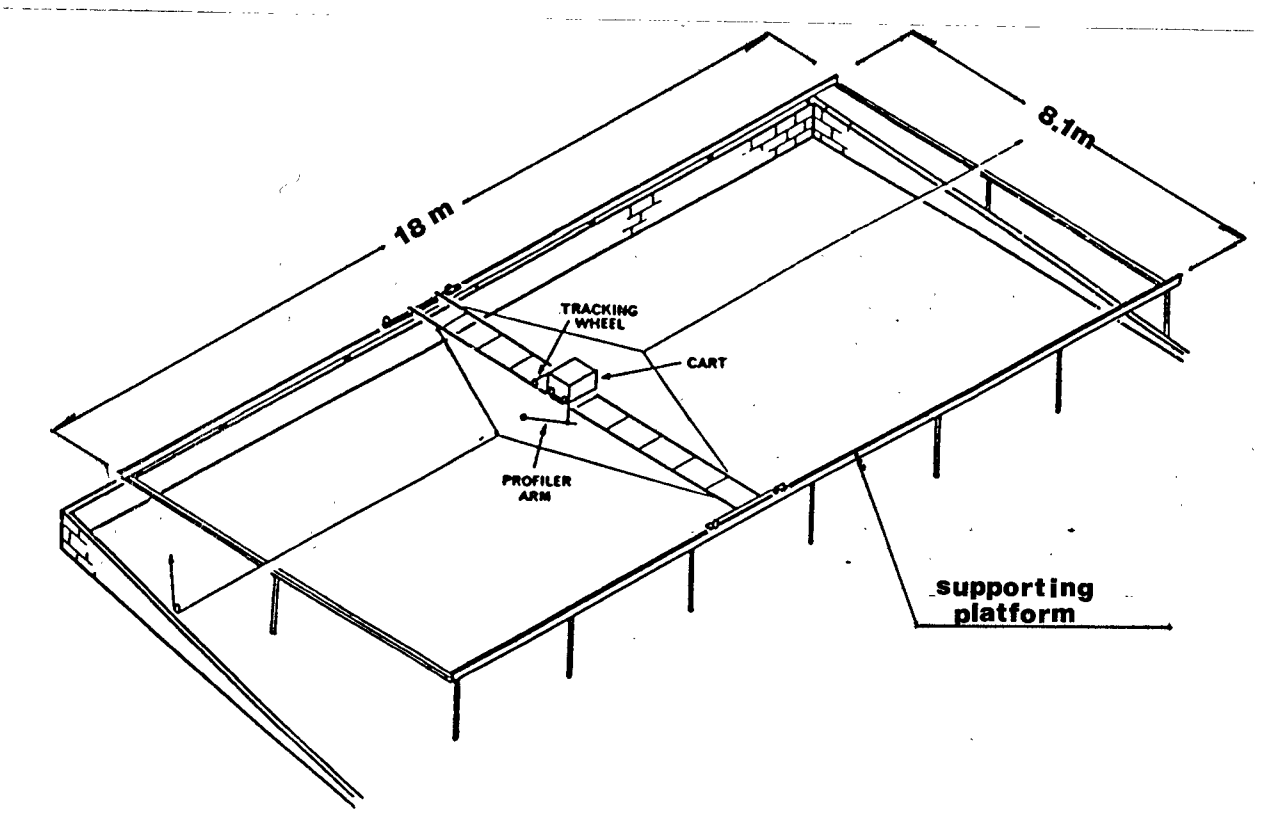

Figure 2.3: General View of the Beach Profile Measurement System (after Bodge, 1986)

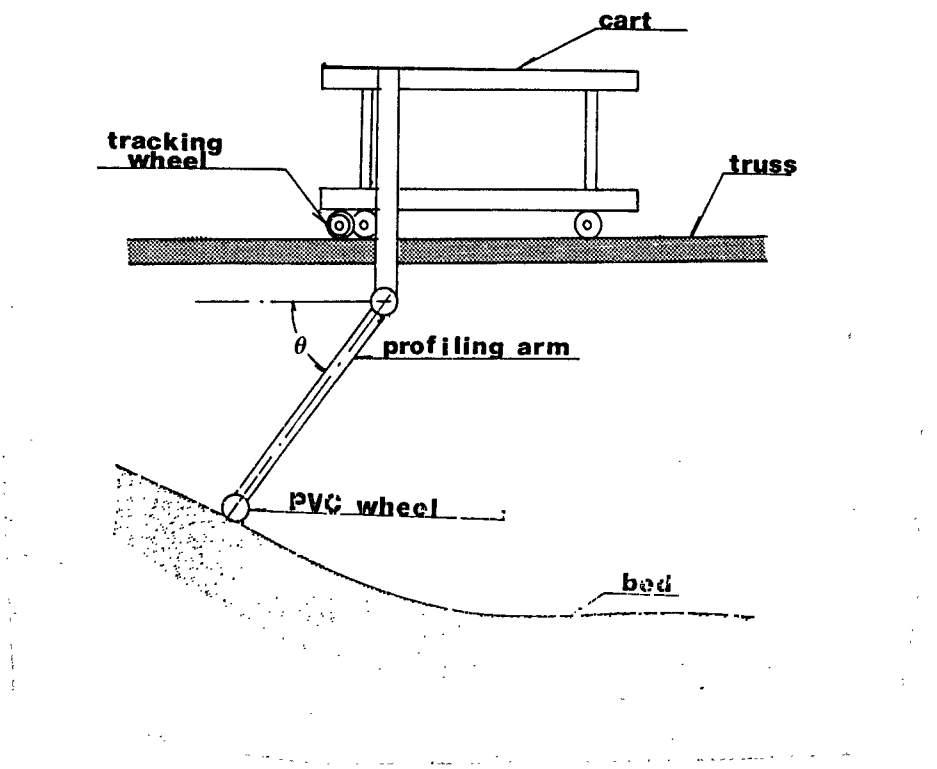

Figure 2.4: Assembly of Beach Profile Measurement System

bed. This assembly is shown in Fig. 2.4. The horizontal position is determined by the voltage change across a potentiometer on the carriage as it is at different locations on the truss. The vertical position is determined by the voltage change across a potentiometer owing to the change of angle of the arm. This angle is then converted into vertical distance. All the signals were collected and stored in the COEL computer system and also recorded on strip charts.

Waves were measured by two capacitance-type wave gauges. One is located in the offshore region between the wavemaker and the toe of the beach and the other one is mounted on the carriage. The offshore gauge monitors the incident wave conditions and the carriage gauge provides the local wave conditions, usually in the breaking zone. Near shore currents were also measured using an electric-magnetic current meter. Video and still photographs were also employed to estimate wave direction and current patterns. Rhodamine dye was used for flow pattern

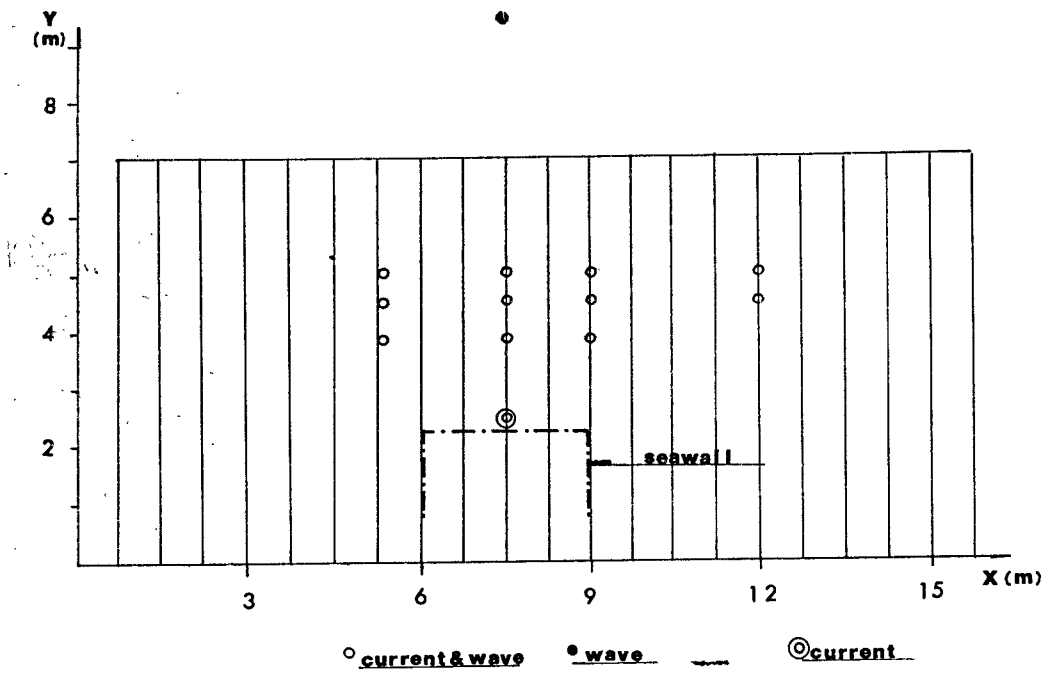

Figure 2.5: Locations of the Wave and Current Measurement Points

visualization.

The locations where wave and current measurements were performed are given in Fig. 2.5 together with beach profile measurement lines.

2.2 Experimental Procedures

The experiments were carried out following the steps outlined here:

Step 1 The initial beach profile was molded in the equilibrium shape according to Eq.2.1 for every test case. First, wooden templates cut into the initial profile were inserted into and across the beach at a spacing of about 3.6 m. The beach between the templates was then molded in shape by a wooden bar along the templates. After completion of one section, the templates were removed and reinserted into the next section and so on until the complete beach was molded into equilibrium profile.

Step 2 The basin was filled to the required water depth and the wave generating machine was adjusted to produce the test wave condition including wave height, wave period and wave incident angle.

Step 3 The initial beach profiles were surveyed after the beach attended certain degree of saturation. A total of 21 profiles were surveyed at equal spacing of 75 cm. The grid system was as shown in Fig. 2.5 with the origin at the left lower corner, the x-axis parallel to shore and y-axis perpendicular to shore.

Step 4 The beach was then subject to the test wave conditions for a designated duration. Each test usually began with waves of erosional nature for about 4 hrs or until the beach reached a state while the erosional process became very slow. The wave condition was then changed to affect beach recovery. The recovery process was much slower and usually took 12 hrs to reach a state of quasi-equilibrium. During this test period, profile measurements were carried out at regular intervals. In the erosional phase, surveys were conducted at 0, 1, 2, and 4 hrs whereas in the recovery phase, the intervals were 1, 2, 3, 8 and 12 hrs.

2.3 Test Condition

A total of six tests were conducted. Table 2.2 summarizes the test conditions. In all tests, the wave height was set at 11cm and the wave period at 1.74 sec during the erosion phase; the wave height was changed to 3.0 cm while keeping the period the same at 1.74 sec during the recovery phase. The corresponding water depths were 45 cm for erosional phase and 35 cm for recovery phase. One of the main parameters was the wave incident angle which was changed from 0 degree to 5 degrees and, finally, to 10 degrees. Of the six tests, three were with seawall and three without so that the effects of seawall can be examined in reference to cases without seawall.

Table 2.2: Test Condition

Case	wave height (cm)	wave period (sec)	water depth (cm)	wave angle (°)	seawall	elapsed time (hour)
Case1	11.0	1.74	45.0	0	no	4.0
Case1[R]	3.0	1.74	35.0	0	no	12.0
Case2	11.0	1.74	45.0	0	yes	4.0
Case2[R]	3.0	1.74	35.0	0	yes	12.0
Case3	11.0	1.74	45.0	5	no	4.0
Case3[R]	3.0	1.74	35.0	5	no	12.0
Case4	11.0	1.74	45.0	5	yes	4.0
Case4[R]	3.0	1.74	35.0	10	yes	12.0
Case5	11.0	1.74	45.0	10	no	12.0
Case6	11.0	1.74	45.0	10	yes	5.0
Case6[R]	3.0	1.74	35.0	10	yes	12.0

CHAPTER 3
EXPERIMENTAL RESULTS AND DISCUSSION

3.1 Evaluation of Model Test

Laboratory experiments serve two basic purposes:

1. To discover and understand the fundamental underlying principle of a physical phenomenon or process such that knowledge gained from the experiments can be applied to prototype project.
2. To faithfully portray the prototype condition so that the laboratory results can be extrapolated to prototype application.

To achieve the first purpose, laboratory experiments are often designed in such a way that the pertinent factors affecting the process are isolated. Experiments are then carried out to establish the relationship between these factors and their corresponding effects. The physical rules derived from the experiments are then applied to the actual engineering works. The difficulty with this approach lies in the fact that we must identify the most pertinent factors which is not always an easy task for a complicated system as the coastal beach. Furthermore, to study the effect of an isolated factor gives no assurance or information on the interactions among the factors.

The second approach does not make an explicit attempt to isolate the factors. Rather, its attempts to duplicate the prototype process as faithfully as possible so that the experimental results can be directly applied to the prototype. The difficulty with this approach is the degree of success of faithfully reproducing the natural system at a reduced scale.

The approach of the present experiments lies in between the above two in that the experiment is designed to portray the prototype condition as closely as possible. However, owing to the inherent difficulty that will be discussed later complete similarity can not be achieved between the model and the prototype. We must supplement our approach by attempting to identify the most pertinent factors in the process and to establish their roles in the whole process. Again owing to the complexity of the phenomenon these factors and their interactions can not always be easily sorted out. Therefore, before the results are presented, it is instructive to first examine here the relevance of the experiment to the prototype process it attempts to replicate.

3.1.1 Design of Model Beach

The experiment is not intended to model a specific prototype condition. However, the model beach must fulfill two basic requirements: it represents initially an equilibrium condition and it realistically portrays a plausible prototype condition. To fulfill these requirements, the original design by Bodge (1987) was closely followed. Bodge's laboratory experiments were designed to model a stretch of sandy beach along Atlantic-coast near Duck North Carolina where he conducted field tests on short-term impoundment tests of longshore sediment transport. Hughes' (1983) moveable-bed modeling law was utilized to scale the model beach based upon typical profiles measured in the field. In Hughes' modelling law, there are two criteria that involve four scale parameters:

$$T_n = \frac{\lambda}{\delta^{1/2}} \tag{3.1}$$

$$\lambda = \frac{\delta^{2/3}}{W_n} \tag{3.2}$$

where λ, δ, T_n, and W_n, are the ratios of prototype to model of the horizontal length, the vertical length, the time scale and the sediment particle fall velocity, respectively. Bodge established $W_n = 1.47$ and selected $T_n = 6$. Thus, based upon the above criteria, he arrived at $\lambda = 9$ and $\delta = 18$, and therefore a 2:1 horizontal/vertical distortion. The details of the model design parameters are given in Table 2.2. The time scale was so chosen that the corresponding vertical and horizontal length scales, when applied to the field profiles, produced a model geometry which closely resembled an equilibrium profile for the median grain size. Therefore, the two basic requirements stated above are fulfilled. Specifically, the submerged portion of the beach profile follows:

$$h(y) = Ay^{2/3} \tag{3.3}$$

where $h(y)$ is the water depth at y, y is the distance from the shoreline and A is the scale parameter.

The scale parameter "A" is shown to be a function of grain size diameter (Moore, 1982), or more appropriately, a function of fall velocity. Based upon Moore's diagram, A = 0.078 m for the model sand. The best fit of the field profiles obtained by Bodge yielded a value of A = 0.13 m. This, when scaled to the model, would give a value of A = 0.098 m. Bodge compromised the selection by choosing A to be the average of the two values, or A = 0.089 m. He also observed that the profile was fairly stable for all experiment waves, of which wave heights were 0.03 m to 0.1 m, and wave periods were 0.85 to 0.19 sec. In the present model design, there appears to be no reason to change the value A as suggested by Bodge; the value of A = 0.089 m is used. Dean (1986) re-plotted the value of A as a function of fall velocity as shown in Fig.3.1. Thus, for the test range of H_b/TW from 1.93 to 7.23, the value of "A" is no longer a constant but varies from 0.15 to 0.06. Consequently, there is no tangible advantage to select one value over the other as long as the A value falls in the mid range of the extremes.

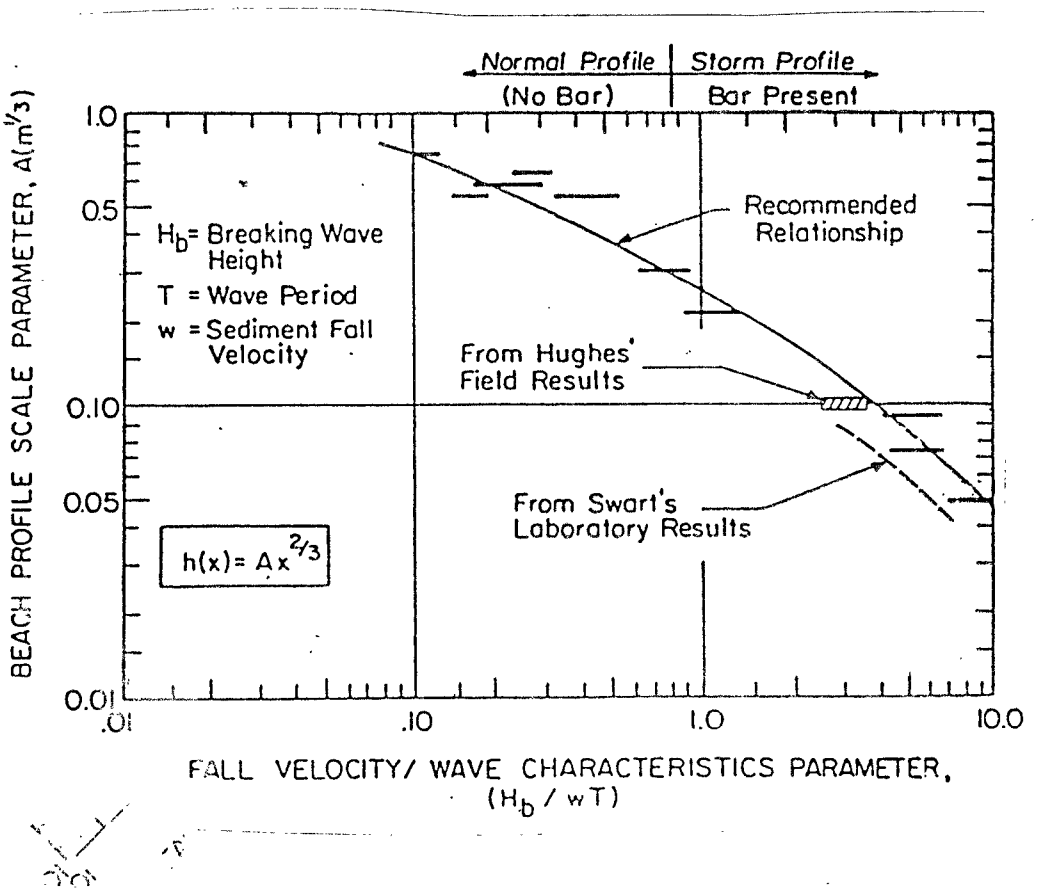

Figure 3.1: Correlation of Equilibrium Beach Profile Scale Parameter, A, with Combined Sediment Wave Parameter, H_b/TW

3.1.2 Assessment of Equilibrium Beach Profile

To assess the applicability of equilibrium beach profile at this laboratory scale, profiles measured at the center of the test section (x = 7.5 m) without seawall were used.

For the erosive wave condition, the fall velocity parameter assumes the value:

$$\frac{H_b}{TW} = \frac{0.13}{1.74 \times 0.017} = 4.39 \tag{3.4}$$

According to Fig. 3.1, the value of "A" is 0.09. Under this condition, it is found that:

a. The over all submerged profiles at the final stage of the tests match well with the equilibrium profile for all wave angles tested 0^o , 5^o , and 10^o. Fig. 3.2 shows the comparisons of the experimental results and the theoretical profile.

b. Moreover, the equilibrium profile also represents the model beach profiles well during the transient stages. Figs.3.3 and 3.4 shows the comparisons for elapsed time of 1 hr., 2 hrs., and 4 hrs. respectively.

For the recovery wave condition, the fall velocity parameter assumes the value of 1.01 and the corresponding "A" value is 0.24. As can be seen in Fig.3.5 the comparison is poor.

3.1.3 Assessment of Normal and Storm Profiles Classification

The classification of normal and storm beach profiles is a tool used by many investigators to determine whether a beach is undergoing or will undergo an erosional or accretional process. The topic has been quite extensively researched since the first attempt by Johnson (1952). A literature review is given recently by Kriebel et al. (1986). Four criteria purposed by four different authors–Dean (1973, 1977), Sunamura (1974), Hattori and Kawamata (1980) and Wang (1985)–are tested here.

Common to all the four criteria are two parameters, the wave steepness, H_o/L_o, for the wave condition and the sediment fall velocity, W, or sediment particle size,

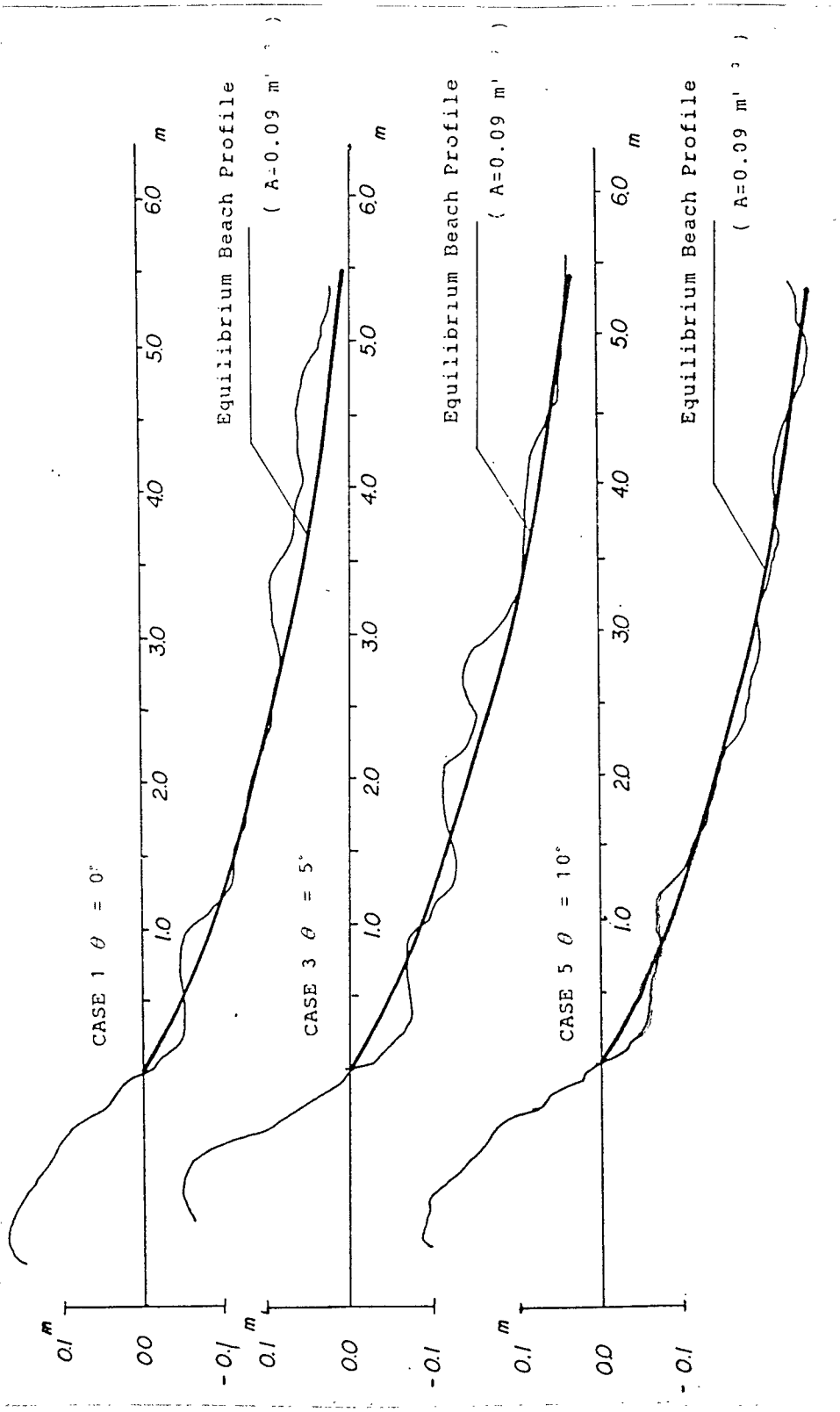

Figure 3.2: Comparison of Equilibrium Beach Profile to the Final Beach Profile in the Model Test

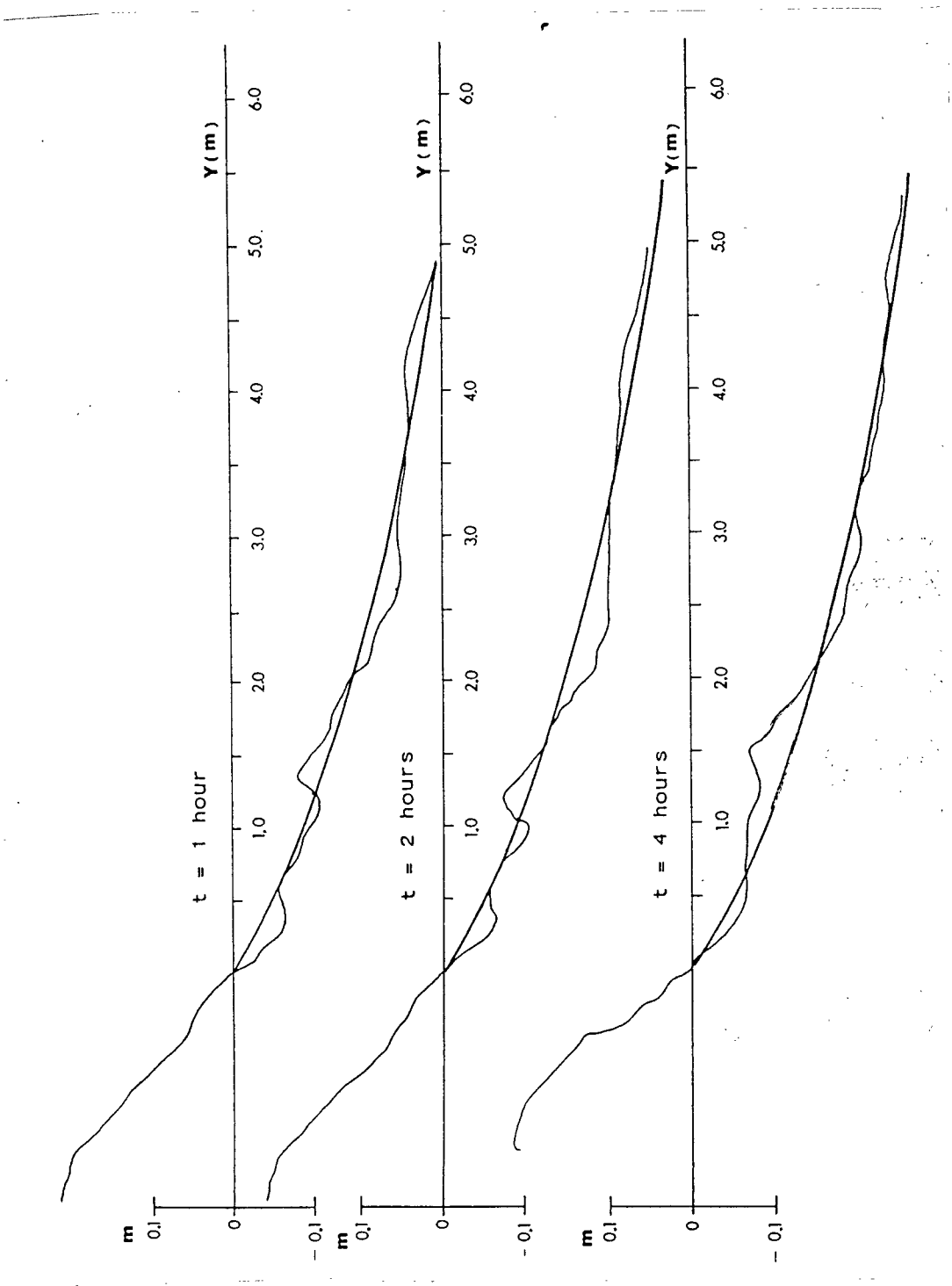

Figure 3.3: Comparison of Equilibrium Beach Profile to the Beach Profile in the Model Test for each elapsed time (Case 1)

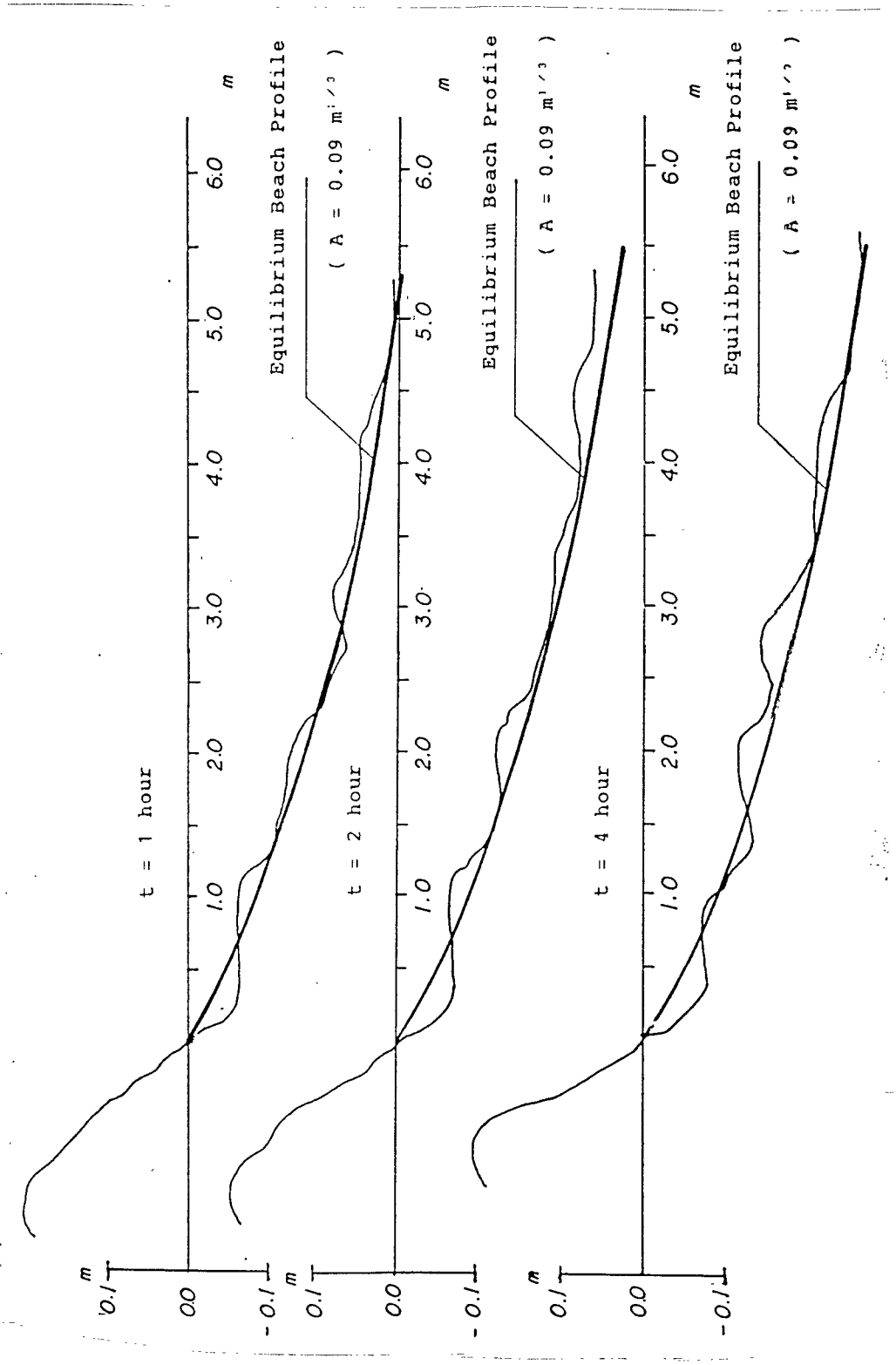

Figure 3.4: Comparison of Equilibrium Beach Profile to the Beach Profile in the Model Test for each elapsed time (Case 3)

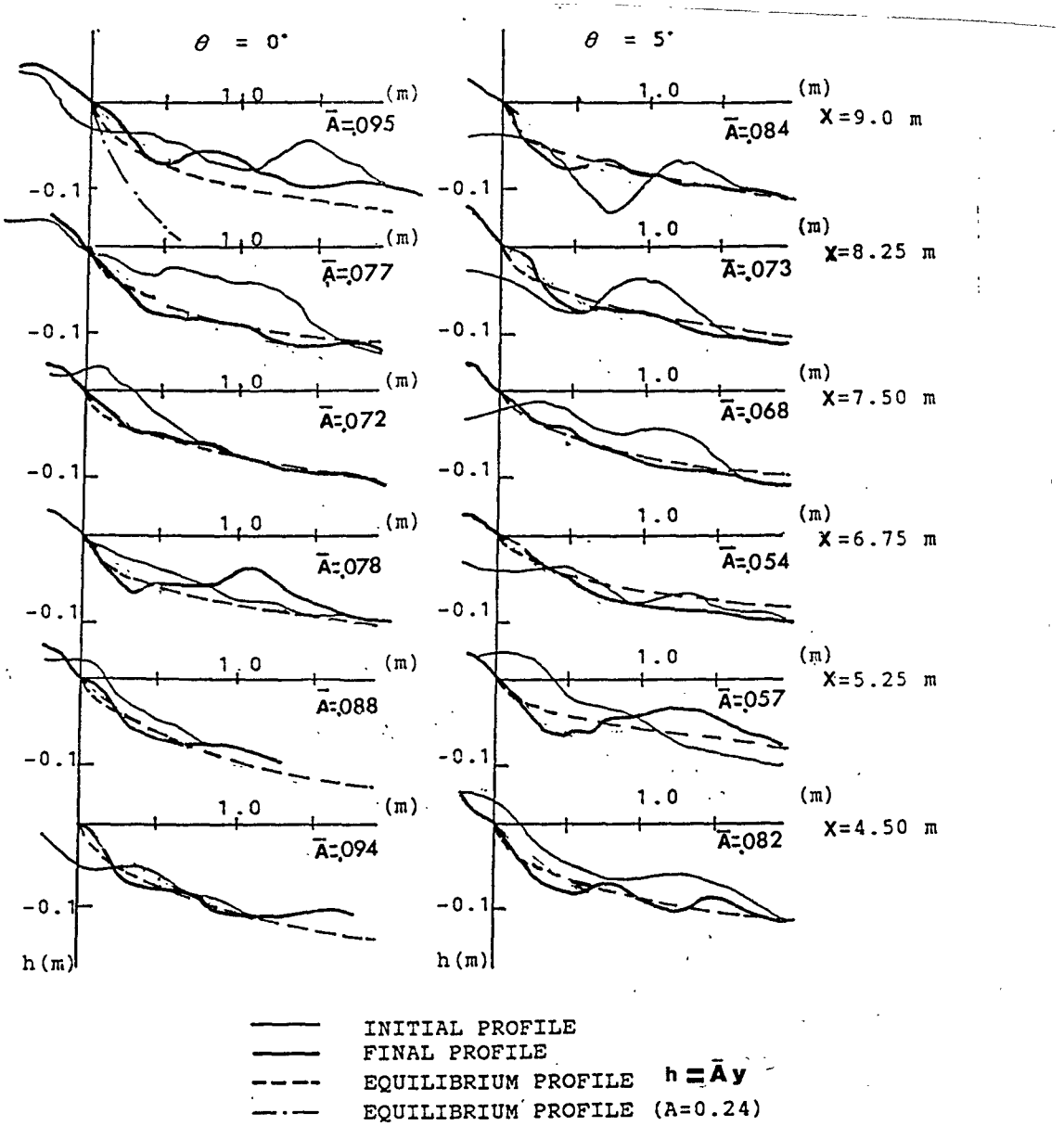

Figure 3.5: Comparison of Equilibrium Beach Profile to the Beach Profile in the Model Test for recovery condition (Case 1)

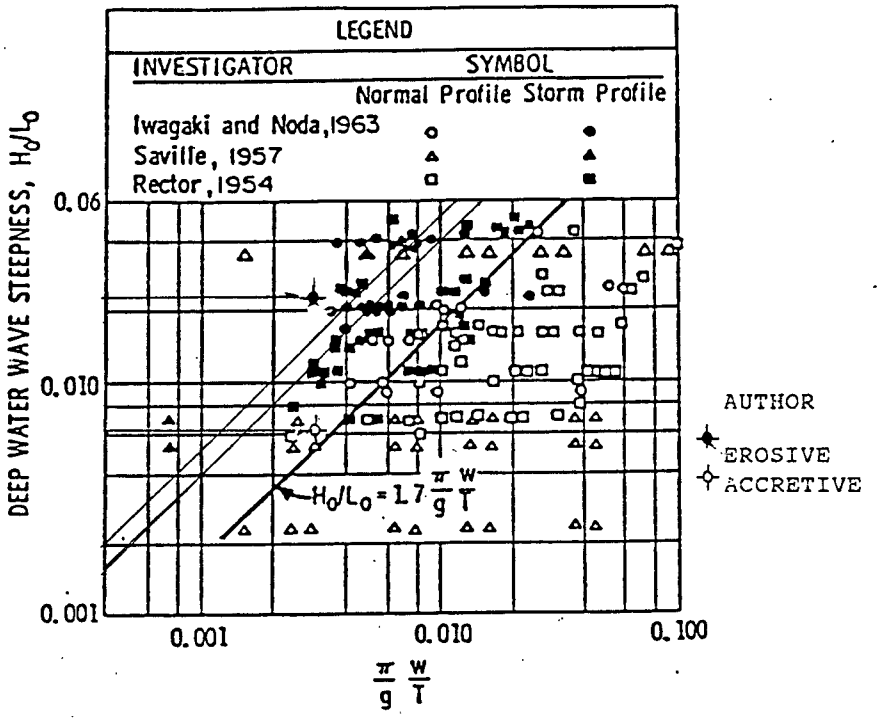

Figure 3.6: Criterion of Normal and Storm Profile (after Kriebel at al., 1986)

D, for sediment characteristics. With the exception of Dean, the other three authors all included an additional parameter of beach slope, $tan\beta$, but for different reasons. Sunamura included $tan\beta$ as the effect of initial condition. Wang and Hattori and Kawamata, on the other hand, utilize this parameter to account for wave breaking forms in the surf zone. Dean (as modified by Kriebel et al.) and Sunamura have different values for laboratory and field data whereas Hattori and Wang have one condition for all the data (Wang, however, used the same data set as Dean's).

In the present comparison, the profiles at x = 7.5 m(at the center of test beach) are used. The results are shown in Figs.3.6 to 3.9. All the four criteria past the test for erosional condition as the data point falls well within the zone of erosive profile. For the accretive profile, Hattori and Kawamata's, and Sunamura's criterion passed the test but both Dean's and Wang's failed.

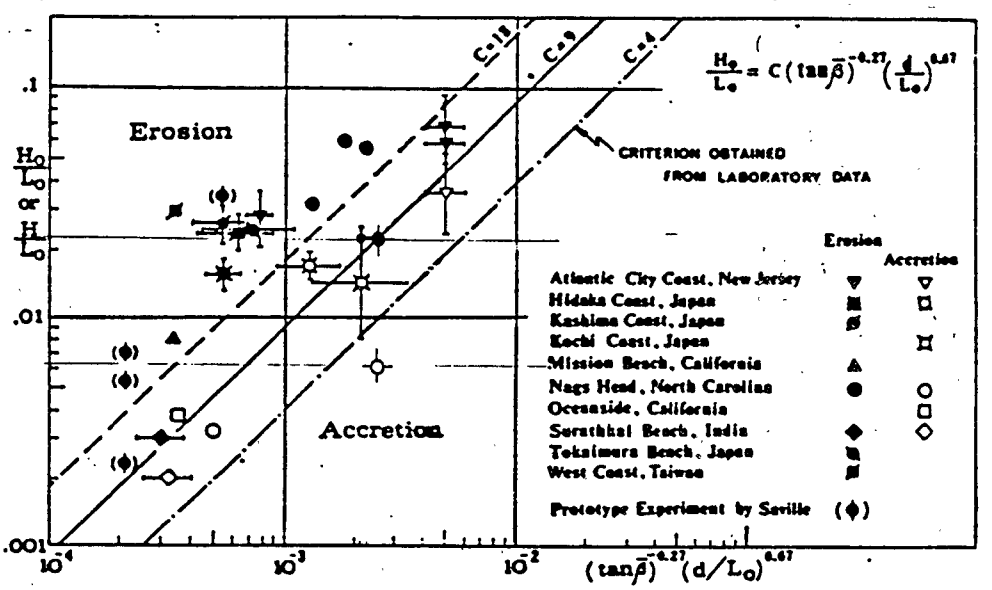

Figure 3.7: Criterion of Normal and Storm Profile (after Sunamura and Horikawa, 1974)

3.1.4 Flow Regime and Mode of Sediment Transport

It was remarked by Wang (1985) that practically all the proposed beach classification criteria were based upon the premise that in the surf zone the suspended sediment transport mode dominates as signified by the presence of the fall velocity parameter. The equilibrium beach profile is also based upon the same concept. This, while well may be the situation under prototype condition, may or may not be true at the laboratory scale. In fact, the results presented above seem to suggest otherwise. To examine the flow regime of the experiment, Jonsson's(1966) flow regime chart is used. His diagram as shown in Fig.3.10 consists of three regimes and three transition zones. The position is determined by two parameters; a roughness parameter defined as

$$a_m/k_s \tag{3.5}$$

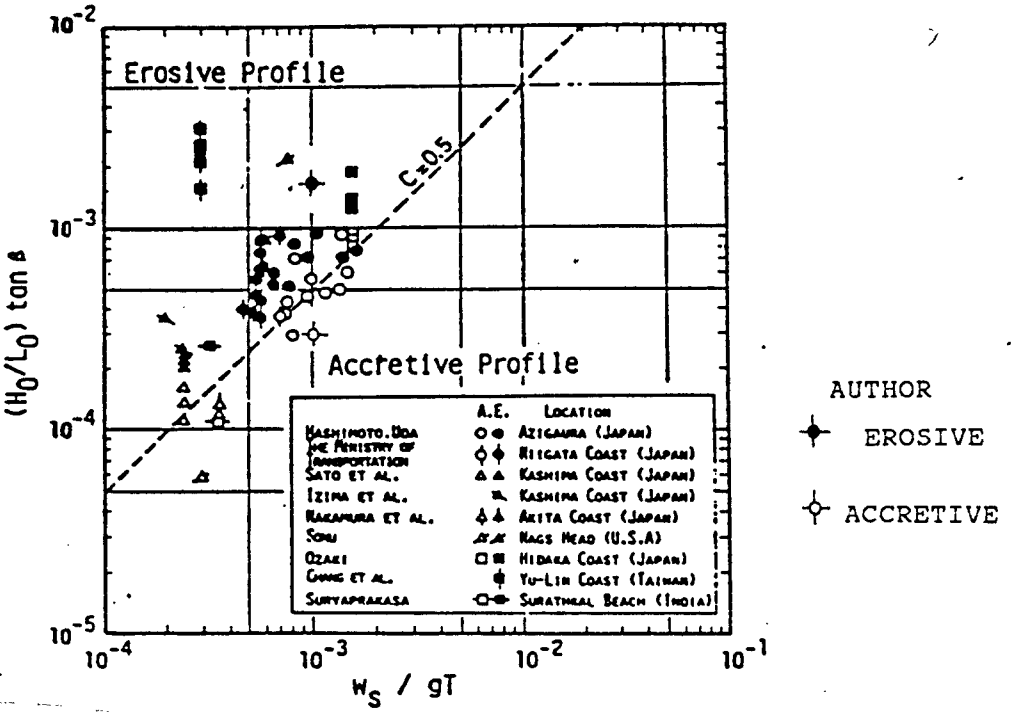

Figure 3.8: Criterion of Normal and Storm Profile (after Hattori and Kawamata, 1980)

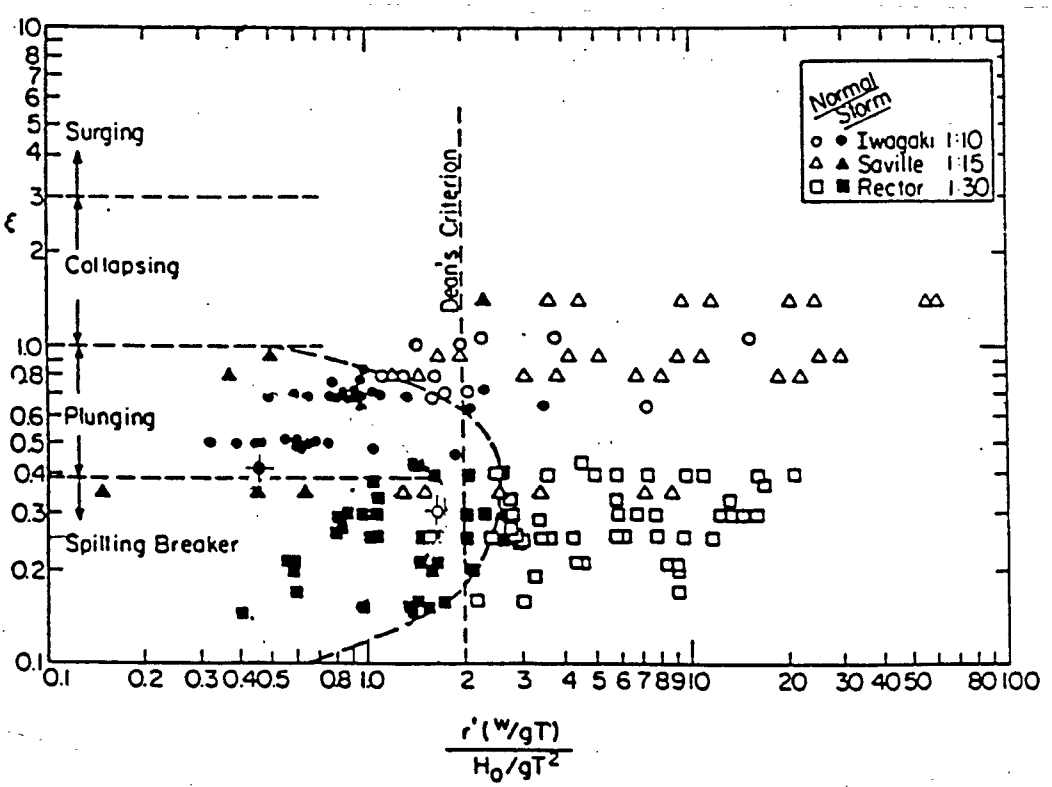

Figure 3.9: Criterion of Normal and Storm Profile (after Wang, 1985)

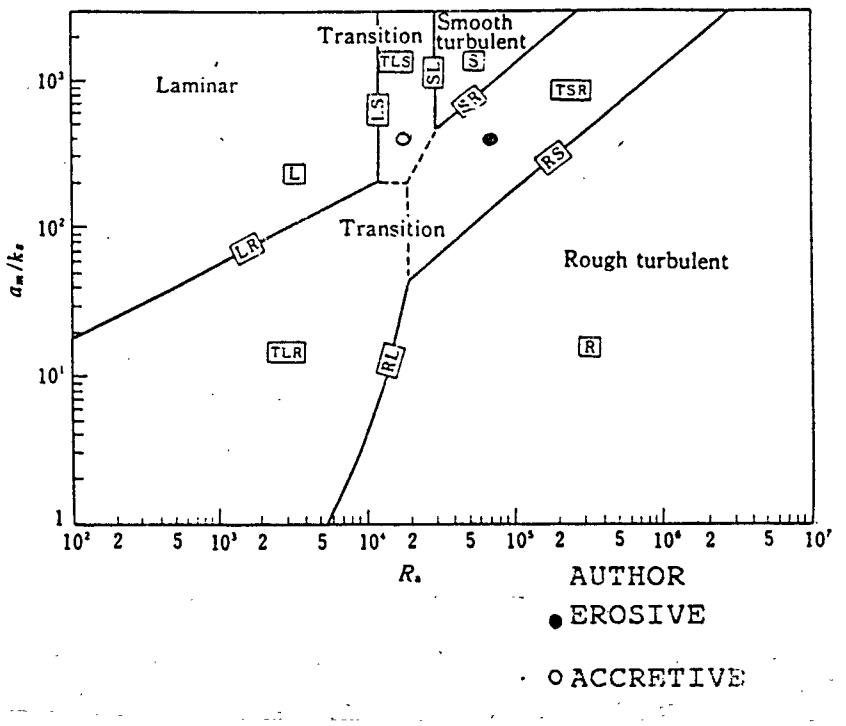

Figure 3.10: Jonsson's Flow Regime

and a Reynolds number given by

$$R_a = \frac{\hat{u}_b a_m}{\nu} \tag{3.6}$$

where $\hat{u}_b$ is the amplitude of the fluid particle velocity near the bed,a_m is the amplitude of the fluid particle displacement, k_s is the roughness length and ν is the kinematic viscosity. Assuming $k_s = D \sim 1.5D$ and using linear wave theory, the flow status at wave breaking point was decided and plotted in Fig.3.10. Therefore, for erosional tests, the flow is in the transition zone between rough turbulent to smooth turbulent and, for accretional tests, the flow is in the transition zone between smooth turbulent to laminar. Since in all likelihood, the field flow condition would be in rough turbulent regime, the results in the recovery tests might not have practical value.

Now we turn our attention to the mode of sediment transport. Shibayama and Horikawa (1980) proposed to use two parameters to classify mode of transport.

These parameters are relative fall velocity and the Shields parameter; they are defined as follows:

$$\hat{u}_b/W \tag{3.7}$$

$$\Psi_m = \frac{f_w \hat{u}_b^2}{2sgD} \tag{3.8}$$

where Ψ_m is the Shields parameter ,f_w is the Jonsson's friction coefficient, s is the sediment specific gravity in the fluid and g is the gravity acceleration.

Again, using linear wave theory, we obtain:

$\Psi_m = 0.828$ for the storm condition

and

$\Psi_m = 0.315$ for the recovery condition.

The positions of these conditions are plotted in Fig.3.11. It is shown that for the storm condition the mode of sediment transport is in the transition zone of bed load and suspended load whereas for the recovery condition the mode is bed load. This result further reinforces the observation that the recovery tests should be viewed with caution to extract any qualitative or quantitative conclusions for field applications. The laboratory results for the storm wave condition, on the other hand, are more realistic and their application to prototype is possible provided proper scaling laws can be established.

3.2 Modeling Law

Modelling law for beach evolution process has been studied by many investigators, notably, Noda (1972), Kamphuis (1975), Hughes (1983), Dean (1983) and Wang (1985). Yet, a completely correct modelling law is still not available. The fundamental difficulty is that the basic mechanism of coastal sediment transport is not well understood. In addition, practical considerations severely limit the choice of material that can be used in the laboratory. Consequently, the scaling of sediment size, specific weight and viscosity are all very limited. Finally, there lacks

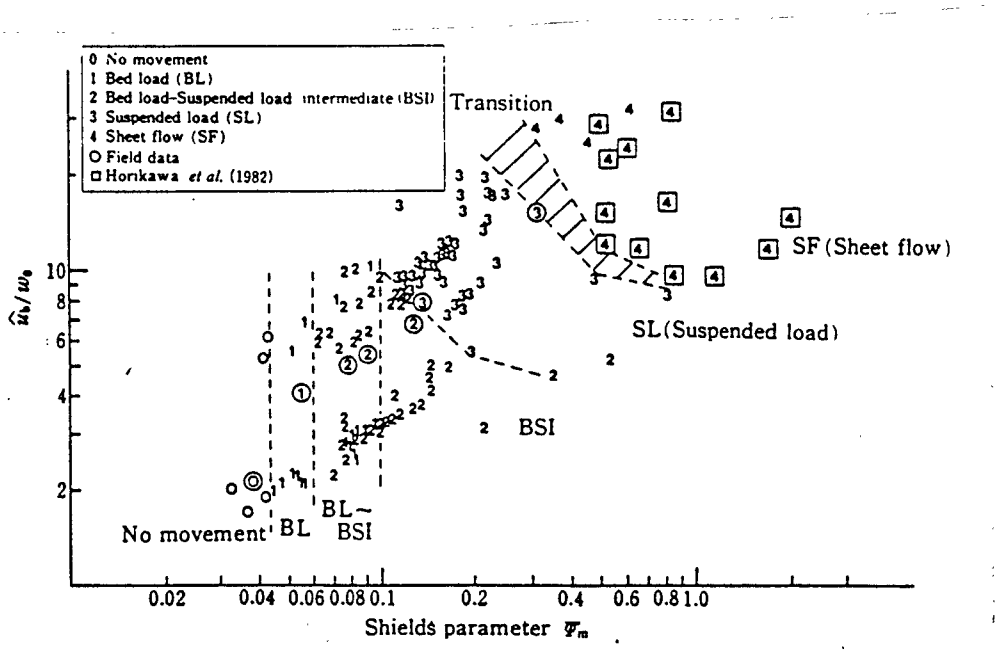

Figure 3.11: Classification of Sediment Transport Model (after Shibayama and Horikawa 1980)

quality prototype data for verification purposes.

In the present study, the initial profile of the model is approximately scaled in accordance with Bodge's field profile (1987) with the assumption that equilibrium is attained at both laboratory and field conditions. There is, however, no field information on beach evolution to compare with the laboratory results. An alternative approach is taken here. Since Dean's (1977) equilibrium profile is derived from an assemblage of field data, it can be treated as a prototype template of some sort. If the beach response is slow, the equilibrium profile should at least match with the final profile. If the beach response is fast, the equilibrium profile should also represent well the transient profiles (the entire profiles as well as the origin could move as a function of time). Based upon this approach, a number of proposed modelling laws are examined here.

3.2.1 Modelling Requirement from Dean's Equilibrium Profile

Let P_p and P_m denote, respectively, the prototype and model values of a physical quantity ,P, and let $P_n = P_p/P_m$ be the scale ratio. We further define λ and δ as the horizontal length scale and vertical length scale of the geometry, respectively.

Then, if the equilibrium profile applies equally well to the prototype and the model, we should have the following scale relationship for the factor "A":

$$A_n = \frac{h_n}{x_n^{2/3}} = \frac{\delta}{\lambda^{2/3}} \tag{3.9}$$

In addition, A should be a function of fall velocity, , following the empirical relationship as given by Fig.3.1 or,

$$A_n = \frac{f_p(H_b/TW)}{f_m(H_b/TW)} \tag{3.10}$$

Therefore, we have two constraints among six physical properties - two geometrical properties ,λ and δ , two flow properties,H and T, one sediment property, W, and one scale coefficient, A. If H is the same as the geometrical vertical scale, the actual variables reduced to five. The dynamic behavior in a gravitational flow field is usually simulated by preserving the Froude number between prototype and model. This scaling law yields for the time variable:

$$T_n = \frac{\lambda}{\delta^{1/2}} \tag{3.11}$$

Therefore, we arrived at a system with two degrees of freedom provided the wave period can be treated as time scale in the Froude similitude.

In the present experiments, if we select $W_n = 1.47$ and $\lambda = 18$, to be consistent with Bodge's values, the following scale ratios are then obtained from the above three equations:

$$\begin{aligned} A_n &= 1.29 \\ \delta &= 8.88 \\ T_n &= 6.04 \end{aligned} \tag{3.12}$$

These are very close to the actual values used by Bodge and the initial condition in the present experiments. Therefore, the initial beach profile conforms with the empirical modeling law as it should.

For the erosive wave conditions tested, the non-dimensional fall velocity is equal to 4.39 and the corresponding A_m value is 0.09. In the previous Section, it was shown that the equilibrium profile represents well the model beach profiles for the final stage as well as for the intermediate stages. This implies that the underlying mechanism of sediment transport is properly modeled under the erosive wave condition. The fact that intermediate stages are also well represented by the equilibrium profile seems to suggest that the morphological time scale is of the same order as the wave time scale, a phenomenon which is often observed in the field under storm wave conditions.

For the recovery wave conditions, on the other hand, the fall velocity parameter becomes 1.01 and the corresponding value of A_m should be 0.24. Neither the shape of the equilibrium profile (controlled by the 2/3 power law) nor the scale of it (controlled by the factor A) appears to compare well with the experiments. A value of $A_m = 0.1$ would be the best choice under this circumstance. Again, as observed in the previous Section, under recovery wave condition, the flow regime is most likely turbulent at field scale but is in a transition regime between laminar and smooth turbulent in the laboratory. Thus, the sediment transport mechanism appears to be not properly modeled in this case.

3.2.2 Hughes' Modeling Law

The Hughes' modeling law which the present model design is partially based upon is examined here. The criteria as specified in Eqs.(3.1) and (3.2) are repeated here:

$$T_n = \frac{\lambda}{\delta^{1/2}} \qquad (3.1)$$

$$\lambda = \frac{\delta^{3/2}}{W_n} \qquad (3.2)$$

Equation (3.1) is essentially a statement of Froude similarity between prototype and model. Equation (3.2) is the preservation of non-dimensional fall velocity parameter, used by Dean in his empirical formula to determine "A". This can be seen by letting wave height H follow the vertical scale and wave period T follow the time scale. Eliminating λ from Eqs. (3.1) and (3.2) we have

$$(\frac{H_b}{TW})_p = (\frac{H_b}{TW})_m \qquad (3.13)$$

This is a more restrictive condition than the Dean's empirical relation given by Eq. (3.10) which only requires A_n to obey the empirical functional relationship. The Hughes' law also has two degrees of freedom and is equivalent to Dean's empirical relationship.

3.2.3 Wang's Modeling Law Revised

Based on the argument that the beach elevation changes must be constrained by the sediment conservation law, Wang (1985) proposed a different set of Modeling Law. A revised version of the Wang's law is discussed here.

The sediment conservation equation states that

$$\frac{\partial z}{\partial t} + K\frac{\partial q_y}{\partial y} = 0 \qquad (3.14)$$

where z is the change of bottom elevation, q_y is the sediment transport rate in the direction of x, and K is the coefficient related to the porosity and is usually taken as unity.

A set of non-dimensional variables are introduced here.

$$\tau = \frac{t}{t_b}\ ;\ \bar{z} = \frac{z}{h_b}\ ;\ \bar{q}_x = \frac{q_x}{q_b}\ ;\ \bar{x} = \frac{x}{x_b} \qquad (3.15)$$

Here the reference values are selected at breaking point signified by the subscript b. Other reference values, of course, can be used as long as they are consistent

and represent the characteristics of the phenomenon. Now, substituting these non-dimensional variables into Eq. (3.14), we arrived at the non-dimensional transport equation in surf zone

$$\frac{\partial \bar{z}}{\partial \bar{t}} = (\frac{q_b t_b}{h_b x_b}) \frac{\partial \bar{q}_x}{\partial \bar{x}} \tag{3.16}$$

To maintain similitude between model and prototype requires

$$(\frac{q_b t_b}{h_b x_b})_m = (\frac{q_b t_b}{h_b x_b})_p \tag{3.17}$$

or

$$\frac{q_n t_n}{h_n x_n} = 1 \tag{3.18}$$

where h_n and x_n are the geometrical scales of δ and λ, respectively, t_n is a morphological time scale and q_n is the sediment transport scale.

Since the mechanisms of bed load transport and suspended load transport are quite different, Wang argued that the Modeling criteria are also different depending upon which mode of transport dominant. Here only the suspended load dominant case is discussed.

Wang proposed that the suspended load transport rate can be expressed by depth averaged properties:

$$q_s = hVC \tag{3.19}$$

Here h=depth; V= mean transport velocity and C = mean sediment concentration. Following Hattori and Kawamata's approach, it is assumed that the suspended sediment concentration is directly proportional to the stirring power due to turbulence, P_t, and inversely proportional to the settling power due to gravity, P_r. The stirring power per unit volume can be expressed as

$$P_t = \rho g u' \tag{3.20}$$

where u' is the turbulent velocity . The resisting power is

$$P_r = (\rho_s - \rho) g W \tag{3.21}$$

with W being the settling velocity. Therefore, we have

$$C \propto \frac{u'}{\gamma' W} \tag{3.22}$$

where

$$\gamma' = (\frac{\rho_s}{\rho} - 1) \tag{3.23}$$

Based on field measurement of kinetic energy and momentum flux in surf zone, Thornton (1978) suggested that the ratio of turbulent velocity intensity and the wave-induced velocity intensity is a function of surf zone parameter, i.e.,

$$\frac{\sigma_u'}{\sigma_u} = f(\xi) \tag{3.24}$$

where σ' and σ are the standard deviations of the turbulent and wave-induced velocities, respectively, and $\xi = tan\beta/\sqrt{H_o/L_o}$. Thus, substituting Eq. (3.24) into Eq. (3.22) and absorbing the proportionally constant into $f(\xi)$, we arrived at

$$C = \frac{\sigma_u}{\gamma' W} f(\xi) \tag{3.25}$$

For steep waves , σ_u can be assumed to be proportional to H/T , the above equation can, therefore, be expressed as

$$C = \frac{f(\xi)}{\gamma'(\frac{WT}{H})} \tag{3.26}$$

Physically, this equation states that the suspended sediment concentration in surf zone is proportional to a function of surf zone parameter (or the breaker type), and is inversely proportional to the specific gravity and the relative fall velocity. Substituting Eq. (3.26) into Eq. (3.19), results in

$$q_s = \frac{hV f(\xi)}{\gamma'(\frac{WT}{H})} \tag{3.27}$$

Substituting Eq. (3.27) into Eq. (3.18) gives

$$\frac{V_n f_n(\xi) t_n}{\gamma_n' W_n T_n / H_n} = 1 \tag{3.28}$$

A number of assumptions are made here

a. The wave height is proportional to water depth, thus, can be treated as a vertical scale, or, $H_n = \delta$.

b. The morphological scale is the same as the wave period scale, or, $t_n = T_n$. This is justified in that during erosional process the rate of erosion is proportional to the number of waves propagated in the duration.

c. $V \propto \delta^{1/2}$. This is based upon the results by Wang, et. al. (1982). That the net transport velocity is found to be

$$V \propto \kappa^2 \sqrt{gh} \tag{3.29}$$

where κ is the wave height to water depth ratio.

d. $\xi_p = \xi_m$. It is a more restrictive but sufficient condition to guarantee $f_p(\xi) = f_m(\xi)$. In fact, if $\xi_p = \xi_m$, we have $f_n(\xi) = 1$ and this parameter can be eliminated from Eq. (3.28). However, for $\xi_p = \xi_m$ requires

$$(tan\beta/\sqrt{H_o/L_o})_p = (tan\beta/\sqrt{H_o/L_o})_m \tag{3.30}$$

Since $L_o = gT^2$ and $(tan\beta)_n = \delta/\lambda$, Eq. (3.30) is equivalent to

$$T_n = \frac{\lambda}{\delta^{1/2}} \tag{3.31}$$

which is the Froude similarity between prototype and model.

Now substituting the above four condition into Eq. (3.28), we arrive at the following modeling criterion

$$\delta = (\gamma_n' W_n)^{2/3} \lambda^{2/3} \tag{3.32}$$

If we define A_w as

$$A_w = \alpha(\gamma' W)^{2/3} \tag{3.33}$$

with α a proportional constant, Eq. (3.32) can be written as

$$\delta = (A_w)_n \lambda^{2/3} \tag{3.34}$$

This equation is almost the same as Dean's equilibrium profile equation, the difference being the functional dependency of the scale parameter, A. Based upon empirical evidence, Dean and Moore suggested A to be a function of sediment particle size, D, or non-dimensional fall velocity, H_b/TW. Based upon sediment mass conservation equation, the correct form of A is suggested here to be (see Eq. (3.28))

$$A_w = (\frac{\gamma' W}{g^{1/2}})^{2/3} \tag{3.35}$$

Wang paid special attention to the scaling of settling velocity in a wave field as the magnitude of the velocity is affected by the nature of the oscillatory flow field (Fig.3.12). Hwang (1985) suggested that

$$\frac{W}{W_o} = f_w(\frac{V_f}{W_o}\ ,\ R\ ,\ \frac{V_s}{V_f}) \tag{3.36}$$

where

W_o is the terminal velocity in calm water,

V_f and V_s are the amplitude of fluid and particle oscillations, respectively and

R is the particle Reynolds number.

Proper modeling requires

$$W_n = (W_o)_n[f_w(\frac{V_f}{W_o}\ ,\ R\ ,\ \frac{V_s}{V_f})]_n \tag{3.37}$$

This is difficult to fulfill. At present, W is treated as equal to W_o. Thus,

$$W_n\ =\ (W_o)_n \tag{3.38}$$

It is further observed here that for small Reynolds number, $WD/\nu < 1.0$,

$$W_o \propto D^2 \tag{3.39}$$

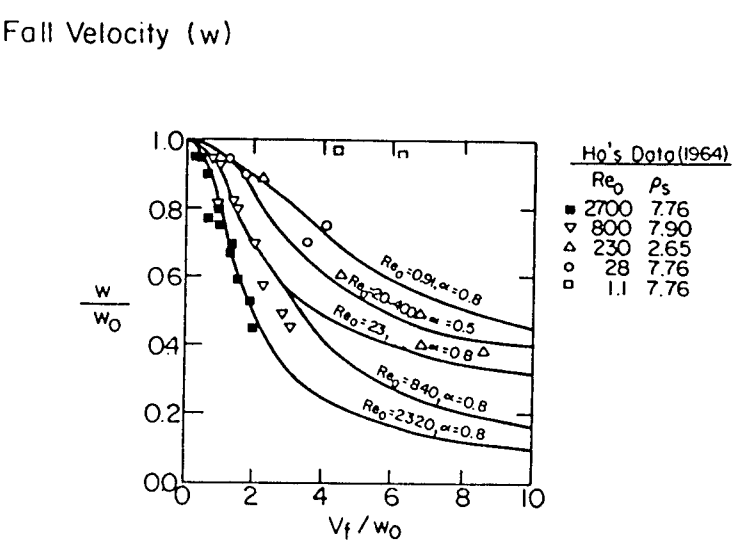

$$\frac{w}{w_0} = f\left(\frac{\hat{u}}{w_0}\ ;\ R\ ;\ \alpha\right)\ ;\ R = \frac{w_0 D}{\nu}\ ;\ \alpha = \frac{V_s}{V_f}$$

Figure 3.12: Reduction of Settling Velocity in the Oscillatory Flow (after Hwang 1985)

for higher Reynolds number but less than 10^3,

$$W_o \propto D \tag{3.40}$$

and finally for high Reynolds number,

$$W_o \propto D^{1/2} \tag{3.41}$$

The corresponding slope of A_w in these ranges are $D^{1.33}$, $D^{0.67}$ and $D^{0.33}$, respectively. They are consistent with the data compiled by Moore (Fig.3.13) in which the slope of curve " A " decreases with increasing D.

For erosive wave condition, this model law is applied to the test results. For horizontal scale $\lambda = 18$ and $W_n = (W_o)_n = 1.47$, the vertical scale should be

$$\delta = (1.47)^{2/3} \times 18^{2/3} = 8.88 \tag{3.42}$$

which is very close to the value of 9 used in model design. The corresponding $A_n = (W_n)^{2/3} = 1.29$. This is very close to the ratio determined from the empirical diagram of Moore's, which gives a ratio of 1.31.

3.2.4 Noda's Modeling Law

Noda gave a set of empirical modeling law as follows:

$$D_n(\gamma_n')^{1.85} = (\delta)^{0.55} \tag{3.43}$$

$$\lambda = (\delta)^{1.32}(\gamma_n')^{-0.386} \tag{3.44}$$

This set of equation has two degrees of freedom. Eliminating γ_n' from the above equations, we have

$$\delta = D_n^{-0.17}\lambda^{0.83} \tag{3.45}$$

The shape factor 0.83 is in the same magnitude as in the previous model laws. The scale factor, on the other hand, has a quite different functional dependency on D

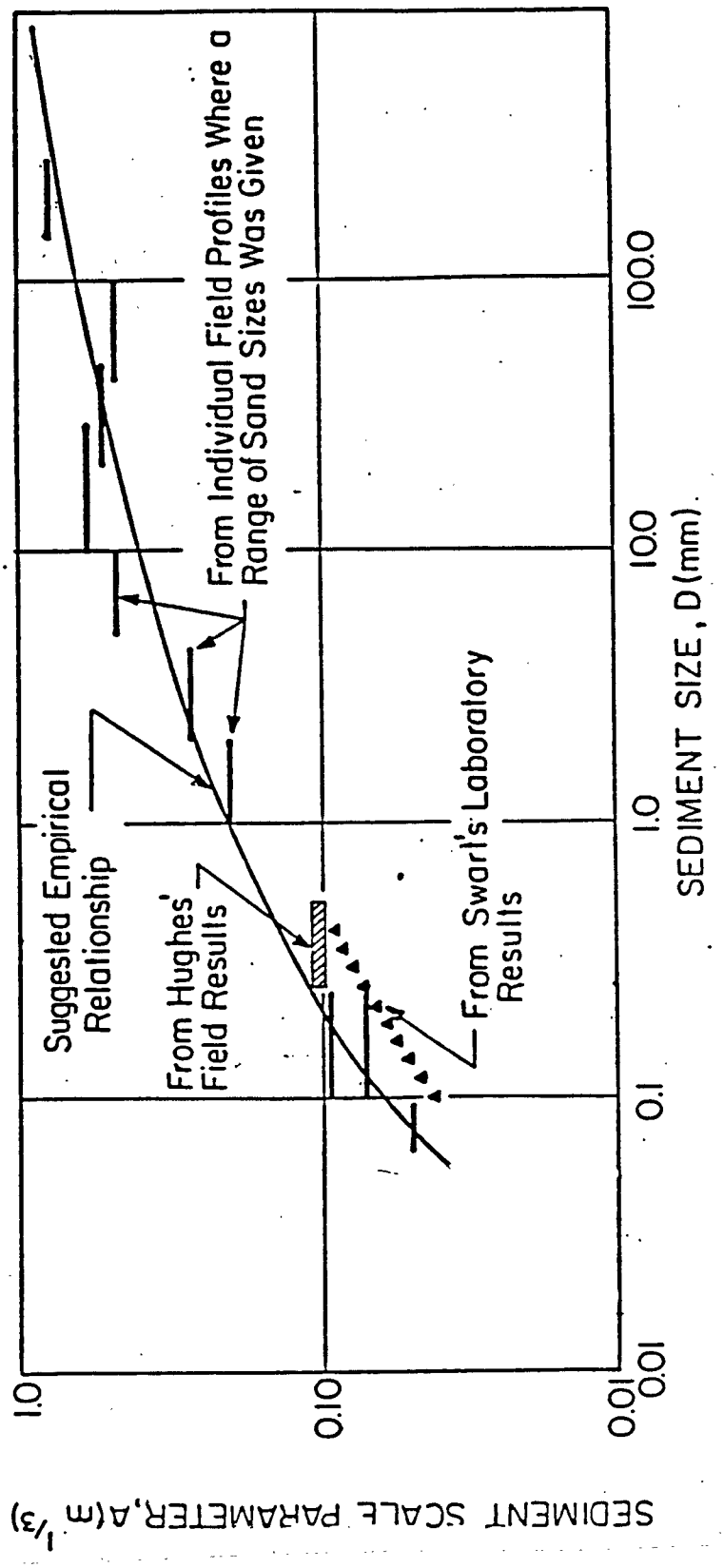

Figure 3.13: Moore's Diagram for Scale Parameter A

given by Moore (1982). If we further let $D_n = 1.21$, the value used in the present experiments, Eq. (3.43) yields

$$\delta = 1.41 \tag{3.46}$$

This is a very restrictive criterion and is quite different from the value used here.

3.2.5 Summary

For the verification of the modeling laws, we have assumed that the equilibrium beach profile can be treated as a prototype template for the model results to be compared to. Four different modeling laws are examined–Hughes, Wang's, Noda's and an empirical law derived from Dean's equilibrium profile concept.

The experimental results show that the model tests were carried out under different flow regime, thus, required different scaling laws for the recovery conditions and for the erosive conditions. Of the four modeling laws, only Wang's can address the problem of different modeling laws for different sediment transport modes. For comparison purposes, only results from the erosive wave conditions are tested.

Noda's model is definitely inadequate. Hughes' model, Dean's equilibrium concept and Wang's model are consistant, although they are derived from significantly different argument. All of them give reasonable results. Finally, Wang's model provides a rational explanation of the scale parameter "A" as well as its functional dependency and how it should be scaled without resorting to empirical graphs. It also addresses bed load dominated case and transient profile modeling that, in principle, can not be addressed by the equilibrium concept.

3.3 Comparison to 2-D and 3-D Model Test Results

Barnett (1987) conducted two dimensional (2-D) model tests of a vertical seawall on beach in a wave tank in the same laboratory here in the Department of Coastal and Oceanographic Engineering, University of Florida. His results are compared with the results of the present study which are from three dimensional (3-D) conducted in a wave basin.

3.3.1 Beach Profile Comparison

The 2-D and 3-D experiments were conducted under rather close but not identical conditions. To facilitate comparison, certain adjustment has to be made first. The test conditions of 2-D experiment are given in Table 3.1. By comparing with the test conditions of the 3-D model given in Table 2.2, a selected sets of data with similar test conditions–Cases 1A and 9C are used for the natural beach without seawall and Cases 3A and 12C are used for beaches with seawall.

Table 3.1: 2-D Model Test Condition (Barnett 1987)

Wave Condition	
Wave Height(cm)	11.75 8.80 4.00
Wave Periods(s)	1.81 1.30 1.81
Sediment Condition	
Diameter(mm)	$d_{50} = 0.15$
Settling Velocity(cm/s)	$W = 0.017$
Water Depth(cm)	46.0 and 56.0
Seawall Location	shoreline and $\pm 0.3m$ from the shoreline
Initial Profile	$A = 0.075m^{1/3}$

Case 1A and 3A are based upon an equilibrium beach profile with scale factor "A" equal to 0.075. Cases 9C and 12C have the same initial profile as Case 1A but with the water level raised by $10cm$ to represent storm surge condition. Therefore, strictly speaking, the initial condition of Case 9C and 12C is not an equilibrium profile. If it were to be treated as an equilibrium profile, the "A" value has to be adjusted according to

$$A_C = A_A(y_C/y_A)(x_A/x_C)^{2/3} \tag{3.47}$$

where subscripts A and C denote Case 1A or 3A and Case 9C or 12C, respectively. If $A_A = 0.075$, $y_A = 46cm$, $y_C = 56cm$ and the x scales are the same then an equivalent A is obtained as equal to 0.091. Table 3.2 summarized the condition of these cases.

As can be seen from Table 3.2, the initial profiles of the cases to be compared are usually not the same because of the slightly different test conditions. Therefore, one can not be assured that the subsequent comparison of profile evolution are meaningful. The first step is to attempt to establish the profile relationship between 2-D and 3-D test so that meaningful comparisons can be made. This is handled by treating the 2-D experiment as a distorted model of 3-D case, or vice versa.

Based on the modeling requirement from Dean's equilibrium beach profile, we have

$$y_2 = A_2^{3/2} h_2^{3/2} \tag{3.48}$$

and

$$y_3 = A_3^{3/2} h_3^{3/2} \tag{3.49}$$

where subscript 2 and 3 refer to 2-D and 3-D cases respectively.
Dividing Eq.(3.48) by Eq.(3.49) gives

$$\frac{y_2}{y_3} = (\frac{A_2}{A_3})^{3/2} (\frac{h_2}{h_3})^{3/2} \tag{3.50}$$

This is the basic equation used for profile adjustment. All the scale adjustment were made by using 3-D case as reference. Since the vertical scale (the water depth) and the "A" values are known, the most convenient adjustment is the horizontal scale, or

$$y_2 = y_3 (\frac{A_2}{A_3})^{3/2} (\frac{h_2}{h_3})^{3/2} \tag{3.51}$$

Figure 3.14 compares the initial conditions of 3-D and 2-D cases with and without profile adjustment. Figure 3.15 compares profile 4 hrs after the test for cases with and without seawall. For the cases without seawall, the agreement is very good within the surf zone. The 2-D tests generally produced bottom undulation due to wave reflections confined in the channel. For cases with seawall, the comparison is

less satisfying. The most significant difference between them is the bar formation. Prominent multiple reflection bars appeared in all the 2-D tests, whereas in 3-D test, no reflection bar were formed in case 2 and 6 and only small ones appeared in case 4.

3.3.2 Offshore Breaking Bars

There are a few studies which examine the relation between the scale of the breaking bar such as the bar height or width and the other property such as wave height or sediment. Keulegan (1948) found in a laboratory experiment that the ratio of the water depth of the bar trough, h_t, to the depth of the bar crest, h_c, has an average value of 1.69, i.e.,

$$h_t = 1.69 h_c \tag{3.52}$$

Sunamura (1985) mentioned that the relation given by Eq. (3.52) was supported by Kajima's large model test, and also suggested the simple relation between h_t and the breaking wave height H_B as

$$h_t = H_B \tag{3.53}$$

Combining Eq. (3.52) and Eq. (3.53), we have

$$h_c = 0.59 H_B = 0.59 h_t \tag{3.54}$$

It is not always easy to examine the relationship between h_c and h_t, because the breaking point bar is not always stable; the breaking bar formed rapidly then disappeared, h_t sometimes is also unrecognizable. Selecting the maximum bar height in the test, the relation given by Eq. (3.53) are examined by both test results as shown in Fig3.16. Since the breaking wave height in 2-D model test is not available, the breaking wave height were estimated by using the breaking wave index shown in Fig.3.17.

The data are scattered but the relation given by Eq. (3.53) agreed with model test results reasonably well. The difference between 2-D and 3-D, however, is not

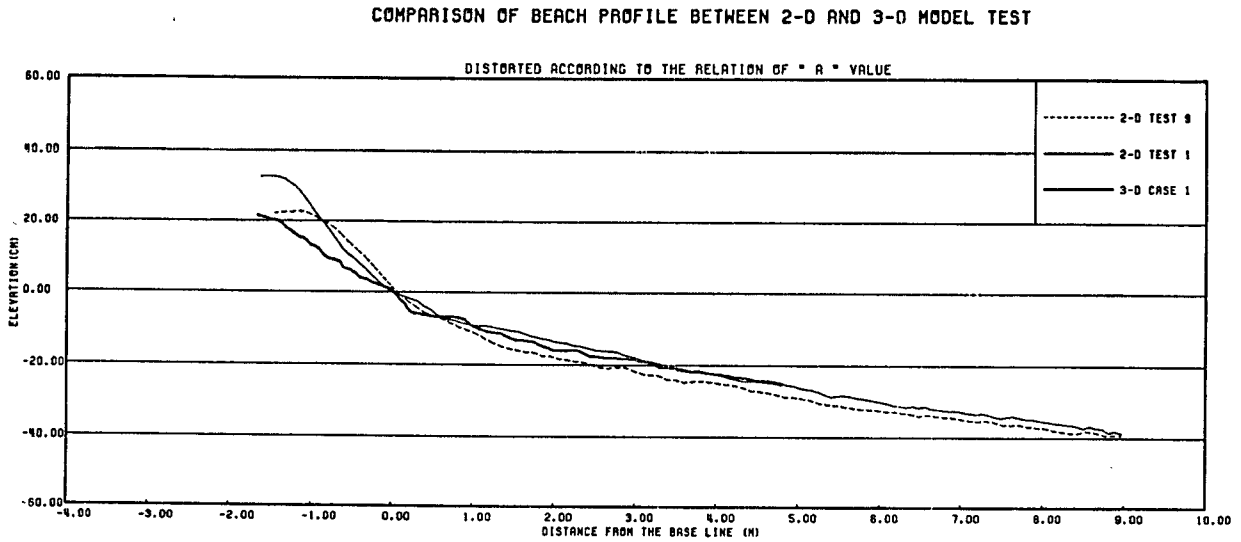

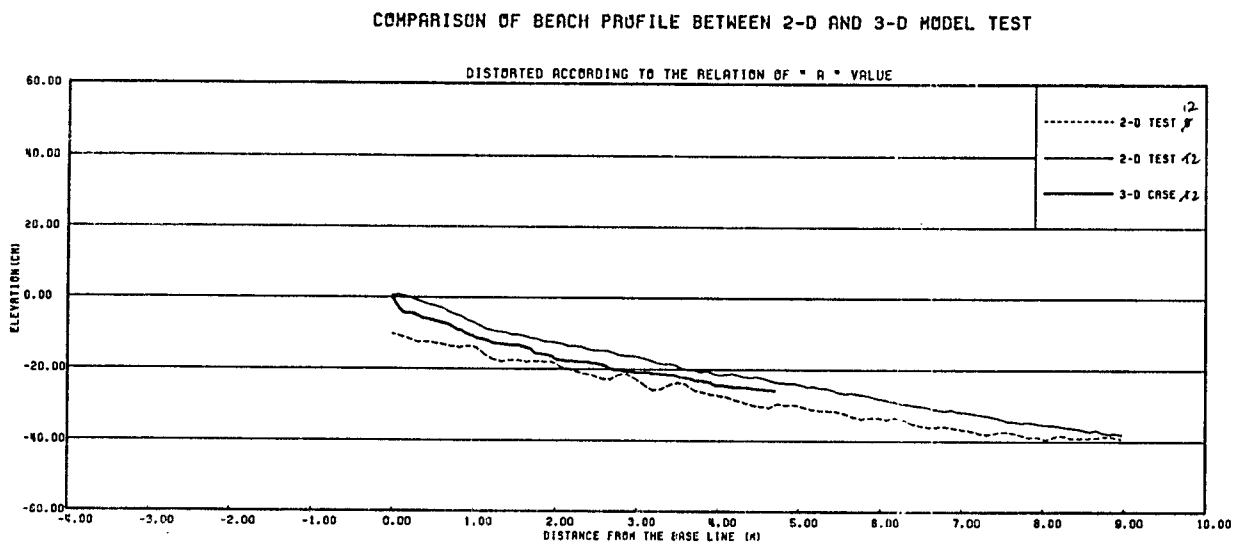

Figure 3.14: Comparison of Initial Beach Profiles between 2-D and 3-D Model Test

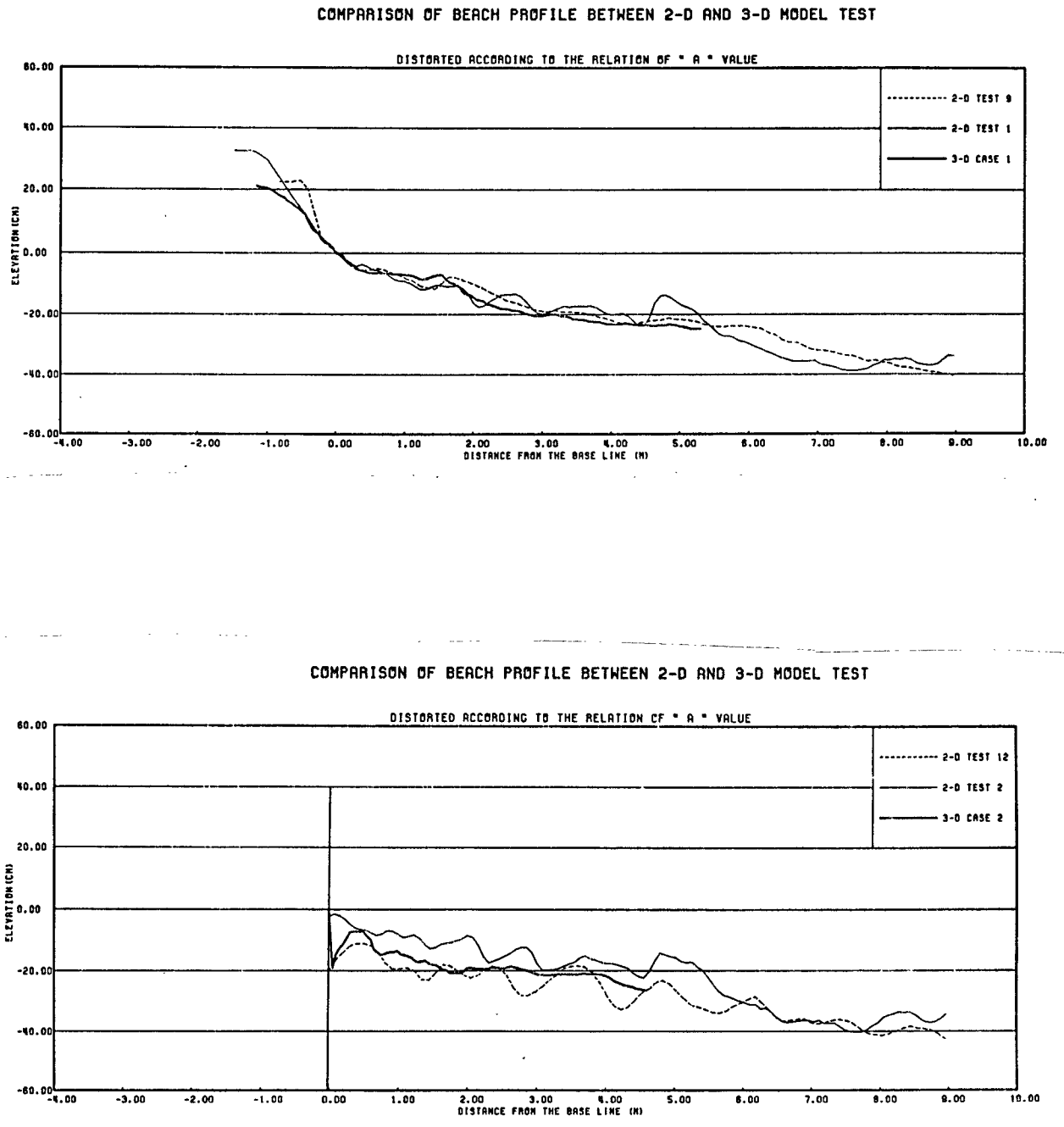

Figure 3.15: Comparison of Beach Profiles after 4 Hours Duration between 2-D and 3-D Model Test

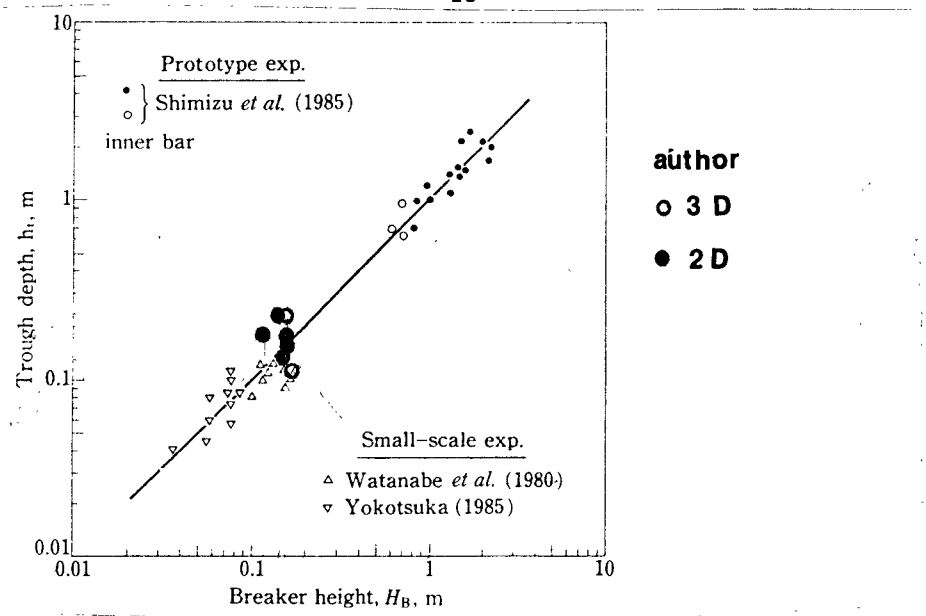

Figure 3.16: Relation between H_B and h_t adopted by Horikawa(1988)

found. The relation between h_c and h_t is also examined in Fig. 3.18. The data are scattered again, but the dashed line in Fig. 3.18 calculated by using least square sense is given by

$$h_c = 0.6h_t \tag{3.55}$$

This coefficient is very close to the value proposed by Keulegan. The scatter of the data points does not permit us to establish the difference between 2-D and 3-D cases.

3.3.3 Reflection Bars

The reflection bars and the offshore bars (or breaking bars) are formed by different mechanisms. The offshore bar is formed by breaking waves while the reflection bars result from the standing waves due to reflection. The location of latter usually coincide with nodes and antinodes of the standing wave system.

Xie (1981) found that there are two types of reflection bar, that is, for fine sediment the bar forms at antinode, but for coarse sediment the bar forms at the node. Irie et al. (1984) also came to the same conclusion and they noted that the criterion of these two formations is a function of Ursell number and the ratio of

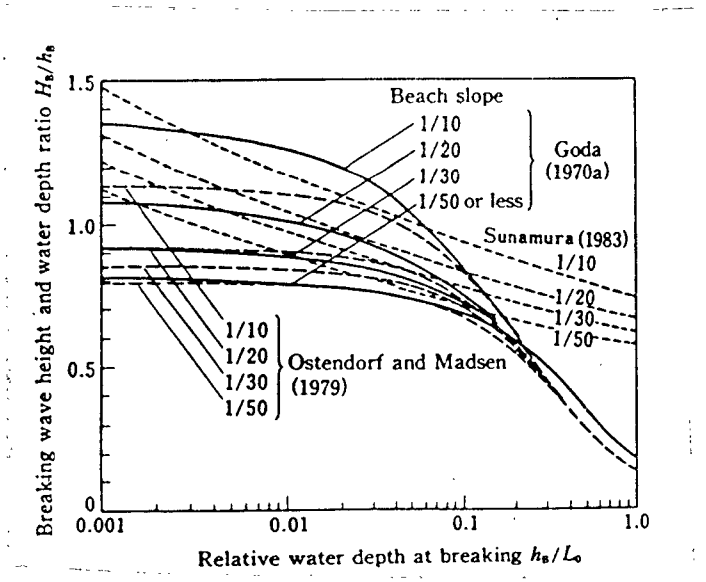

Figure 3.17: Breaking Wave Index adopted by Horikawa (1987)

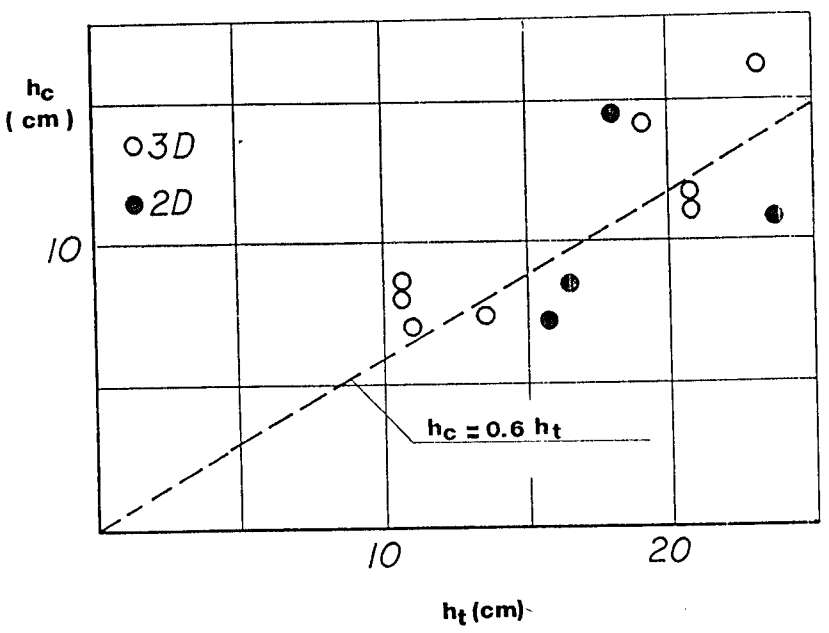

Figure 3.18: Relation h_t and h_c

the fluid velocity at the bottom to sediment settling velocity. Both studies are two dimensional. Irie et al. (1984) and Silvester (1987) also conducted three dimensional tests on breakwaters and seawalls. Their results also showed similar reflection bar pattern. Hsu and Silvester (1989) demonstrated that with angled waves bar and trough occurrence also dependant upon the obliquity. These are determined in fractions of the distance of island crests, formed at wave interactions, termed the crest length. Katsui and Toue (1988) examined the bathymetric change around a large offshore structure by 3-D model test and found that well defined reflection bars formed in front of the structures. It should be noted here that all the studies cited above were carried out at non-breaking waves.

In the present study, reflection bars in 2-D test are prominent even within breaking zone. In 3-D tests, the reflection bar is far more difficult to maintain; it appears and then disappears. This is probably because the energy flux reflected from seawall tends to propagate along the wave crest (a diffraction phenomenon) and the fact that the wave induced current is less organized to sustain stable bar formation.

3.3.4 Scour

The scour depth and the other quantity are defined in Fig.3.19. Two scour depths, S_l and S_g, are defined. S_l is the depth from the elevation of the nearest bar crest to the elevation of the scoured bed at the toe of the seawall, and S_g is the depth from the initial bed to the bar crest. The reason for defining two scour depths is that S_l and S_g might be caused by the different mechanisms. As can be seen in Fig.3.15, the beach is eroded from the entire region in front of seawall in Test 2A, while the erosion occurred only in the vicinity of the seawall in Test 12C and Case 2. In other word, S_l is caused by strong vortices due to interaction of wave and structure, while S_g is caused by the sediment depletion to form offshore bar. As to the parameter s which is relevant to the scouring, (1) incident wave height,H_o, (2)

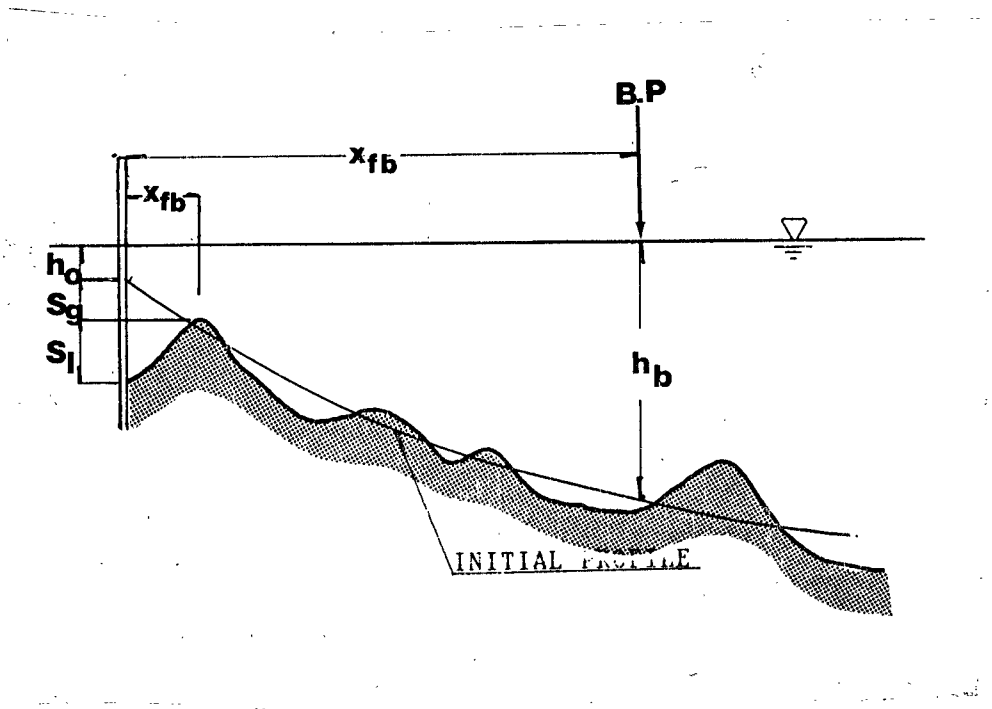

Figure 3.19: Definition of Scour Depth and Other Parameters

wave period, T, (3) initial water depth at the seawall, h_o and (4) distance from the seawall to the nearest bar, y_{fb} are considered. After several attempts to examine their relation, the clear relation between S_l and h_o was found in Fig.3.20. The following observation based on physical reasoning are made:

(1) The scour depth might be directly related to the wave height.

(2) For the case that the elevation of the toe is above the still water level, if the elevation of the toe is so high that the wave can not reach the seawall, the scouring does not occur. Thus, some variables which define the relation of h_o to the wave run up height must be included, and the wave run up is related to the beach slope and the wave steepness.

(3) The waves which reach the seawall must be influenced by the breaking wave condition.

Consequently, based on the relation obtained in Fig.3.20 and the physical reasoning above, the scour depth, S_l is given as a function of H_o, L_o, h_o and the surf similarity parameter based on the $tan\beta_b$ (Figure 3.21).

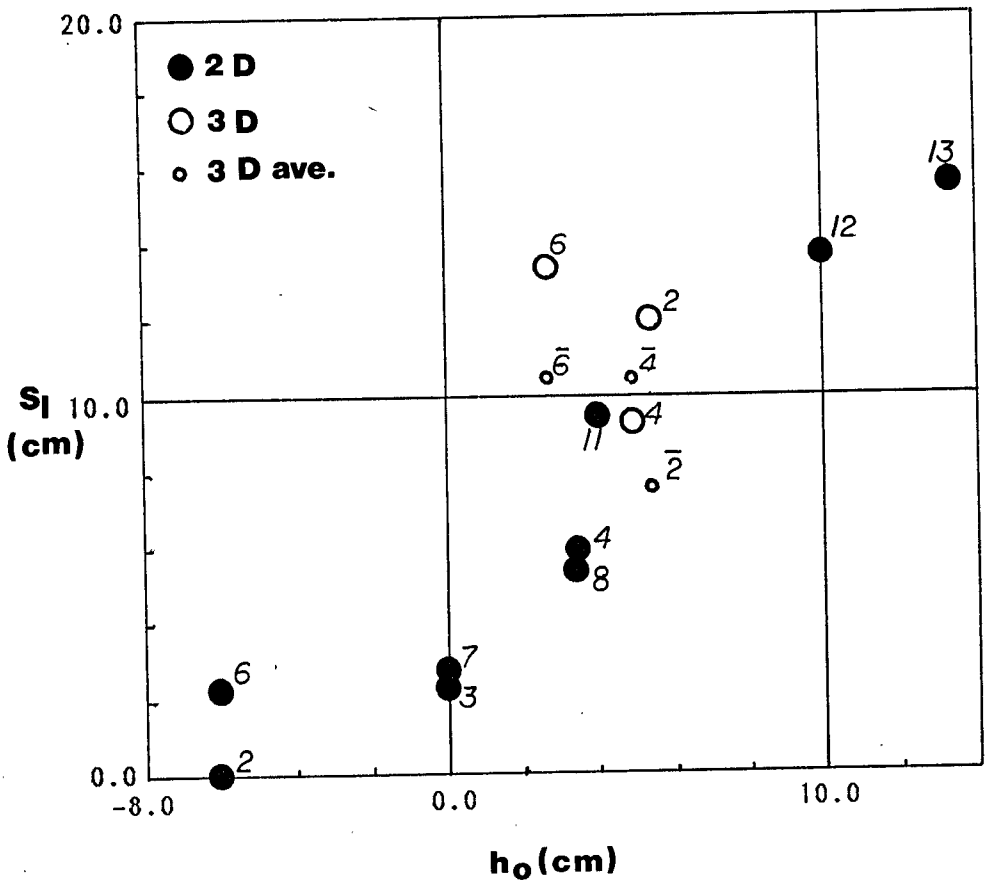

Figure 3.20: Relation of S_l and h_o

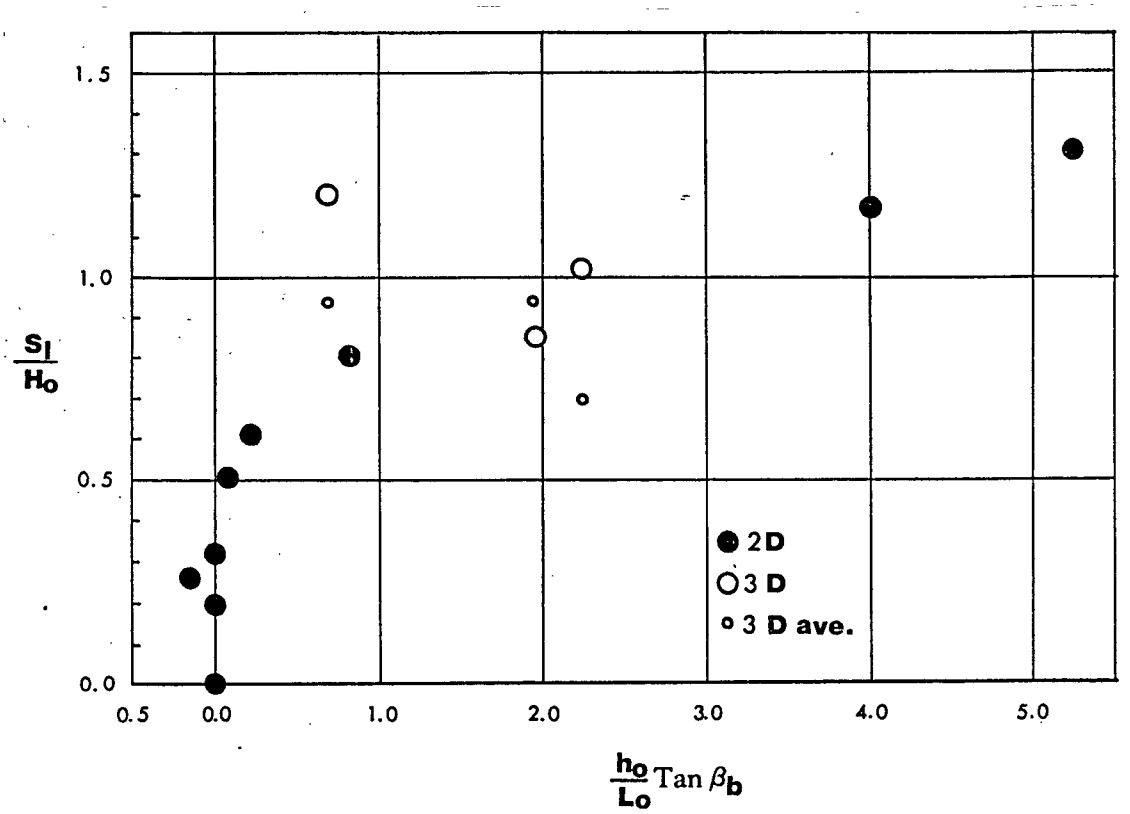

Figure 3.21: Relation between S_l/H_o to $h_o \times tan\beta_b/L_o$

Table 3.2: Comparison of Scale Parameter "A" in 2-D and 3-D Model Test

	3-D model test	Cases 1A and 3A	Cases 9C and 12C
water depth	$45cm$	$46cm$	$56cm$
wave height	$11.75cm$	$11.0cm$	$11.0cm$
wave period	$1.73sec.$	$1.7sec$	$1.7sec$
scale parameter	$0.09m^{1/3}$	$0.075m^{1/3}$	$0.089m^{1/3}$

CHAPTER 4
VOLUME CHANGE ANLYSIS

The effects of seawall on beach changes are evaluated using two major indices– the effects on volumetric changes of beach material and the effects on shoreline and contour-line changes in foreshore and backshore region. The effects on volumetric changes is addressed here first.

4.1 Definition of Volumetric Changes

The basic equation used to compute the sediment volumetric changes is the sediment mass conservation equation given by

$$\frac{\partial z}{\partial t} = -(\frac{\partial q_x}{\partial x} + \frac{\partial q_y}{\partial y}) \tag{4.1}$$

Referring to Fig.4.1, the terms in Eq. (4.1) are defines as

x=shore-parallel axis, y=shore-perpendicular axis; z=profile elevation;

The origin is set at the undisturbed still water level at the down wave boundary of the test region 7.5 m from the center of the seawall. Three different types of volumetric changes are computed; their definitions are shown in Fig.4.2.

(1) Rate of Volumetric Changes along a Profile, $\dot{v}_p(x,t)$

The volume change along a profile can be obtained simply by integrating Eq. (4.1) along a profile from $y = 0$ to $y = y_o$

$$\begin{aligned} v_p(x,t) &= \int_0^{y_o} \frac{\partial z}{\partial t} dy \\ &= -\{q_y(y_o) - q_y(0) + \int_0^{y_o} \frac{\partial q_x}{\partial x} dy\} \end{aligned} \tag{4.2}$$

where y_o is the offshore boundary. Since $q_y(0) = 0$, the above equation becomes

$$\dot{v}_p(x,t) = -q_y(y_o) - \int_0^{y_o} \frac{\partial q_x}{\partial x} dy \tag{4.3}$$

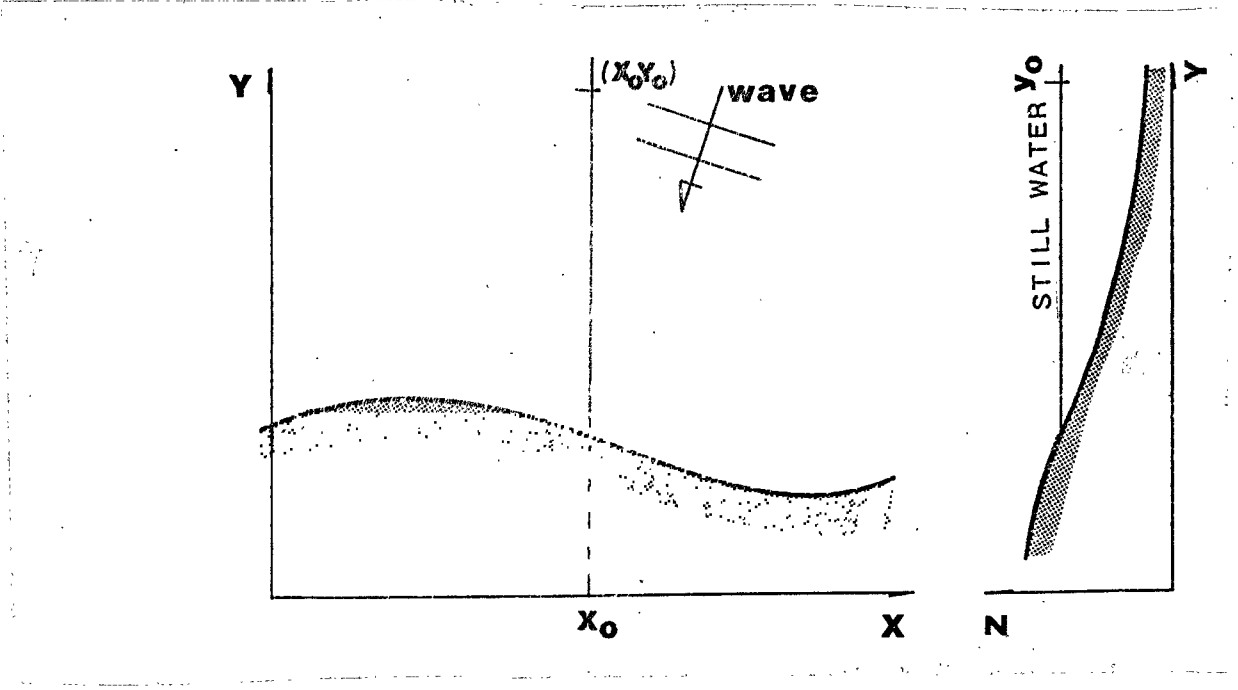

Figure 4.1: Sketch of Coordinate System

The units of $\dot{v}_p(x,t)$ are volume per unit length per unit time.

(2) Cumulative Rate of Volumetric Changes Referenced to Down-Wave Boundary, $\dot{v}_c(y_o,t)$.

If Eq. (4.3) is integrated along shore from $x = 0$ to $x = x_o$, we have

$$\dot{v}_c(x_o,t) = -\int_0^{x_o} q_y(y_o)dx - \int_0^{y_o}\{q_x(x_o) - q_x(0)\}dy \tag{4.4}$$

This represents the cumulative rate of volumetric changes in a control area bounded along shore from $x = 0$ to $x = x_o$

(3) Rate of Volumetric Changes in a Local Control Area Centered around the Seawall, $\dot{v}_l(t)$

In this case, the integration of Eq. (4.3) is carried out from $-W/2$ to $W/2$, where $W/2$ is the long shore distance measured from the centerline of the seawall location, i.e.,

$$\dot{v}_l(t) = \int_{x_c-W/2}^{x_c+W/2} \dot{v}_p(x,t)dx$$

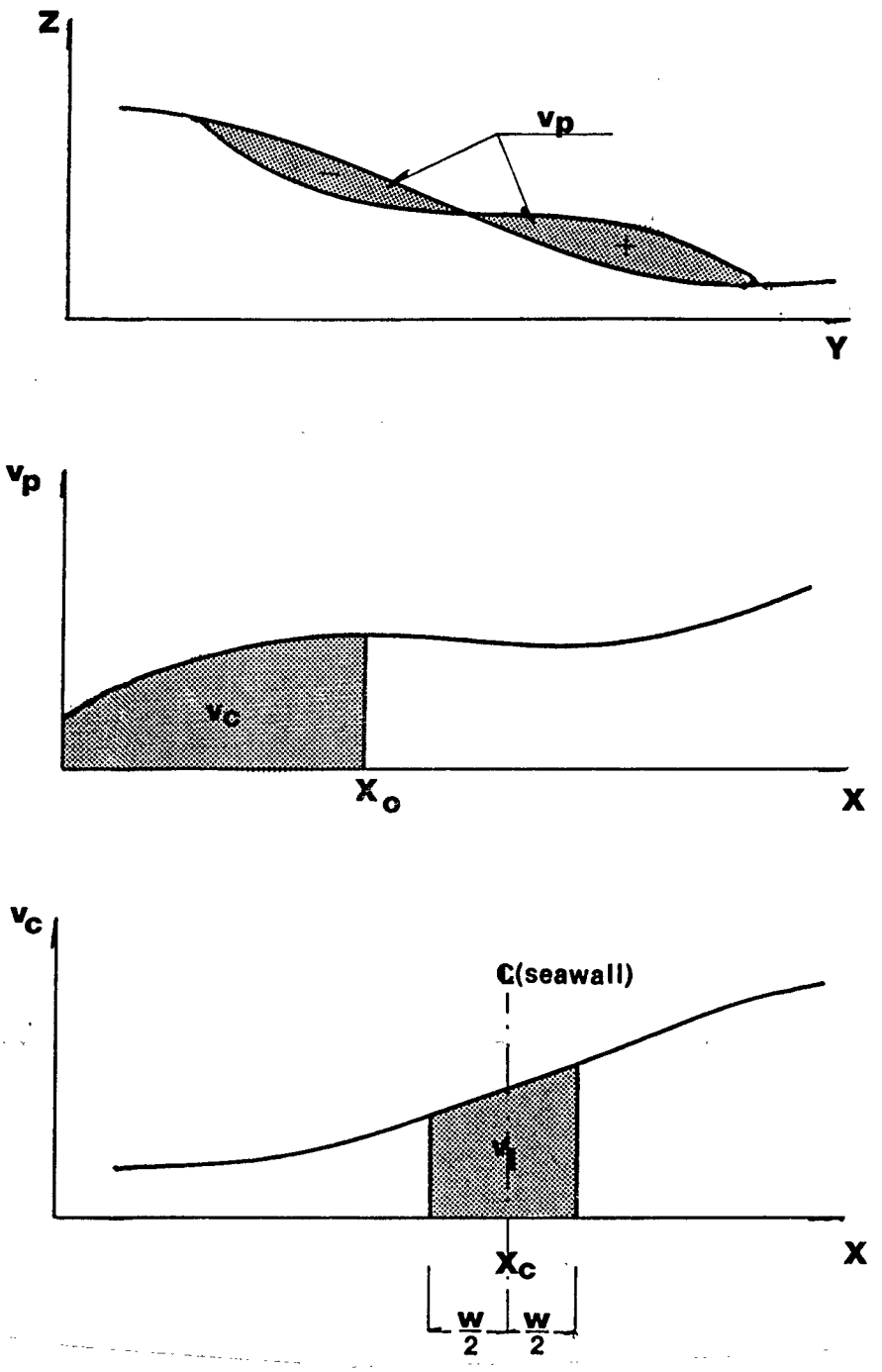

Figure 4.2: Definition of Three types Volumetric Changes

$$= Q_x(x_c + W/2, t) - Q_x(x_c - W/2, t) + \int_{x_c - W/2}^{x_c + W/2} q_y(y_o)dx \qquad (4.5)$$

where

Q_y is the longshore transport rate, x_c is the location of center of seawall and $-W/2$ and $W/2$ are the variable down-drift and the up-drift boundary of the local control area respectively.

4.2 Results and Discussion

Based on Eqs. (4.3), (4.4) and (4.5), $\dot{v}_p$, $\dot{v}_c$ and $\dot{v}_l$ are calculated. The integration are carried out by the following discrete formulas

$$(\dot{v}_p)_j^k = \frac{\Delta y}{\Delta t} \sum_{i=1}^{I} (z_{i,j}^{k+1} - z_{i,j}^k) \qquad (4.6)$$

$$(\dot{v}_c)_j^k = \sum_{j=j}^{J} (\dot{v}_p)_j^k \Delta x \qquad (4.7)$$

$$(\dot{v}_l)_j^k = (\dot{v}_c)_{j_2}^k - (\dot{v}_c)_{j_1}^k \qquad (4.8)$$

where

i, j and k denote y, x and t respectively,

$\Delta y = 0.05m$, $\Delta x = 0.75m$, $\Delta t = 3600s, 7200s$, and $14400s$,

I is the integer so that $I\Delta y = 7.0m$

J is the integer so that $J\Delta x = 15.5m$

j_1 and j_2 are the integer so that $j_1\Delta x = x_c - W/2$ and $j_2\Delta x = x_c + W/2$ respectively. The results are presented in Figs. 4.3, 4.4 and 4.5. In the case of $\dot{v}_p$ and $\dot{v}_c$, the abscissa is the longshore distance measured from origin. In the case of $\dot{v}_l$, the abscissa is the width of the local control areas non-dimensionalized with respect to the seawall length, or W/L_s where W is the width of the control area and L_s is length of the seawall. The ordinate of all three cases represents the rate of volume change per hour. All the computations are carried out to a total of four hours duration even though some of the experimental runs were carried out to a much

longer duration. Since the topographic changes were measured at 1 hour, 2 hours and 4 hours after the test began, the computed points denoted as t=4 hours in the graphs actually represent the average values from t=2 hours to t=4 hours.

The rate of volumetric change along individual profile is examined first. In Fig. 4.3, the seawall is located at $x = 6m$ to $9m$, and the wave incident angle is defined as shown. Therefore, the updrift boundary is at the right hand side for all the cases shown. Under normally incident waves, the rate of erosion in the center portion of the test region is almost uniform with or without the seawall. Also, in this center region, the rate of volumetric erosion is seen to be smaller on profiles fronting the seawall than that of natural beach. This is similar to the 2-D results by Barnett. Towards the two sides of the test region, the volumetric rate of change along individual profile becomes erratic, perhaps owing to boundary effects.

For the cases of oblique wave of 5^o and 10^o incident wave angles, Erosional rate along individual profile becomes more irregular due to the three dimensional flow pattern in the near shore zone. For natural beach, there is a definite appearance of rhythmic feature. For beach with seawall, the rate of changes along individual profiles are very irregular. However, if a line is drawn across the region to represent the averaged rate, one clearly sees trend of increasing erosion forward the downdrift side. And, the slope of the line also appears to increase with increasing wave angle, which means the difference of the averaged rate of erosion between the updrift and downdrift sides becomes larger as the incident wave angle becomes larger.

In the next case, the cumulative volumetric change with reference to a fixed down-wave boundary is given in Fig.4.4. For the case of normal incident waves, the slopes of the cumulative curves are almost uniform, an additional indication of uniform erosional rate. For cases with oblique waves angles on natural beaches, the cumulative curves reveal an undulation superimposed upon uniform erosion. If mean straight lines are fitted on the curves, the effects on wave angle in rate of

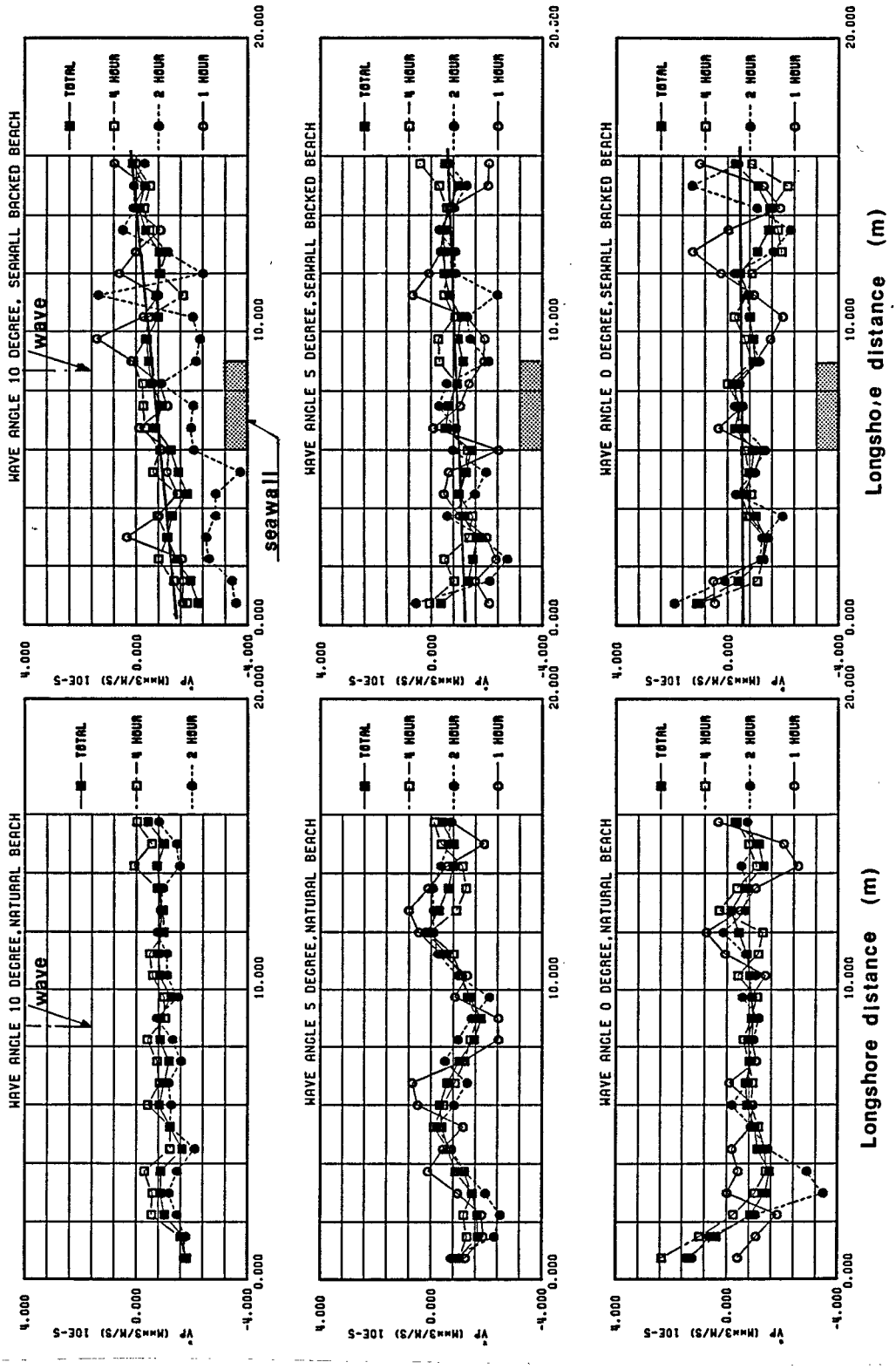

Figure 4.3: Rate of Volumetric Change along a Profile, $\dot{v}_p$

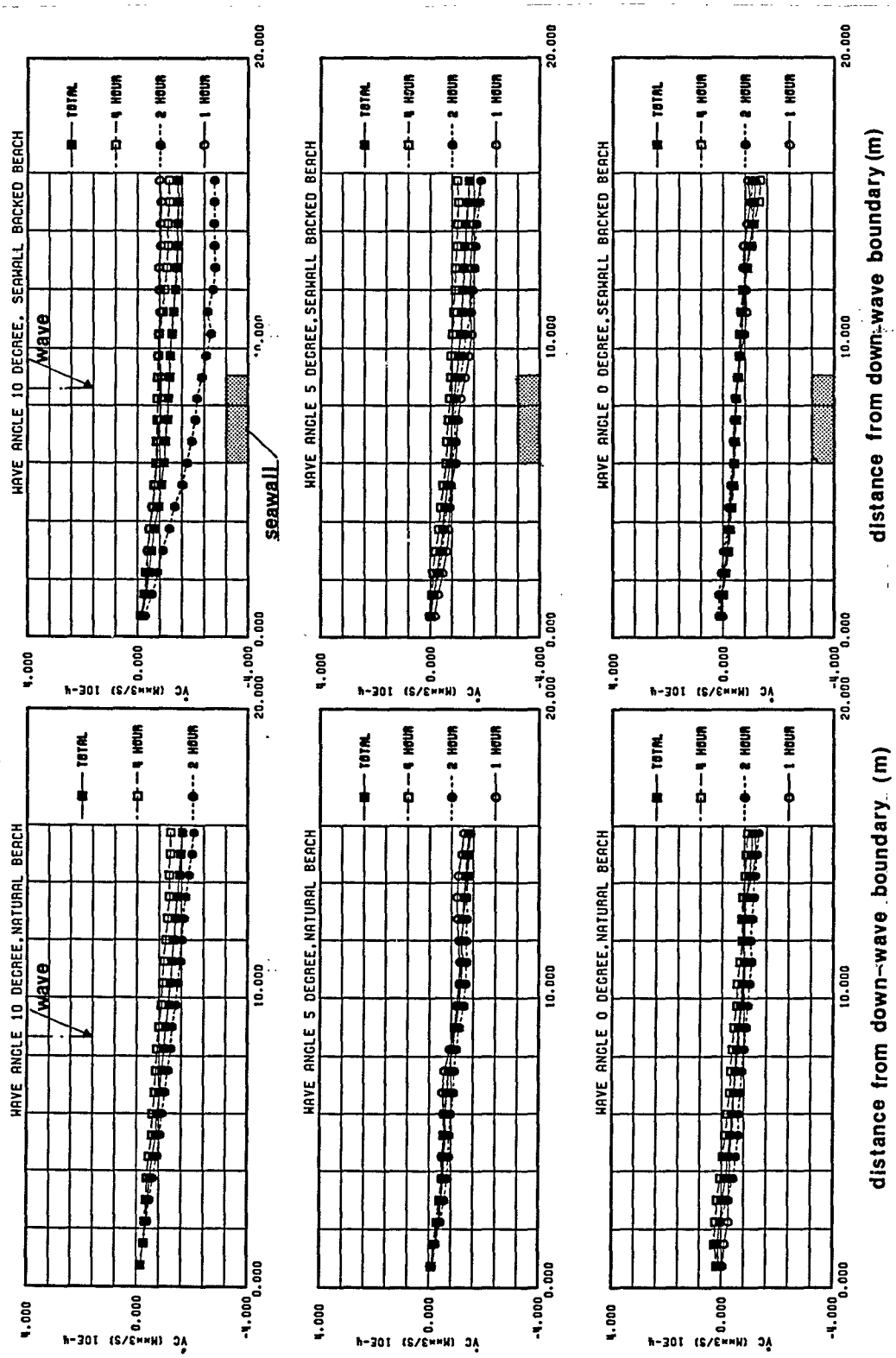

Figure 4.4: Cumulative Rate of Volumetric Change Referenced to Down-wave Boundary, $\dot{v}_c$

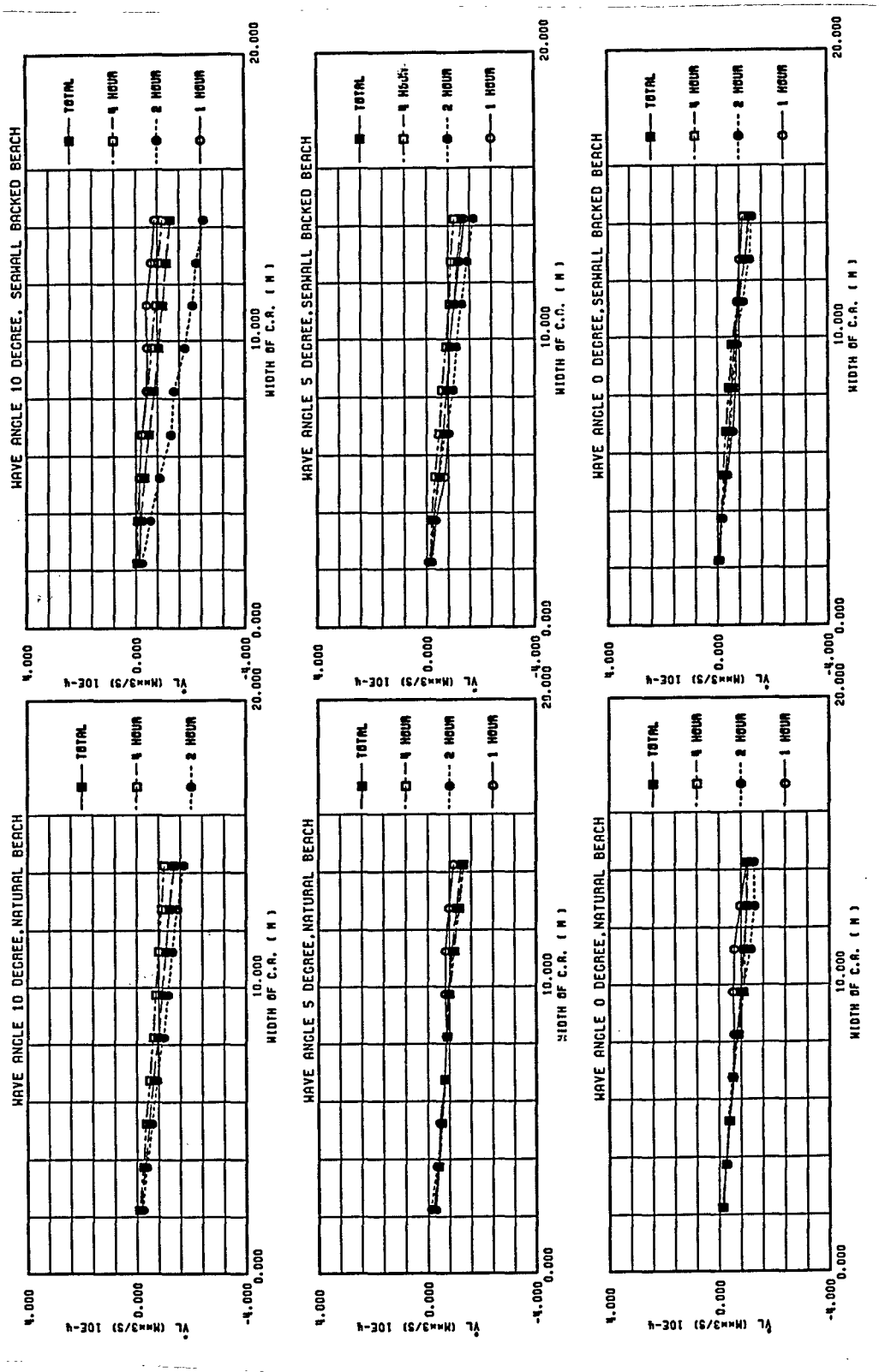

Figure 4.5: Rate of Volumetric Change in a Local Control Area, $\dot{v}_l$

Table 4.1: On/Offshore and Longshore Transport Rate for Natural Beach

wave angle (deg.)	on/offshore transport rate	gradient of longshore transport rate
	$m^3/m/s \times 10^{-6}$	
0	8.18	0.
5	8.18	0.54
10	8.18	1.68

Table 4.2: On/Offshore and Longshore Transport Rate for Seawall Backed Beach

wave angle (deg.)	on/offshore transport rate		gradient of longshore transport rate	
	$m^3/m/s \times 10^{-6}$			
	updrift	downdrift	updrift	downdrift
0	9.75	9.58	0.0	0.0
5	9.75	9.58	-3.31	3.55
10	9.75	9.58	-4.49	5.1

erosion is clearly revealed. If we further assume that under normal wave incident wave angle, the spatially averaged transport is in the on/offshore direction only, the longshore and on/offshore component of transport rate can be separated by the following equation

$$\dot{v}_T(\alpha) = \dot{v}_o + \dot{v}_l(\alpha) \tag{4.9}$$

where $\dot{v}_T(\alpha)$ is rate of the gradient of the transport; $\dot{v}_o$ is the on/offshore component assumed here to be independent of wave angle, α, and $\dot{v}_l(\alpha)$ is the longshore component. Based upon this equation, the longshore and on/offshore component for the three cases of the natural beach are given in Table 4.1. Now, for the cases with seawall, the slope on the down drift and on the updrift are different. Comparing with the case of 0^o, the slope are steeper in the downdrift side but milder in the updrift side. By using Eq. (4.9), the on/offshore component and the longshore component are established separately for the downdrift and the updrift sections. These results are also given in Table 4.2. The negative longshore components in the updrift side are the consequence of groin effects.

We now turn the attention to examine the extent of seawall on the rate of volumetric change within a control region centered around the seawall. The results are plotted in Fig.4.5 with various width of the control region. Using the same data set, the ratio of volumetric change, with($\dot{v}_s$) and without($\dot{v}_n$), is plotted against the non-dimensional control width (W/L_s)(Fig.4.6). If the ratio is larger than 1.0, the rate of erosion is larger with seawall than without seawall and vice versa. From this Figure, a number of observations can be made.

(a) For normal incident waves, the rate of erosion in the vicinity of seawall including the fronting beach is generally smaller for the case of seawall than without. This is particular apparent for beaches fronting the seawall (or when $W/L_s < 1$)
(b) Under oblique wave condition, the rate of erosion is considerably faster for seawalled beach than natural beach in the early stage of wave attack, but this trend is reversed as time progresses. In the final stage of reaching a new equilibrium condition, this ratio is either less than 1 or approach 1 as the control width increases. Thus, the effects of seawall in volumetric erosion appears to be localized.

Considering the final total volume change, the results are given in Fig.4.7. In Fig.4.7a, the ratio of total volume change with(v_s) and without(v_n) seawall is plotted for the updrift and downdrift region separately. In the updrift region, v_s/v_n is always less than 1 irrespective the width of the control region and the wave angles. Thus, in the case of normal incident wave, this value less than one because more sand is retained by the seawall in the backshore than the additional material being eroded in front of the seawall, when compared with the natural beach case. For cases with oblique waves, on the other hand, sand is retained in the updrift due to groin effect; they also makes this ratio less than unity. On the downdrift side, the situation is different. As expected, under normal incident waves,v_s/v_n is less than onemuch the same as the updrift side. Under oblique waves, v_s/v_n is less than 1 when $W/L_s = 0.5$,

or when the control region coincides with the seawall length. Apparently, even under oblique wave, the material retained from the scouring trough in front of the seawall. However, when W/L_s becomes larger than 0.5, v_s/v_n also becomes larger than 1. The presence of seawall now interrupt the normal longshore transport and causes downdrift erosion to be greater than the natural beach condition. Finally, in Fig.4.7b, the ratio of total volumetric changes including both updrift and downdrift region are given. It can be seen that when $W/L_s < 1.25$, $v_s/v_n < 1.25$. When $W/L_s > 1$, the ratio of v_s/v_n quickly becomes constant and approaches 1 as it should when W/L_s becomes large. Therefore, the effects of seawall appears to be quite localized, certainly within 3 to 4 seawall length for the cases tested.

To examine the volume change in more detail, we divide the region surrounding the seawall into 12 sections as shown in Fig.4.8. The seawall is located at the center section C1; Sections L1, C1 and R1 are on the beach and the rest sections are in offshore. The total volume changes after four hours duration within each sections are then computed and the results expressed in percentages of change are presented in Fig.4.9. From this Figure, it can be seen that for the case of zero incident wave angle, flanking effects and toe scouring are evident. Material lost from flanking and toe scouring are deposited offshore to form offshore bars. Since the material saved on backshore is more than offset the increased material loss to the offshore owing to the presence of the seawall the total volume loss in the control area is generally less for the case with seawall than without seawall. However, as the control area becomes large, this difference of losses becomes small. For the case of oblique waves, the scouring hole in front of the seawall remains prominent. The decrease in updrift erosion and increase in downdrift erosion, mainly in the beach sections (L1,R1) are also evident.

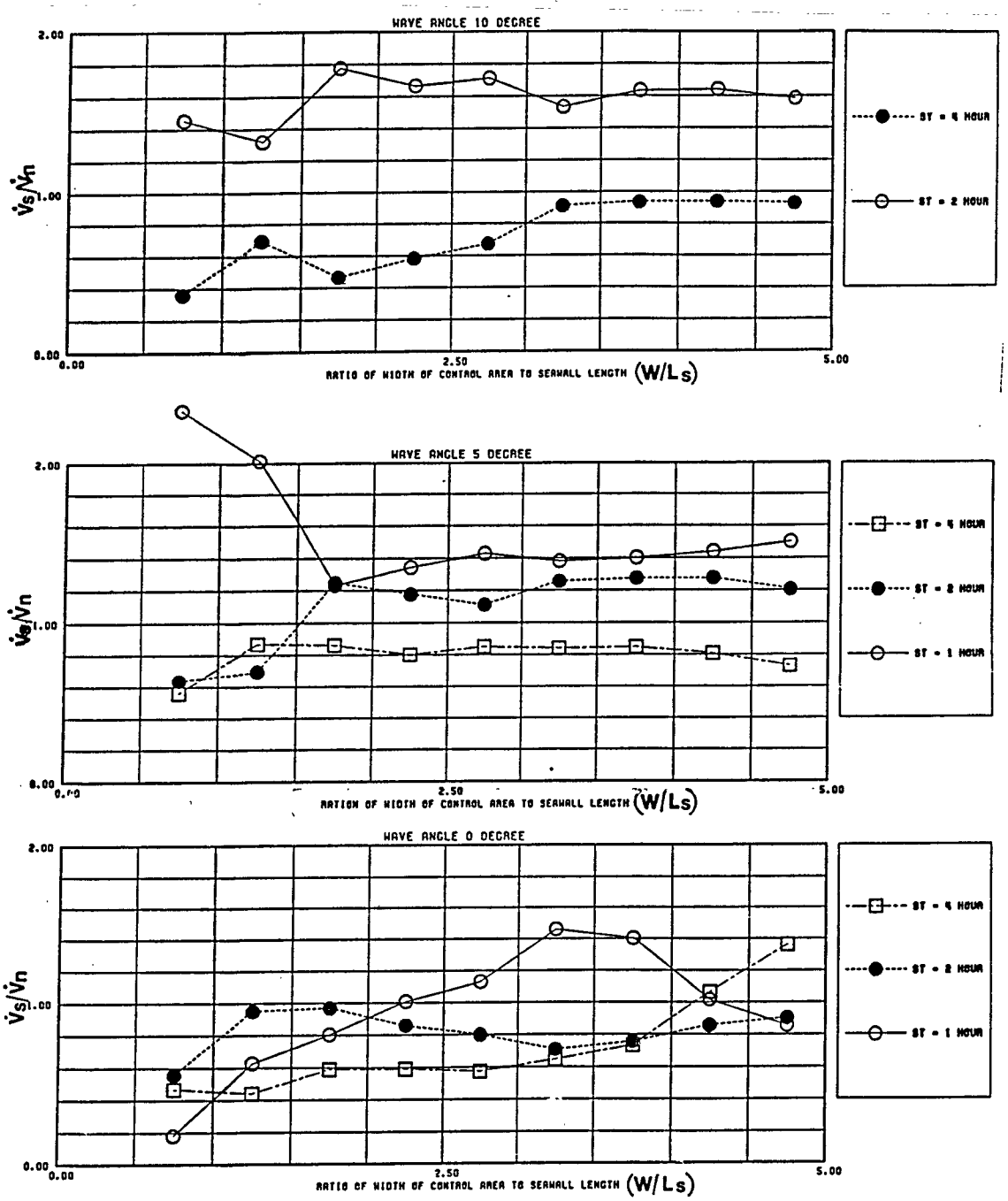

Figure 4.6: Ratio of the Rate of Volumetric Changes with and without Seawall

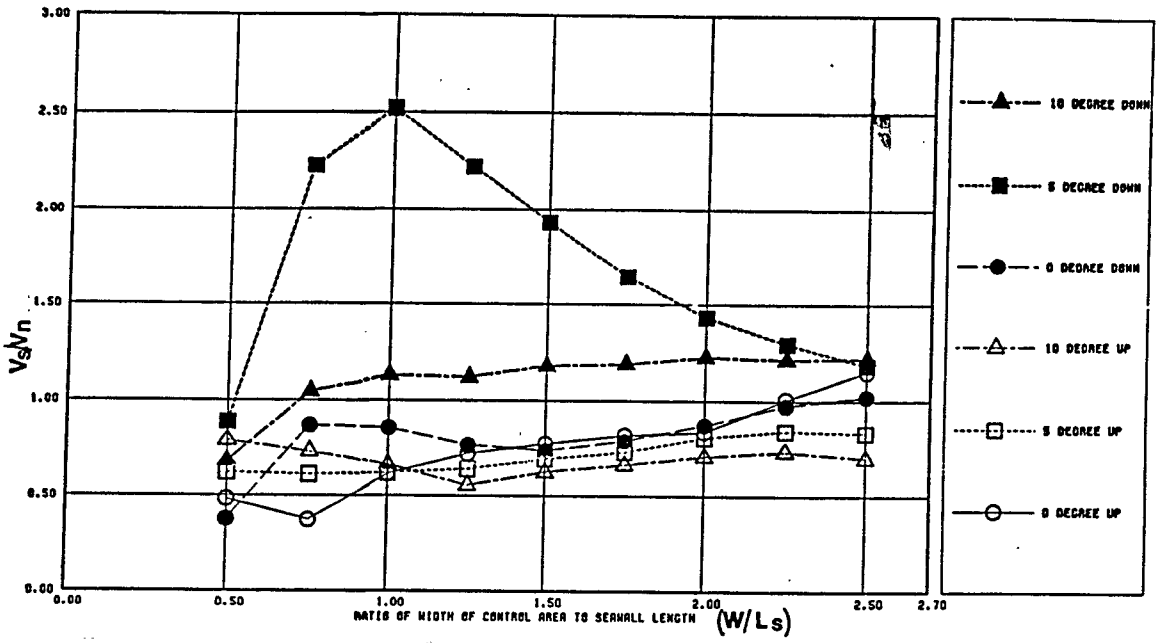

(a) Up-Drift and Down-Drift Separately

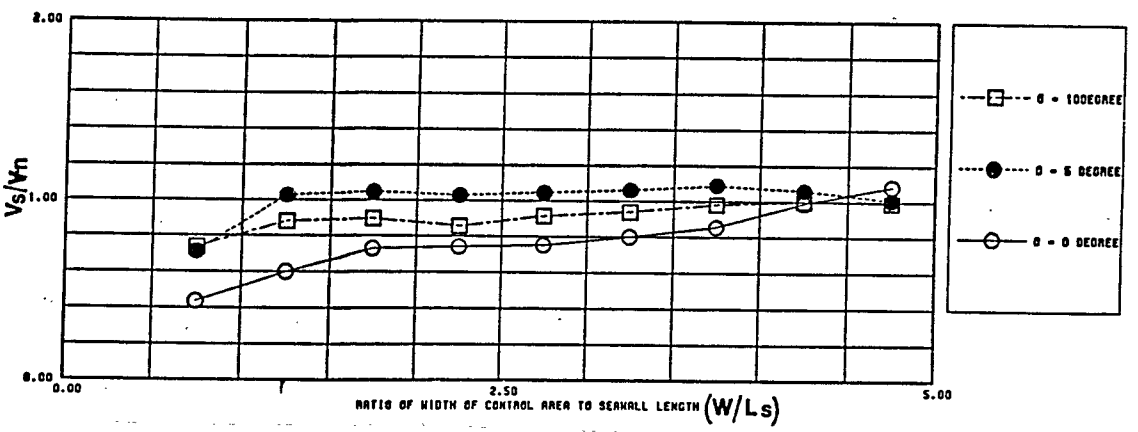

(b) Total Region

Figure 4.7: Ratio of Volumetric Changes with and without Seawall for 4 Hours Duration

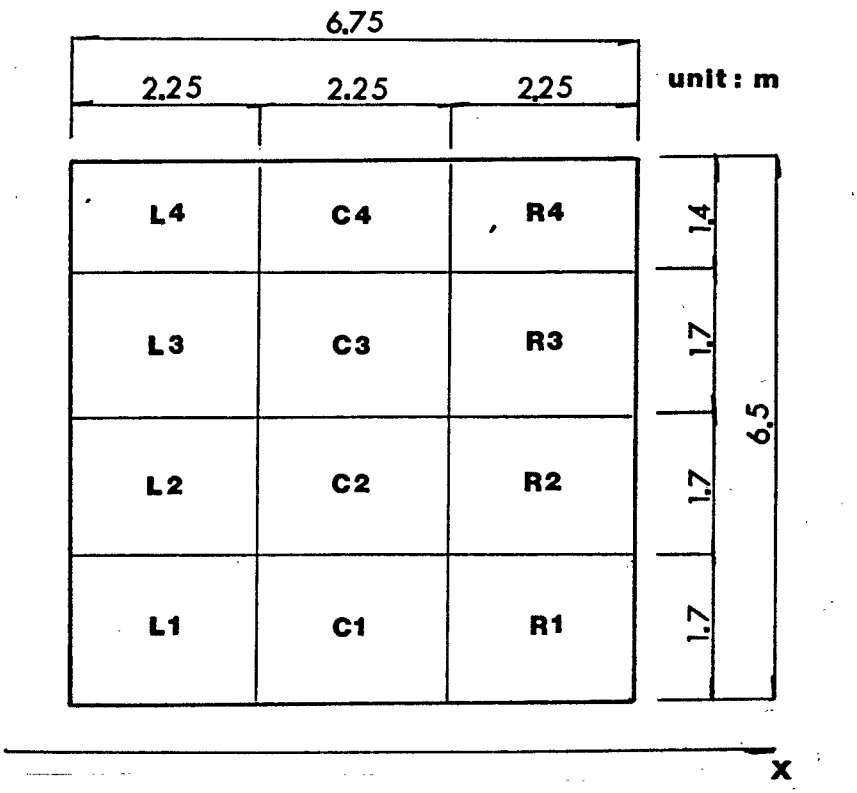

Figure 4.8: Sketch of 12 Sections Surrounding Seawall

NATURAL BEACH

	L	C	R
4	- 2.0	+ 0.2	- 1.4
3	-12.4	- 8.9	- 0.9
2	-11.0	- 6.0	-14.5
1	-13.1	-13.2	-16 6

(A) CASE 1 0°

SEAWALL BACKED BEACH

	L	C	R
4	+ 6.5	+ 7.1	- 1.1
3	-13.9	- 4.7	+ 8.5
2	-10.8	-19.0	-27.2
1	-18.2	SEAWALL	-27.1

(B) CASE 2 0°

4	+ 1.5	- 1.2	- 5.3
3	- 4.9	+ 1.3	- 2.9
2	- 8.2	- 8.7	-18.0
1	- 6.1	-18.8	-28.7

(C) CASE 3 5°

4	+ 0.5	+ 0.6	+ 3.8
3	- 5.3	- 0.5	- 5.9
2	-15.8	-20.5	-27.8
1	-20.4	SEAWALL	-20.4

(D) CASE 4 5°

4	- 2.4	+ 2.0	- 2.0
3	-11.3	- 9.5	- 8.1
2	-15.3	-11.9	- 6.4
1	-11.0	-10.8	-13.0

(E) CASE 5 10°

4	- 0.5	+ 4.3	+ 1.8
3	- 4.9	- 7.8	+ 2.5
2	-24.1	-24.2	-10.5
1	-28.1	SEAWALL	- 8.5

(F) CASE 6 10°

Figure 4.9: Volumetric Changes in Sections for 4 hours Duration

CHAPTER 5
SHORELINE AND HYDROGRAPHIC CHANGES

As stated in Chapter 2, hydrographic surveys were carried out at regular time intervals. In the erosional phase, surveys were conducted at 0, 1, 2, and 4 hours whereas in the recovery phase, the intervals were 1, 2, 3, 8 and 12 hours. The time-elapsed contour plots are illustrated in Fig. 5.1. The complete data sets are presented in Appendix A. In this Chapter, the three dimensional shoreline and hydrographic changes are examined by means of Empirical Eigenfunction (EEF) analysis and One-Line Model (OLM) analysis.

5.1 Empirical Eigenfunction (EEF) Analysis

5.1.1 Literature Review

Since Winant et al. (1975) showed the usefulness of empirical eigenfunction (EEF) analysis or empirical orthogonal function (EOF) analysis, many investigators have utilized EEF to examine beach profile changes. In applying EEF to the bathymetric data, the solution is usually not unique, thus several EEFs for the bathymetric changes can be defined and examined their physical meanings.

Winant et al. (1975) applied EEF to data set obtained from two years monthly surveys at Torrey Pine Beach, California. The analysis separates the temporal and spatial dependance of data, i.e.

$$h(x,t) = \sum_{m} e_m(x) c_m(t) \tag{5.1}$$

where

$e_m(x)$ is the spatial eigenfunction and $c_m(t)$ is the temporal eigenfunction.

They found that only first three eigen vectors explain the original data well. They

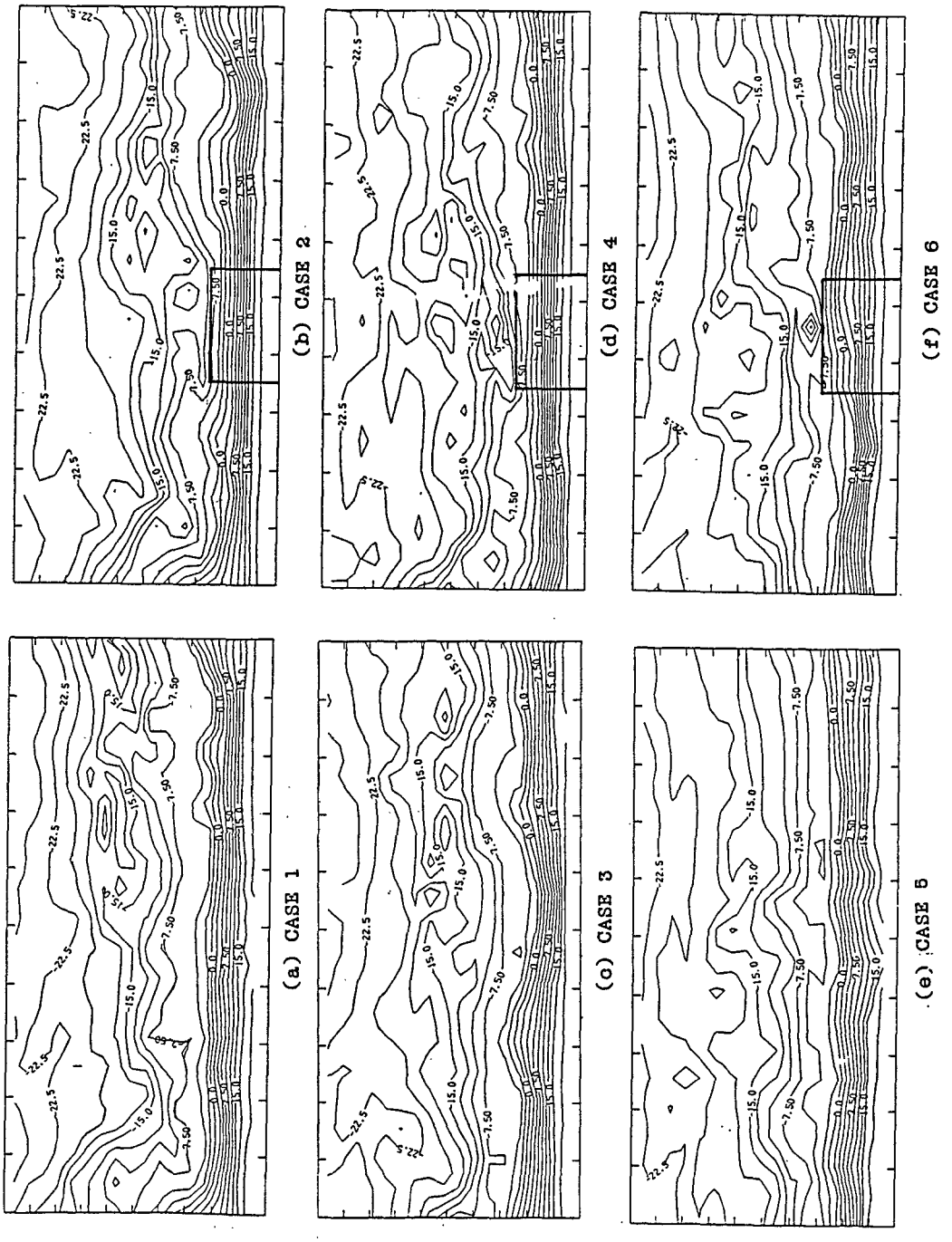

Figure 5.1: Contour Maps for Four Hours Elapsed Time

named the first, second and third spatial EEF as mean function, bar-berm function and terrace function respectively. The physical meanings of these three function are described below:

(1) mean function. Mean beach function is the arithmetic mean profile of the data. If the beach is stable, it has a constant time dependance.

(2) bar-berm function. This is the seasonal eigenfunction, characterized by a strong seasonal temporal dependance.

(3) terrace function. This function has a broad maximum near the position of the low-tide terrace with complicated time dependance.

Aubrey (1979) applied EEF to beach profile changes. He found two pivotal points where beach profile does not change seasonally. The pivotal points are defined as the zero crossing points of the second spatial eigenfunction. Based on a dual pivotal points, he calculated seasonal volume change or sediment movement at Torry Pine Beach California as shown in Fig. 5.2

Hashimoto and Uda (1982) investigated the response of beach profiles to incident waves at Ajigaura beach, Japan. Defining the original data set as the difference from the mean value, they examined the relation between the eigenfunction and wave characteristics. They found that the time derivatives of the first temporal eigenfunction has clear relation to the wave angle given by

$$\frac{d\bar{C}_1}{dt} = -0.42 + 0.067\bar{\theta}(t - 12) \tag{5.2}$$

where θ is the wave angles and $\bar{}$ denotes the average over five weeks. For the second temporal function, they found the following relation to wave characteristics

$$\frac{d\bar{C}_2}{dt} = 1.13 - 0.53H_{mean,max} \tag{5.3}$$

where $H_{mean,max}$ is the weekly mean value of the daily maximum significant wave height.

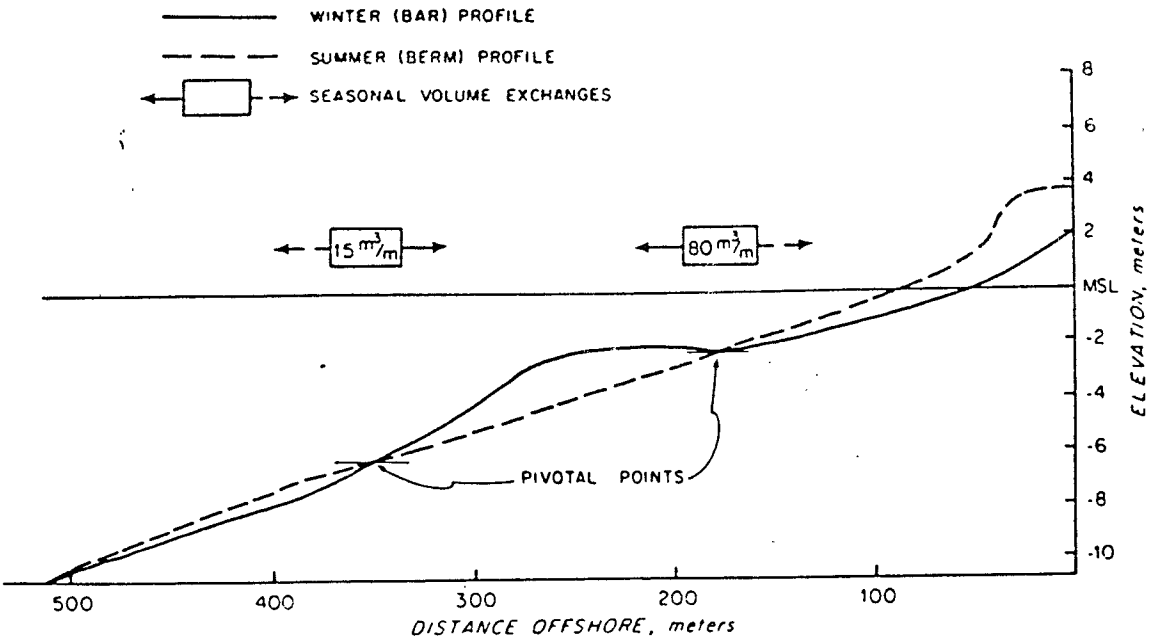

Figure 5.2: Schematic of Seasonal Sand Volume Changes at Torry Pine Beach California, based of a Dual Pivotal Points (after Aubrey 1979)

These two studies showed how to utilize EEF analysis to quantify or predict beach profile changes.

Similar analysis to Winant et al. were carried out also by Birkemeier (1984), Wright et al. (1984) and Kriebel et al. (1986). In Birkemeier's study, the original data set is the same as that of Hashimoto and Uda. From the shape of the first eigen function shown in Fig. 5.3, he concluded that the first eigenfunction describes the changes of the profile from a single bar configuration to a double bar shape, and the first and second eigenfunction appear to result from two unique sequence of storm recovery activities, rather than being controlled seasonally. Moreover, although the third eigenfunction accounted for 1/2 of the variance of the second eigenfunction, its weightings (temporal vectors) have the most well-defined annual cycle.

Wright et al. conducted two types of eigenfunction analysis. The first type used the same method as Winant's, and the second is called "floating datum" analysis. He

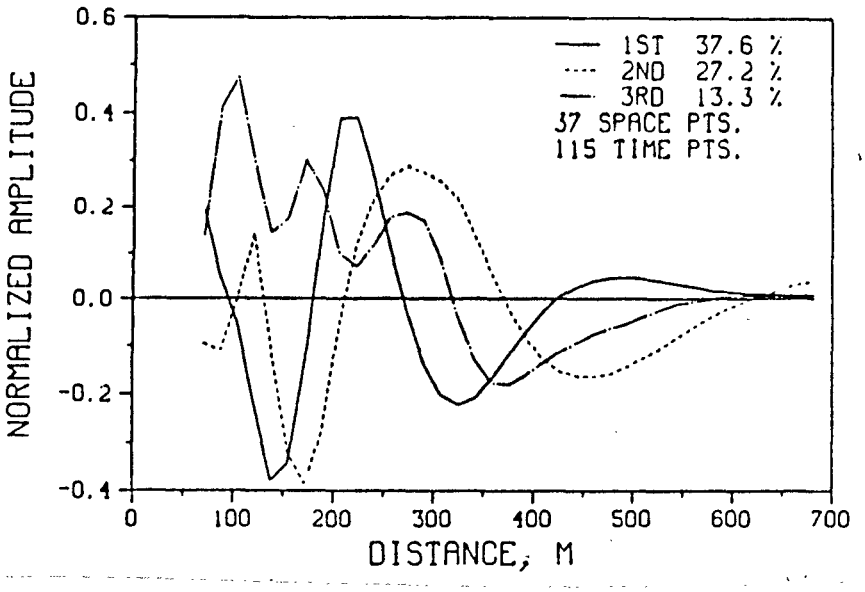

Figure 5.3: Spatial Eigenfunction in Birkemeier's Study

mentioned "floating datum" analysis best express profile changes and can be related to beach profile. In the "floating datum" analysis, the variability is referenced to the instantaneous positions of the shoreline and is independent of absolute degree of accretion or erosion.

Kriebel et al used EEF to examine the beach recovery process at Clearwater, Florida. They compared eigenfunctions of seawall-backed beach and natural beach, and found the eigenfunction has no significant difference between them except in the vicinity of seawall.

Barnett (1987) used EEF in his two dimensional laboratory experiment, and examined EEF characteristics for the seawall-backed beach. The original data set is defined as the difference from the initial beach profile. He found the first eigenfunction describes the bar trough features and the second describes the reflection bars.

The method mentioned above is basically based on the same idea as Winant et al. As the usefulness or powerfulness of EEF analysis to beach profile changes has been demonstrated, different versions were developed.

Uda and Hashimoto (1982) and Dick and Dalrymple (1984) calculated the two spatial eigenfunction in the direction of cross-shore and long-shore at a certain time. Uda and Hashimoto examined the beach profile changes at Misawa fishery port where 180 m long break water is constructed. They assumed the beach profile data is represented by

$$h(x,y,t_o) = \sum_k e_k(y,t_o)c_k(x,t_o) \tag{5.4}$$

where

$e_k(y,t_o)$ is the spatial eigenfunction in the direction of cross-shore.

$c_k(x,t_o)$ is the spatial eigenfunction in the direction of long-shore.

They found all e_k and c_1 are independent of time, and c_2 and c_3 are time dependant, and have clear correlation to the shoreline changes. They described the characteristics of the eigenfunction, as follows:

> The first eigenfunction e_1 corresponded to a mean profile. The second eigenfunction e_2 turned out to correspond to profile changes due to longshore sand transport, because its value was positive over a broad region of the shore, and the second time function c_2 corresponding to it, which gave longshore change of the beach profile, was correlated with shoreline position, y_s. The third eigenfunction e_3 corresponded to profile changes due to the influence of the breakwater, because e_3 took positive values near the shoreline and negative value in the offshore zone, and function c_3 was correlated with the offshore distance y'' of the four meter depth line from the shore. (Uda and Hashimoto, 1982, p. 1414).

Then, combining one line theory, they developed the prediction model of beach profile changes. The results obtained from their model explained the field data well.

Dick and Dalrymple calculated three types of EEF to examine the beach profile changes at Berthany Beach, Delaware. The first type is the same as the Winant et

al. and called the "temporal analysis"; the second is the same as the Uda et al. and named the "spatial analysis," and the third is very similar to the second, but the original data sets are defined as the difference between two surveys, called "difference spatial analysis." In their spatial analysis, the second spatial eigenfunction in the direction of longshore was named the "rotation function" which explain the beach rotation. They also examined the sensitivity of EEF. The seasonal movement of beach can be determined by the "spatial analysis" from two surveys, one taken from the summer profile and other from the winter, instead of using repeated surveys that are necessary for the "temporal analysis."

Garrow (1984) applied EEF to examine the rhythmic feature of shore line and contour lines in the field. First he examined the EEF calculated based on the hypothetical data matrices representative of ideal beach topography. He found that if the sinusoidal pattern remained stable but varied in amplitudes, the analysis produces a sinusoidal mean and a single sinusoidal eigen vectors 180 degree out of phase with the mean. From the analysis of the field data, three important morphologic components are found, those are, overall accretion/erosion of the shoreline, configuration of 800-850m wavelength beach rhythmic topography, and longshore profile or phase of rhythmic features. But they could not be easily separated.

The same type of EEF analysis sometimes produced different results. For example, the second eigenfunction obtained by Birkemeier explained the movement of the single bar to the double bars or vise versa, while the function from Winant et al. or Aubrey is defined as the bar-berm function. The spatial eigenfunction in the direction of cross– shore calculated by Uda and Hashimoto is independent to time, while the function calculated by Dick and Dalrymple is time dependant. The main cause of these difference might be the differences of time scale, survey intervals (sampling time) and local geographic characteristics.

Some comments on EEF by several examiner are summarized here.

Birkemeier: EEF has a number of significant limitations. First, the eigen vectors do not necessarily have any physical significance. Secondly, the analysis assumes that every survey is equally spaced in time and that all cases are equally weighted, an assumption that is not usually the case with field data. Finally, when analyzing data from a single profile line, the EEF analysis does not separate cross-shore effects from long- shore effects

Dick and Dalrymple: The EEF method is an efficient way to describe beach profile changes, however, it should be emphasized that it is a descriptive process and therefore does not reveal any information regarding the governing process.

Garrow: This mathematical technique has two main goals. One goal is to determine a new set of variables which are independent each others. The second goal is to define the fewest new variables possible that can completely describe the original data.

EEF analysis, of course, is not used only in beach profile but other natural phenomena such as wave spectrum parametric study (Vincent and Resio, 1977) edge wave analysis (Kato 1984). In meteorology and geology, EEF analysis has often been conducted to quantify stochastic data (Kutzbach 1967).

5.1.2 Basic Concept on Empirical Eigenfunction Analysis

The usefulness of EEF analysis is to reduce the number of data from original data sets. In the present study, the data are the hydrographic survey, and since the measurement is carried out four times at 21×140 points, the number of variables would exceed $4 \times 21 \times 140 = 11760$. If Uda and Hashimoto's representation (Eq. 5.4) is possible and the first three EEF can represent most of the original data, the number of data needed would reduce to $4 \times (3 \times (21 + 140)) = 1932$. The EEF that will be presented here, reduces the number of necessary data to 384. Furthermore, In EEF analysis, since the two eigenfunction is assumed to be independent to each

other, the new set of variables can be examined independently. Hereinafter, the basic concepts of EEF is described.

Suppose, for example, we have some survey data at M points, and N times surveys are carried out. Thus, the number of data is M×N, this would compose M by N matrix, say, **F**. **F** can be represented as

$$\mathbf{F} = \begin{pmatrix} f_{11} & f_{12} & \cdot & f_{1N} \\ f_{21} & \cdot & \cdot & f_{2N} \\ \cdot & \cdot & \cdot & \cdot \\ \cdot & \cdot & \cdot & \cdot \\ f_{M1} & f_{M2} & \cdot & f_{MN} \end{pmatrix} \tag{5.5}$$

In the analysis of bathymetric changes, the variables f_{nm} would be the water depth at a point of space and time. Defining a vector $\mathbf{f}_i$ as

$$\mathbf{f_i} = \begin{bmatrix} f_{1i} \\ f_{2i} \\ \vdots \\ \vdots \\ f_{Mi} \end{bmatrix}, \tag{5.6}$$

then we have

$$\mathbf{F} = [\mathbf{f}_1 \mathbf{f}_2 \cdots \mathbf{f}_N] \tag{5.7}$$

One wants to determine which vector **e** has the highest resemblance to all the observation vectors **f**, simultaneously, where resemblance is measured with the squared and normalized inner product between a vector **f** and **e**. This is the equivalent to maximizing

$$\mathbf{e}^t \mathbf{R} \mathbf{e} \tag{5.8}$$

subject to the condition

$$\mathbf{e}^t \mathbf{e} = 1 \tag{5.9}$$

where **R** is an M × M symmetric matrix whose element, r_{ij} is given by

$$r_{ij} = N^{-1} \sum_{n=1}^{N} f_{in} f_{jn} \tag{5.10}$$

or

$$\mathbf{R} = N^{-1}(\mathbf{F}\mathbf{F}^t) \tag{5.11}$$

This problem yields to eigen value problem, i. e.

$$\mathbf{R}\mathbf{e} = \mathbf{e}\lambda \tag{5.12}$$

In fact, one obtains not just one eigenvector, but series $\mathbf{e}_i$, $i = 1, 2....M$ associated with M eigen values of $\mathbf{R}$. It can be shown that $\mathbf{e}_i$ are orthogonal and that λ_i are real and positive. Thus, writing eq. (5.12) for all eigen vectors

$$\mathbf{R}\mathbf{E} = \mathbf{E}\mathbf{L} \tag{5.13}$$

where $\mathbf{E}$ is an M by M orthogonal matrix whose column are eigen vectors, $e_{i1}....e_{iM}$. Note that

$$\mathbf{E}^t\mathbf{E} = \mathbf{I} \tag{5.14}$$

and $\mathbf{L}$ is an M by M diagonal matrix whose ith diagonal element λ_i is the eigenvalue associated with $\mathbf{e}_i$. Combining eqs. (5.11) and (5.12)

$$\begin{aligned} N^{-1}\mathbf{F}\mathbf{F}^t\mathbf{E} &= \mathbf{E}\mathbf{L} \\ \mathbf{F}\mathbf{F}^t\mathbf{E} &= \mathbf{E}\mathbf{L}N \\ \mathbf{E}^t\mathbf{F}\mathbf{F}^t\mathbf{E} &= \mathbf{E}^t\mathbf{E}\mathbf{L}N \\ &= \mathbf{L}N \end{aligned} \tag{5.15}$$

Defining

$$\mathbf{C} = \mathbf{E}^t\mathbf{F} \tag{5.16}$$

where $\mathbf{C}$ is M by N matrix

it follows that

$$\mathbf{F} = \mathbf{E}\mathbf{C} \tag{5.17}$$

From eq. (5.17), it is clear that the observation vector $\mathbf{f}_n$, representing the nth observation of the M variables, can be expressed as a linear combination of the M

eigenvectors. The c_{in}th element of C will be referred to as the coefficient associated with the ith eigenvector for the nth observation. From Eq. (5.16), it can be shown that c_{in} play the same role in Eq. (5.17) as the coefficients in, for example, a Fourier series representation. The N observations refer to N different time and, therefore, the elements in the ith row of C represent time variations of the coefficient associated with the ith eigenvector. Different representations are possible, the basic concept is the same as presented.

5.1.3 Formulation and Procedure of EEF for Contour Lines

In essence, EEF analysis is similar to harmonic analysis with the exception that the functional form is not determined a priori but is part of the solution. For a multivariate function such as the three dimensional contour line represented by $h(x,y,t)$ there are several possible combinations of eigenfunction representation such as

$$h(x,y,t) = \sum_m w_m c_m(t) e_m(x) f_m(y) \tag{5.18}$$

$$h(x,y,t) = \sum_m w_m c_m(t) e_m(x,y) \tag{5.19}$$

$$h(x,y,t) = \sum_m w_m c_m(x,t_o) e_m(y,t_o) \tag{5.20}$$

These combinations are, however, not independent of each other. The hope is to have the right choice such that most the variance in the data set will be accounted for in fewest terms. Unfortunately, at present, there is no criterion for making such a choice and one has to rely on intuition and trial and error. After a number of preliminary tests, it is decided to use the distance from a baseline to particular contours as the dependent variable. Thus, we assume that this distance can be represented by the linear sum of spatial eigenfunctions, $S_m^n(x)$, and temporal eigenfunctions, $T_m^n(t)$, of the following form

$$d^n(x,t) = \sum_{n=1}^{\infty} \bar{w}_m^n S_m^n(x) T_m^n(t) \tag{5.21}$$

where w_m^n is the weighting function, m is the mode and n denotes nth contour line. But, if we apply EEF analysis based of Eq. (5.21), the influence of the initial profile dominates the other modes. Since in the laboratory the initial profile is the same, it is logical to eliminate this effect in the EEF analysis and to use the following form

$$D^n(x,t) = d^n(x,t) - d_n(x,t_o) \tag{5.22}$$

$$= \sum_{m=1}^{\infty} w_m^n S_m^n(x) T_m^n(t) \tag{5.23}$$

or, in the discrete form neglecting superscripts m for brevity

$$D_{ij} = \sum_{m=1}^{\infty} w_m S_{mi} T_{mi} \tag{5.24}$$

where i and j denote x and t respectively.

In applying the procedure outlined here to the present experiment data set, a number of problems are identified that require special attention:

(1) Owing to the existence of offshore shoals and bars, the $d^m(y,t)$ has, at times, multi-values as illustrated in Fig. 5.4. Care must be exercised to select the depth contour that is physically meaningful. (2) In EEF analysis, the contour lines are assumed to be continuous. But, in the case of seawall, the contour lines near it are clearly not continuous. In such case, the contour lines are divided into segmented continuous lines and EEF analysis is performed to each line individually. (3) In the recovery process, the final profile in the stormy wave condition is taken as the initial profile and is eliminated in the EEF analysis.

5.1.4 Results and Discussion

EEf analysis is performed for eight contour lines for each test case, they are -0.5, 0.0, 5.0, 7.5, 10.0, 12.5, 15.0, and 20.0 cm respectively. They are measured with respect to the still water level in the erosional wave condition. Thus, 0.0 corresponds to shoreline in the erosional cases and 10.0 corresponds to shoreline in the recovery cases. The results are presented in Figs. A.1 to A.9 in the appendix. In these results, with the exception of Case 5, all the case have both erosional and

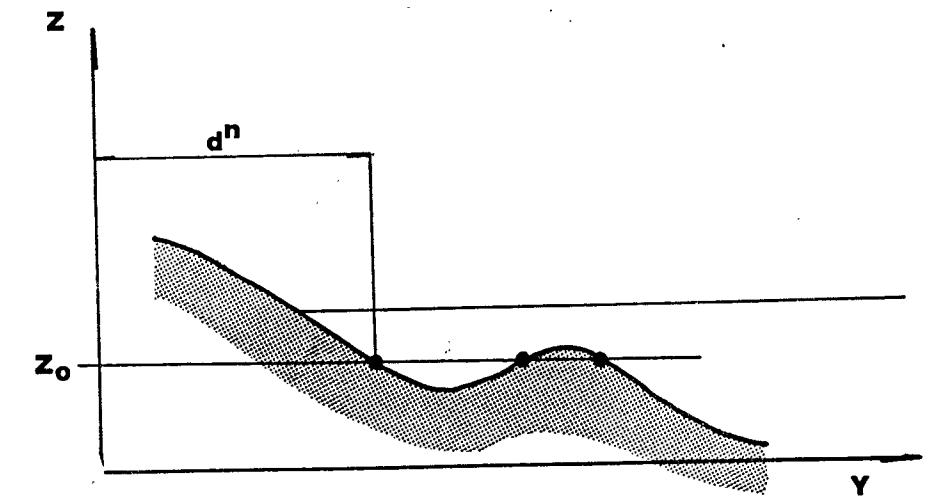

Figure 5.4: Definition of d^n

recovery phases. The recovery processes are identified with a "R" following the caption. Case 5 has erosional phase only. Also, duration of test is 12 hours in Case 5, 5 hours in Case 6 and 4 hours for the rest. In the spatial eigenfunctions, the ordinate represents the eigenvectors multiplied by the associated weighting value. It should be noted here that if the spatial and temporal eigenfunction are of same sign the contour line progresses whereas if they are of opposite sign the contour line regresses.

Figures 5.5 to 5.10 compare the real shoreline changes and shapes of eigenfunctions for each tested. In the figures, the top graph gives the real shoreline changes at different elapsed times as measured, the middle graph provides the net change of measured profile at different time from the initial profile. The bottom graph plots the first two spatial eigenvectors.

Table 5.1 summarized the contribution of each eigenvector (mode) to the total

variance. Based upon these results, a number of qualitative observations are made.

Shoreline Changes

Shoreline change is the primary signature of beach erosion and accretion. For all the cases tested, the first eigenvector appears to account for more than 90% of the variance. Therefore, there is no surprising that the real shoreline change is similar to the first spatial eigenvector. For cases of erosional waves with normal incident angle, ideally the shoreline would recede uniformly as there should be no longshore component of sediment transport. By examining Fig. 5.5 for the case of no seawall, the first spatial eigenvector is almost a parallel line with the exception near the edges where the three dimensional effect comes into play. For the case with seawall (Fig. 5.6), the first spatial eigenvector is also almost a parallel line. The flanking effects, if any, is not visible. The temporal vectors are almost identical for both cases.

Under oblique waves, for the case of no seawall, the first spatial eigenvector exhibits a rhythmic feature in addition to a uniform recession (Fig 5.7). The first temporal vector appears to be similar to the case of normal incident waves. With the presence of seawall, the rhythmic feature on the updrift sides becomes more pronounced. Again, the temporal vectors possess similar characteristics as the previous cases. Now, as the wave angle increases (to 10 degrees), this rhythmic features diminishes in amplitude. The groin effect becomes more evident that results in severe down- drift erosion immediately in the shadow of the seawall.

It is not clear at this moment whether this rhythmic feature is both induced and controlled by the basin characteristics alone or it is induced by the basin characteristics but eventually controlled by the nearshore topography. Since the rhythmic feature is an often observed phenomenon, particularly immediately after storm attack, there is a strong possibility that it is controlled by the nearshore topography.

Table 5.1: Contribution of Each EEF

case	modes	Water depth of Contour Lines(cm)							
		-5	0	5	7.5	10	12.5	15	20
Erosive Condition [D]:downdrift [U]:updrift									
case 1	1 st	92.1	94.5	93.1	79.7	72.7	64.7	80.5	85.4
	2 nd	5.9	4.7	5.6	18.7	18.7	23.2	17.7	10.9
case 2	1 st	95.4	96.3	90.4	89.2	88.2	87.5	83.1	70.9
[D]	2 nd	3.4	3.6	9.4	6.2	8.3	8.0	10.8	18.5
case 2	1 st	94.2	98.0	96.3	**	**	**	**	**
[U]	2 nd	4.3	1.4	2.1	**	**	**	**	**
case 3	1 st	95.8	97.8	95.8	83.7	86.5	85.7	86.3	76.9
	2 nd	3.4	1.7	3.1	13.0	11.2	11.8	8.5	17.6
case 4	1 st	98.3	99.3	95.6	86.7	88.9	88.2	91.2	84.0
[D]	2 nd	1.5	0.5	3.5	10.5	7.1	8.3	5.8	11.8
case 4	1 st	97.3	98.4	96.7	**	**	**	**	**
[U]	2 nd	1.9	1.3	2.7	**	**	**	**	**
case 5	1 st	97.1	98.7	92.8	94.8	95.0	97.3	98.4	92.6
	2 nd	7.0	9.0	7.1	5.2	5.0	2.7	1.6	7.4
case 6	1 st	98.6	99.7	96.3	92.8	92.0	93.7	91.2	92.8
[D]	2 nd	0.9	0.2	3.0	5.1	5.9	3.7	5.6	4.3
case 6	1 st	91.5	97.1	90.3	**	**	**	**	**
[U]	2 nd	3.9	2.3	6.2	**	**	**	**	**
Recovery Condition									
case 1[R]	1 st	**	**	**	85.7	90.3	91.6	85.8	84.9
	2 nd	**	**	**	9.9	7.3	6.2	7.2	9.1
case 2[R]	1 st	**	**	**	83.5	86.1	86.6	90.4	79.7
	2 nd	**	**	**	11.9	10.3	10.5	7.3	9.7
case 3[R]	1 st	**	**	**	92.0	94.5	83.6	84.5	91.4
	2 nd	**	**	**	6.1	4.4	12.8	10.1	5.7
case 4[R]	1 st	**	**	**	92.1	91.7	90.0	84.5	94.5
	2 nd	**	**	**	5.7	6.2	8.4	8.4	4.8
case 6[R]	1 st	**	**	**	82.0	81.3	78.2	85.8	88.0
	2 nd	**	**	**	11.1	12.4	18.3	9.1	7.0

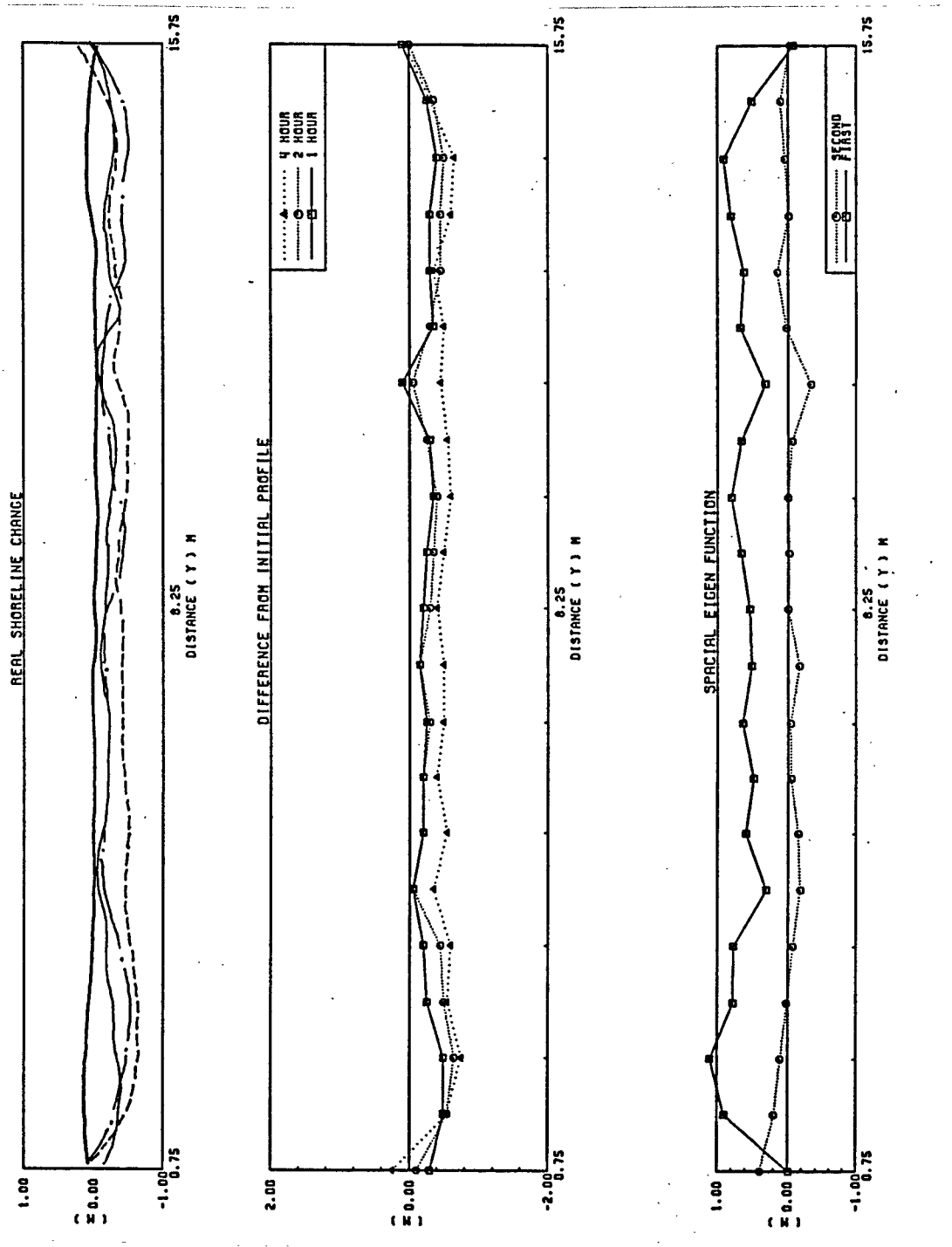

Figure 5.5: Real Shoreline Changes, Net Shoreline Changes and Results of EEF (Case 1)

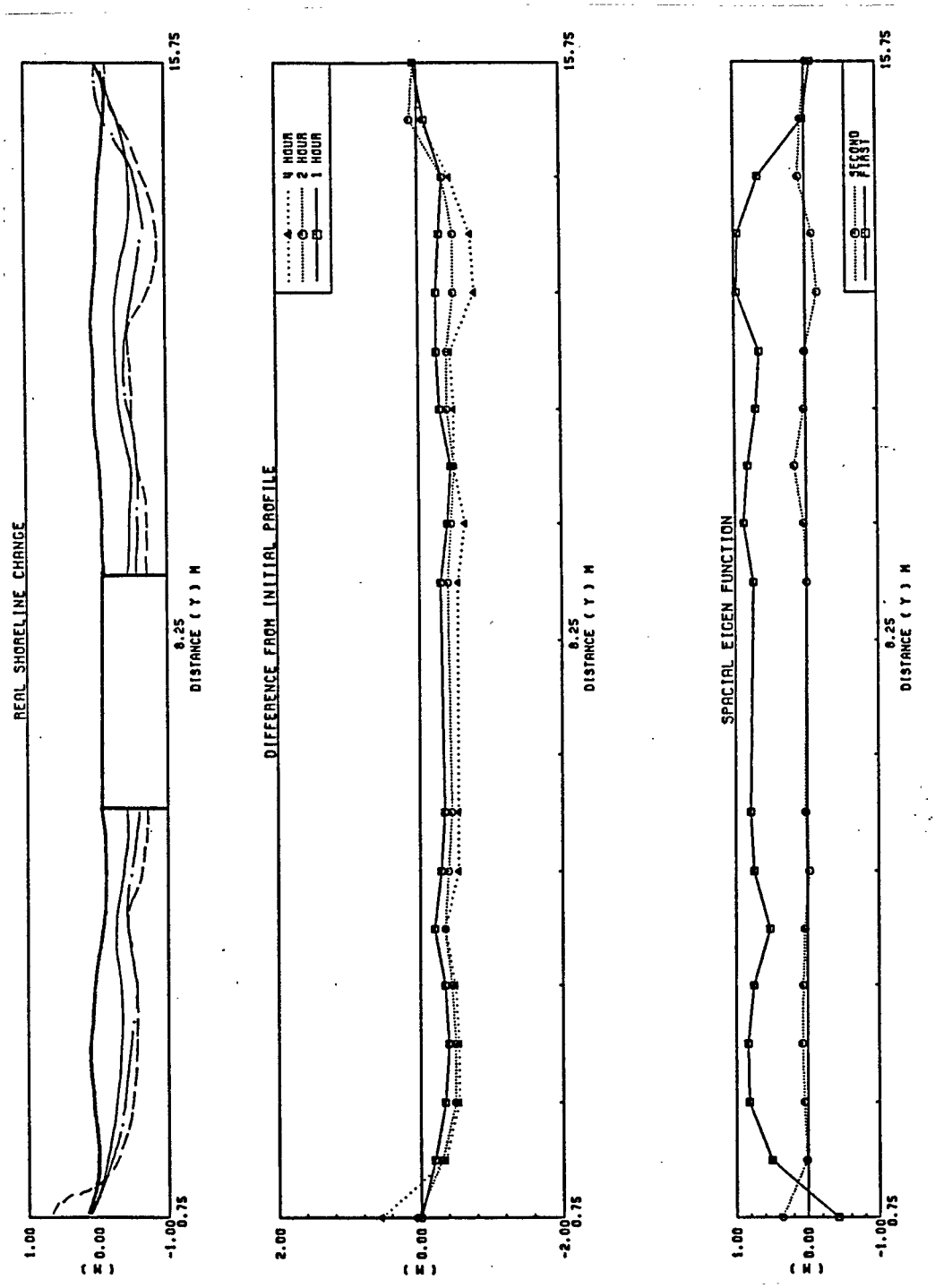

Figure 5.6: Real Shoreline Changes, Net Shoreline Changes and Results of EEF (Case 2)

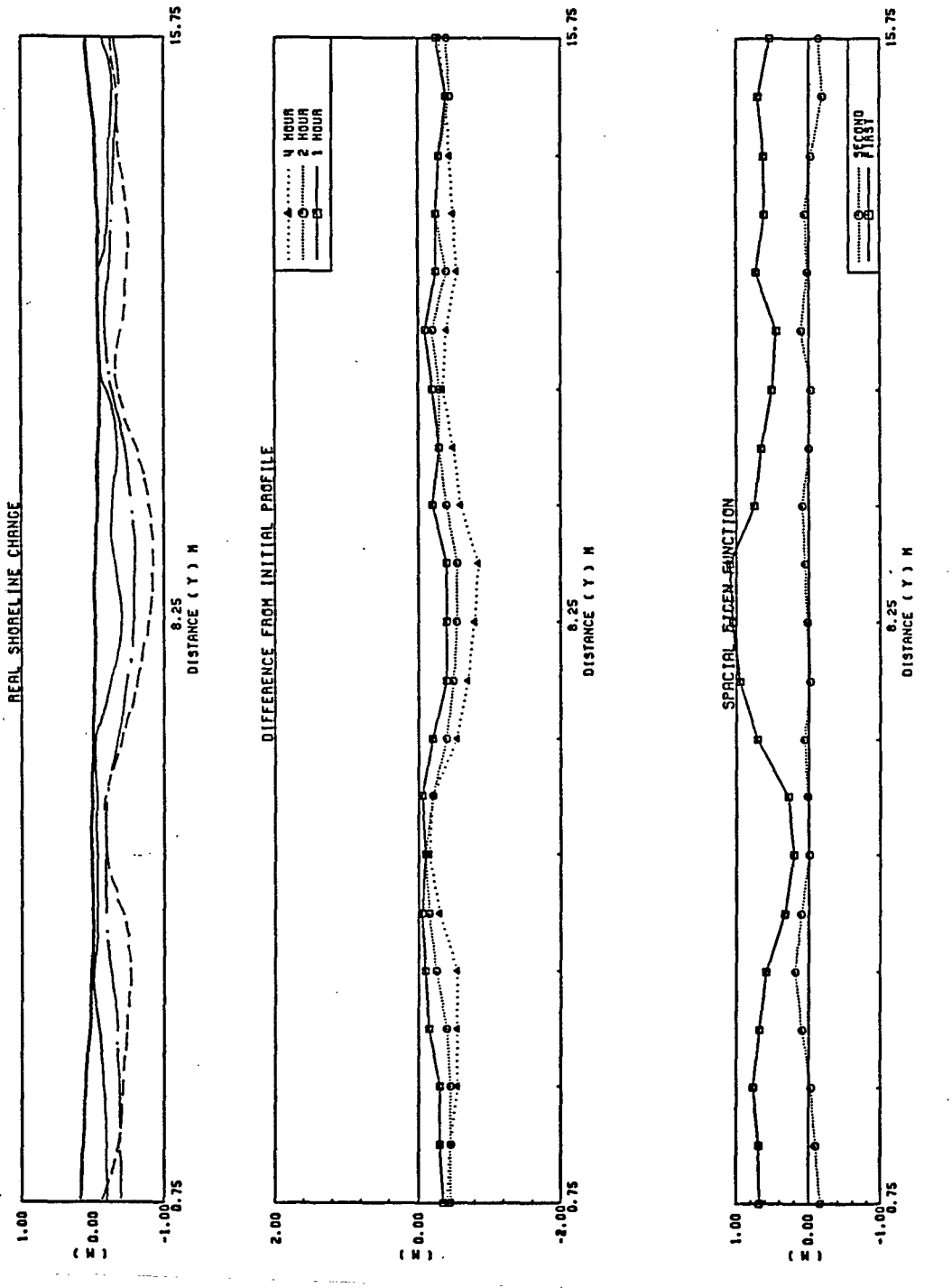

Figure 5.7: Real Shoreline Changes, Net Shoreline Changes and Results of EEF (Case 3)

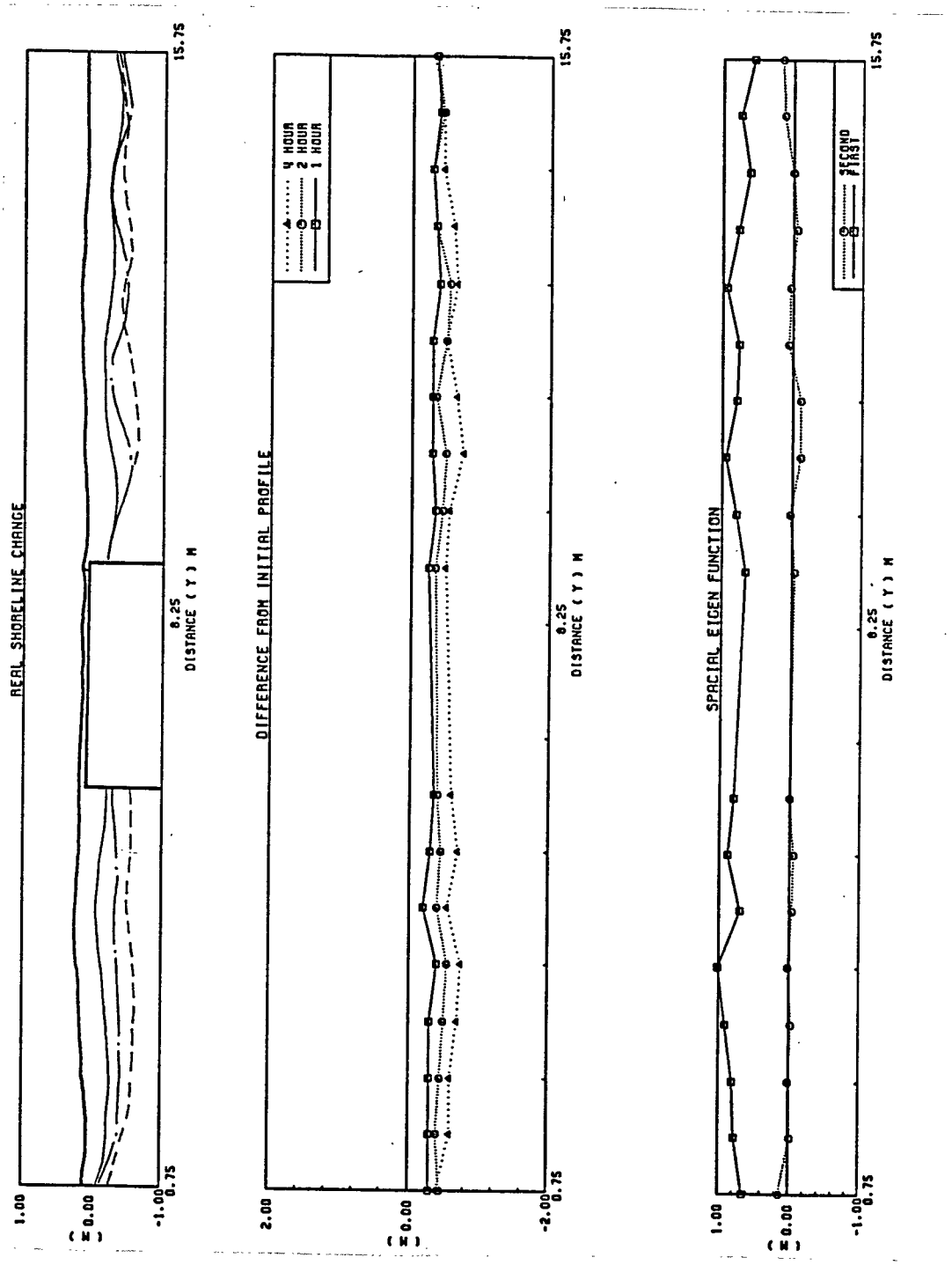

Figure 5.8: Real Shoreline Changes, Net Shoreline Changes and Results of EEF (Case 4)

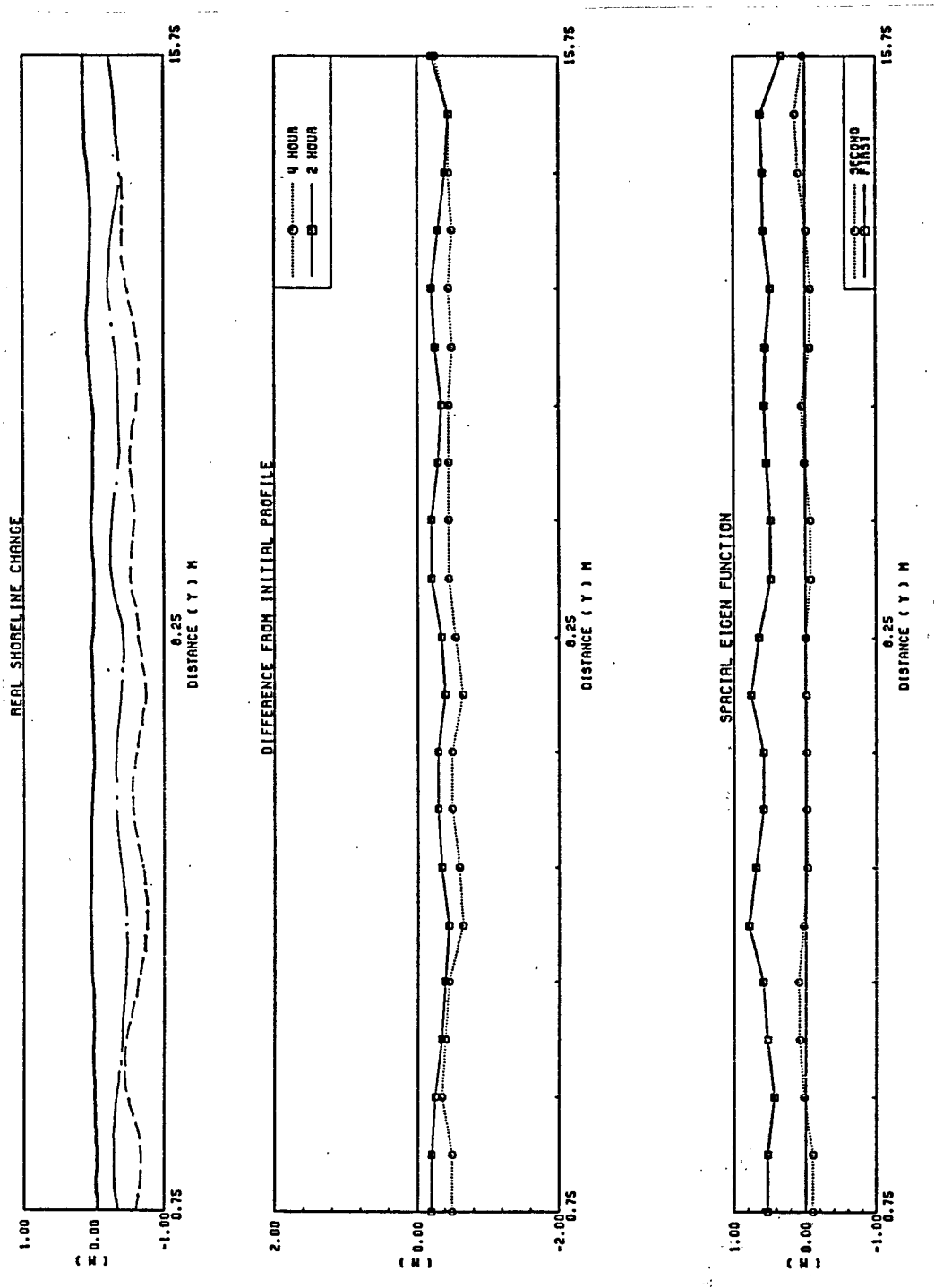

Figure 5.9: Real Shoreline Changes, Net Shoreline Changes and Results of EEF (Case 5)

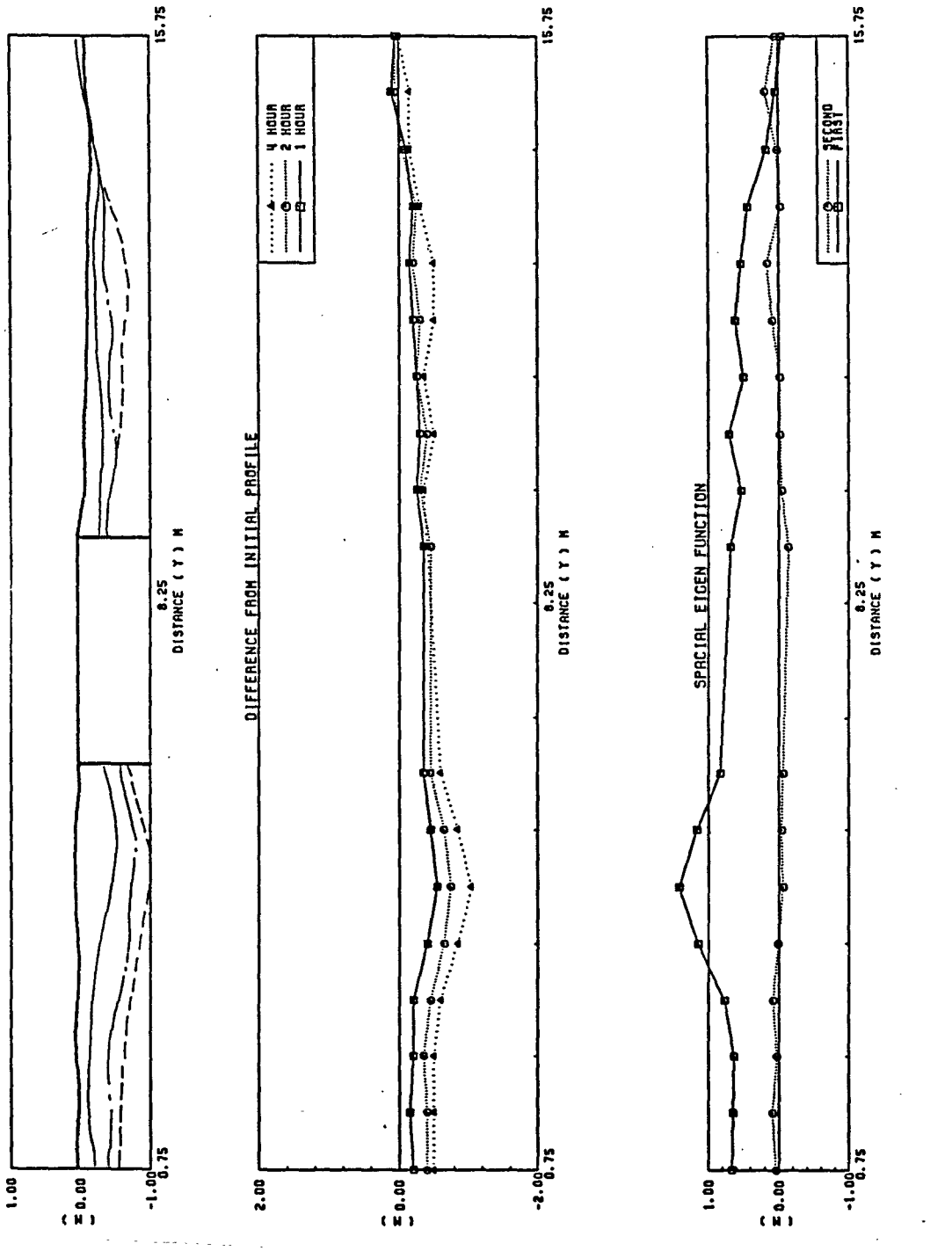

Figure 5.10: Real Shoreline Changes, Net Shoreline Changes and Results of EEF (Case 6)

In the section to follow, a theoretical basis is provided to support this argument.

In the recovery cases, the spatial eigenvectors are much more irregular. One can also easily detect by the shape of the spatial eigenvectors that the recovery in front of seawall is a rapid process.

Hydrographic Changes

In general, hydrographic changes are much more irregular than shoreline changes under both erosional and recovery processes as bars, shoals, troughs, scouring holes, etc. develop, evolve and shift under the influence of the three dimensional flow field. Also, unlike the shoreline changes with their variance largely accounted for by the first eigenvector, the second eigenvector now plays a more important role. And, as the water depth increases, the weight of the second eigenvectors also appears to increase.

In erosional cases, significant scour in front of the seawall is evident as all the spatial eigenvectors up to the 20 cm contour line exhibit a marked bulged shape in the center. However, in the recovery process, one also finds that these scour holes are filling in rapidly.

5.2 Shoreline Changes Based on One-Line Theory

The one-line theory for shoreline change is based of the following continuity equation of sediment flux of a schematic beach profile shown in Fig. 5.11

$$\frac{1}{h}\frac{\partial S}{\partial x} + \frac{\partial d_s}{\partial t} + p' = 0 \tag{5.25}$$

where

d_s denotes shoreline, S is the longshore sediment transport,

h is the water depth of the schematized beach profile,

p is the sink/source of sand,

x is the axis in the direction of longshore and

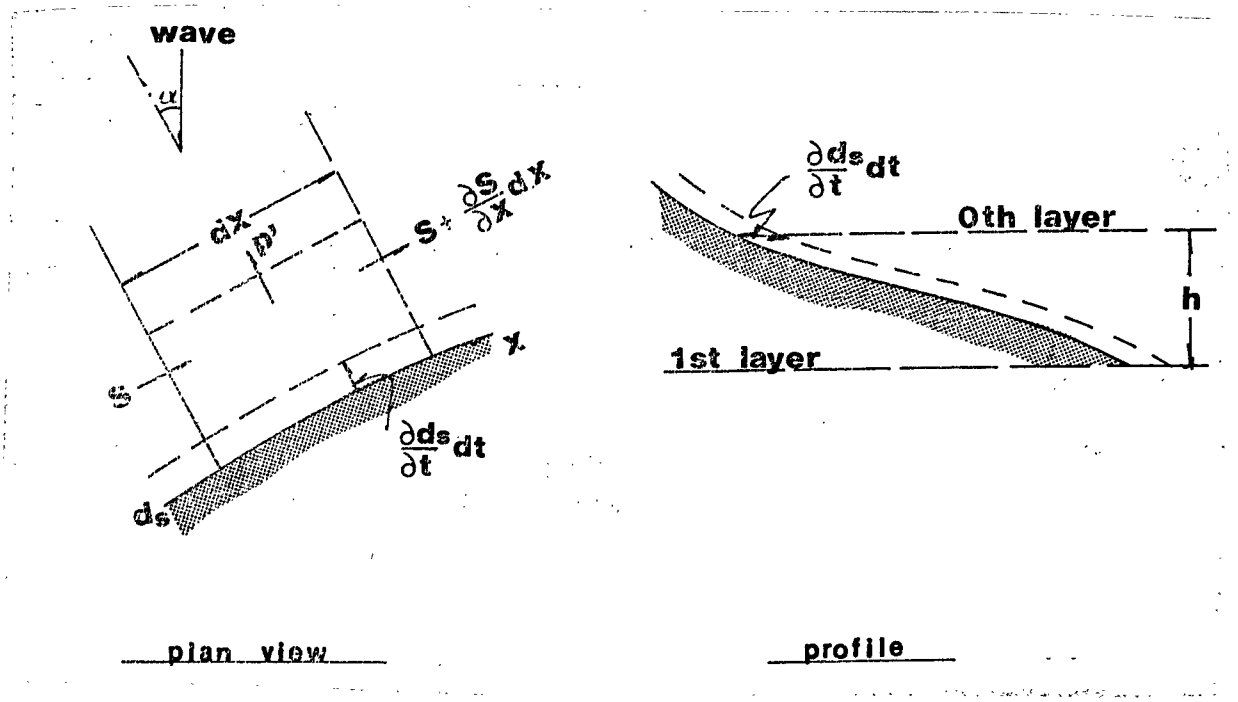

Figure 5.11: Schematic Concept of One-Line Theory

t is the time.

If the longshore transport is a function of the coastline direction only, we have

$$S = S(\alpha) \tag{5.26}$$

where α is the angle of shoreline normal with respect to incident wave angle (Fig. 5.11). By Taylor's expansion and Eq.(5.26) becomes:

$$S = S_o + \alpha(\frac{dS}{d\alpha})_{\alpha=0} + \frac{1}{2}\alpha^2(\frac{d^2S}{d\alpha^2})_{\alpha=0} + \cdots \tag{5.27}$$

where $\alpha = \partial d_s/\partial x$. Substituting Eq.(5.27) into Eq.(5.25) and neglecting terms higher than second order gives the following one-line shoreline equation:

$$\frac{\partial d_s}{\partial t} - \epsilon(\alpha)\frac{\partial^2 d_s}{\partial x^2} + p' = 0 \tag{5.28}$$

where

$$\epsilon(\alpha) = -\frac{1}{h}\frac{\partial S}{\partial \alpha} \tag{5.29}$$

If p' is set equal to zero in the above equation, it reduces to the familiar form of diffusion equation, also known as the Pelnard-Considere (1956) equation of shoreline evolution

$$\frac{\partial d_s}{\partial t} - \epsilon \frac{\partial^2 d_s}{\partial x^2} = 0 \tag{5.30}$$

Furthermore, if ϵ is constant , analytical solutions exist . The standard solution of the P-C equation has the form of an error function which clearly does not apply in the present case . Another possible solution has the following form

$$d_s = e^{-\varsigma t} \sum_i^{\infty} (A_i cosk_i x + B_i sink_i x) \tag{5.31}$$

This represent a spatially rhythmic and time decaying function. By examining the first eigenfunction of shoreline change of a natural beach under oblique wave attack, the following functional form appears to be a reasonable representation (see Fig. 5.7 for example)

$$d_s = (e^{-\varsigma t} - 1)(C_1 + C_2 cos(kx + \delta)) + d_{so} \tag{5.32}$$

where d_{so} is the initial shoreline configuration. This function represents a rhythmic shoreline changes with diminishing amplitude superimposed upon a time-dependant uniform shoreline retreat. Since the solution given by Eq. (5.32) includes not only shoreline change due to long-shore transport but also that due to on/off shore transport, the above function is not a permissible solution of Eq. (5.30). But mathematicaly, the solution is a possible solution of Eq. (5.28) provided the following conditions are satisfied

$$\epsilon k^2 = \varsigma \tag{5.33}$$

and

$$p = C_1 \varsigma e^{-\varsigma t} + \epsilon C_2 k^2 cos(kx + \delta) \tag{5.34}$$

Equation (5.33) provides a condition between the net longshore transport rate (per length) and rate of shoreline retreat, ς, and the wave length of the rhythmic features. The meaning of Eq. (5.34) is explained as follows; Even there is no sink

in the model test, if the shoreline change due to on/off shore transport which is not included in one- line theory can be converted to the shoreline change due to sink/source of sands, the equation above gives the relation of shoreline changes and the value of sink/source. Therefore, the value of p given by Eq. (5.34) is not an actual value. Since ς, k, C_1, C_2 and δ are physical quantities measurable from the experimental data, Eq. (5.33) permits estimation of ϵ, i.e., alongshore duffusivity. Of the five physical quantities, ς and C_1 can be estimated rather accurately from the temporal eigenfunction as it is a monotonically decreasing function. On the other hand, C_2, k and δ are related to the spatial eigenfucntion and this function is sinusoidal. Owing to the limitation on the test basin size, estimations from the data are difficult, particularly, for cases with seawall as only half of the test beach can be utilized for either the updrift or the downdrift section. Therefore, these three factors are evaluated for the cases of natural beach only. Even here, the estimate entails subjective interpretations.

Table 5.2 provides the values of parameters, ς, k, C_1, C_2 and δ together with ϵ as computed from Eq. (5.33). The duffusivity can be calculated by Eq. (5.35)

$$\epsilon = \frac{kH_b^{5/2}\sqrt{\frac{g}{\kappa}}}{8(s-1)(1-p_o)(h_* + B)} \tag{5.35}$$

where p_o is the porosity(=0.35), s is the specific weight of sand(=2.65), k is the longshore transport coefficient (=0.2~1.5), κ is the breaking wave parameter (=0.78) and $h_* + B$ is the active water depth (=0.5m). Based on the equation above, the calculated diffusivity is $1.46 \times 10^{-3} \sim 1.1 \times 10^{-2}$, which reasonably agreed with the value calculated by Eq. (5.33).

The coefficient C_1 is the spatially averaged ultimate mean shoreline position and the coefficient C_2 is the amplitude of perturbation superimposed upon the mean shoreline retreat. As we have observed earlier we are less certain about the true nature of the rhythmic feature. The mean shoreline retreat are more firmly established. The ratios of ultimate shoreline position with and without seawall are

Table 5.2: Estimated Values of ς, ϵ, C_1, C_2, k and δ

Case	ς $(1/s) \times 10^{-4}$	C_1 (m)	C_2 (m)	k $(1/m)$	δ (rad)	ϵ $(m^2/s) \times 10^{-4}$
Natural Beach						
Case 1	0.99	0.595	****	****	****	****
Case 3	0.87	0.644	0.192	0.652	0.36	2.04
Case 5	1.24	0.567	0.064	0.508	0.17	4.81
Seawall Backed Beach,[d] downdrift [u]updrift						
Case 2[d]	0.94	0.570	*****	****	****	****
Case 2[u]	1.22	0.631	*****	****	****	****
Case 4[d]	1.00	0.819	*****	****	****	****
Case 4[u]	0.67	0.757	*****	****	****	****
Case 6[d]	1.15	0.907	*****	****	****	****
Case 6[u]	1.17	0.415	*****	****	****	****

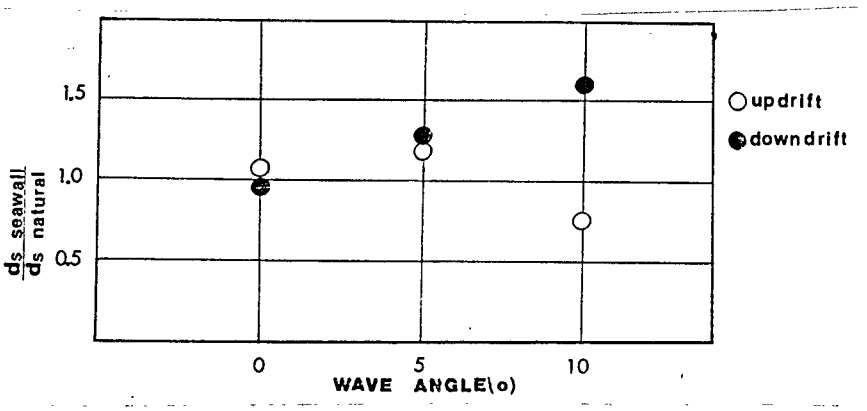

Figure 5.12: Ratios of Ultimate Mean Shoreline Position with and without Seawall

plotted in Fig. 5.12.

5.3 Correlation Between Shoreline Changes and Volumetric Changes

To further examine the validity of the one-line model, the correlation between shoreline changes and volumetric changes are examined here. Equation (5.25) can be written in the following finite difference form

$$\Delta d_s = -\frac{1}{h}(\frac{\Delta s}{\Delta x} + p)\Delta t = -\frac{1}{h}\Delta V \tag{5.36}$$

where ΔV is the volumetric change per unit length along shore. The value of h which is the water depth of the schematized beach profile is usually treated as a constant.

Therefore, for one-line model to work one assume the shoreline change, d_s, has a linear relation to the cross-sectional changes. Fig. 5.13 shows the comparison of the calculated shoreline changes based of Eq. (5.36) to the measured shoreline changes, as can be seen comparison are good for beach with no seawall. The agreement actually becomes better as the test duration increases. This is because the profile gradually reaches its new equilibrium configurations. For beaches with seawall, the agreement is poor at the initial stage but improves progressively as the duration of test become longer. Obviously, during the early stage of profile adjustment, the main mode of sediment transport is in the cross-shore direction. The one-line model which assumes no profile adjustment between time step does not apply. As the time progresses the profile becomes stabilized and longshore transport takes over as the main mode of sediment movement. The presence of seawall will create profile disturbance in both up-wave and down-wave directions away from the seawall as can be seen in Fig. 5.13 b and c. However, as time progresses, the disturbances, instead of spreading further, actually tend to diminish and the beach will revert back to the natural state of no seawall with the exception of the very localized effects just adjacent to the seawall.

In summary, based upon the results presented above the one-line model appears to be reasonable for natural beach under erosive condition. For seawalled beach, the applicability of one-line model is questionable as the profiles are under continuous adjustment. A simple solution as suggested in Eq. (5.32) is no longer valid. The EEF results suggest that in the presence of seawalls, in addition to the modes of translation and oscillation, a shoreline rotational mode appears. This mode becomes more prominent as the incident waves angle increases. This suggests that the longshore transport rate can no longer be treated as constant. Unless the mechanism can be established, one-line model will not yield valid results.

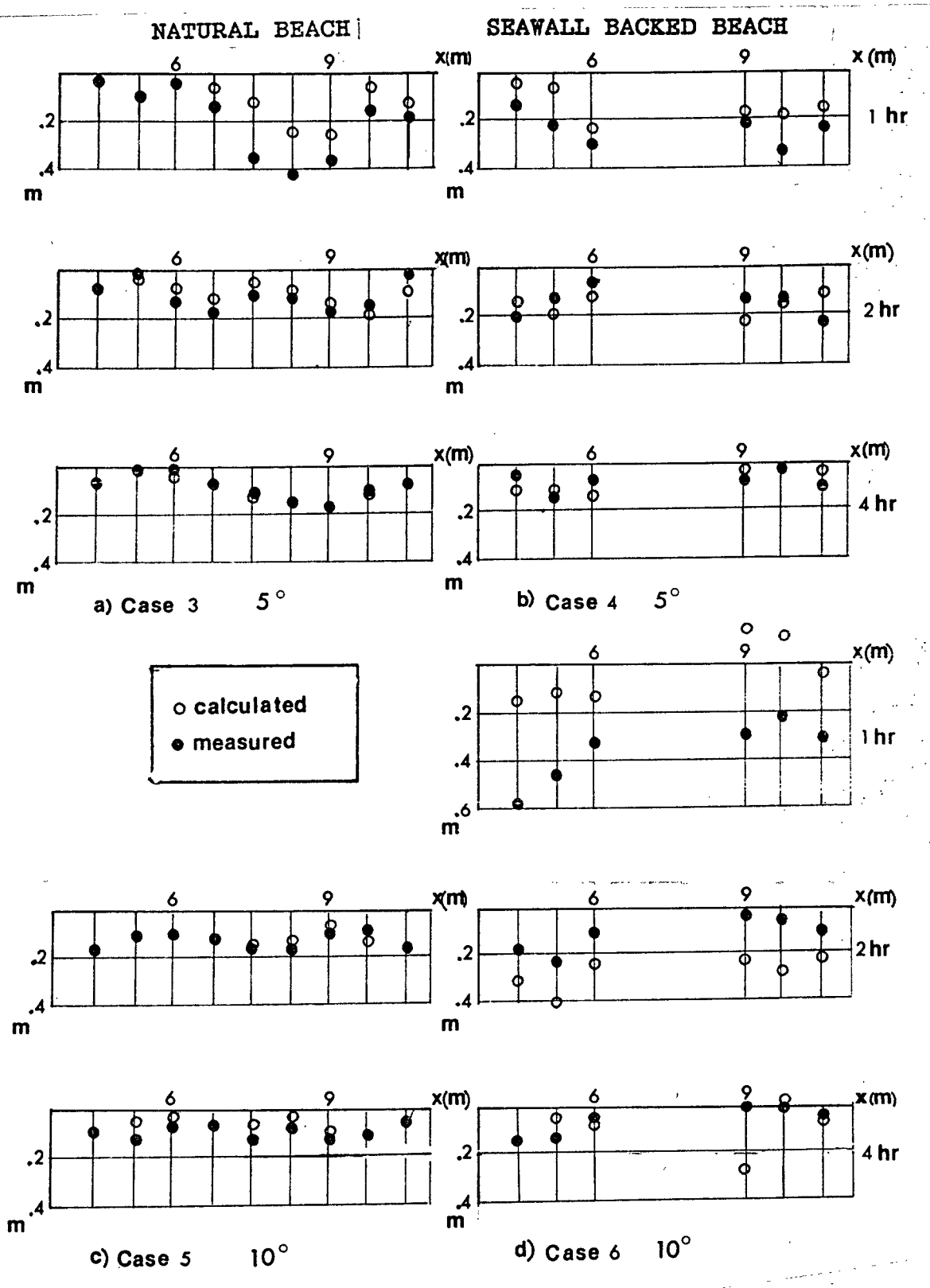

Figure 5.13: Compariosn of Shoreline Change between Measured and Calculated

CHAPTER 6
PROTOTYPE APPLICATION

In this study, it appeared that the scaling law for erosional shoreline is rather firmly established, that is

$$\delta = (\gamma' W_n)^{2/3} \lambda^{2/3} \tag{6.1}$$

and

$$T_n = \frac{\lambda}{\delta^{1/2}} \tag{6.2}$$

Thus, with given input conditions, prototype volumetric rate of erosion and shoreline position can be extrapolated from the laboratory results. A small conflict, however, needs to be resolved first. In arriving at Eq. (6.2), the breaking wave height assumed to be depth controlled, therefore, should be treated as vertical length scale. Eq. (6.2), however, is based upon deep water characteristics; henceforth the deep water height should be used as the vertical scale. If one had to choose between these two vertical scales, it is judged that Eq. (6.2) can be relaxed and the breaking wave height should be used.

Based upon the model scales established here, with $\delta = 8.88$, $\lambda = 18$, W_n=1.47 and $\gamma' = 1$, we have

the shoreline retreat scaling

$$\lambda = 18 \tag{6.3}$$

the volumetric loss scaling

$$\Delta V_n = \delta\lambda = 160./\text{unit length} \tag{6.4}$$

Table 6.1: Example of Prototype Quantities Based upon Laboratory Results

	Case 5(10°, Natural Beach)		Case 6(10°, Seawalled Beach)	
	Labratory	Prototype	Labratory	Prototype
(1) mean shoreline (final) (m)	-0.567	-10.2	-0.907(D) -0.415(U)	-16.3(D) -7.5(U)
(2) time to reach 98%final position (hour)	8.8	53	9.4(D) 9.3(U)	57(D) 56(D)
(3) time to reach 50% final position (hour)	1.6	9.4	1.7(D) 1.7(U)	10(D) 10(U)
(4)volumetric chamnge (spatially averaged) (m^3/m)	-0.142	-23	-0.211(D) -0.076(U)	-34(D) -12(U)

D and U denote down-drift and up-drift respectively
Item (1),(2),and (3) are based on Eq.(5.32 and values in Table 5.2.
Item (4) is based on values in Table 4.1 and 4 hours laboratory testing data

and the time scale

$$T_n = \frac{\lambda}{\delta^{1/2}} = 6.04 \tag{6.5}$$

An example is given here to illustrate the prototype quantities based upon the experimental values.

The laboratory results can also be applied to scales somewhat different than that observed in the model. For such applications, we must recognize the following constraints

1. The wave period in the prototype should fulfill Eq. (6.2), for example, if $\delta = 15$ owing to large prototype wave, thus, $\lambda = 39.5$ and $T_n = 10.2$ which translates into a prototype wave period of $17.7sec.$

2. As remarked, the wave period constraint could probably be relaxed somewhat as long as the types of breakers are preserved.

CHAPTER 7
CONCLUDING REMARKS

The important findings obtained from the present study and the recommendation for future study are presented here.

7.1 Important Findings

To examine the effects of seawall, volumetric change analysis and shoreline and hydrographic change analysis were employed.

In volumetric change analysis, three types of rate of volumetric change were defined and examined. Those were (1) rate of volumetric change along a profile, $\dot{v}_p$, (2) rate of cumulative volumetric change, $\dot{v}_c$, and (3) rate of volumetric change in a local control area, $\dot{v}_l$. It was found that under normal incident wave, the rate of volumetric erosion as well as the total eroded volume in front of seawall was smaller than that of natural beach much the same as the 2D case by Barnett and Wang (1988). For oblique waves, the on/offshore component of the transport rate on both updrift and downdrift sides were found to be only slightly larger than that of the natural beach. On the other hand, the littoral drift rate and the shoreline recession rate, in comparison with the natural beach, increased significantly on the downdrift side but also decreased by the same order of magnitude on the updrift side. This phenomenon was evidently due to the groin effect. Under the wave angles tested, this groin effect was found to be localized within a region spanning 3 to 4 seawall length of fronting beach centered around the seawall. Consequently, in terms of total volumetric changes, the seawall effect is also very localized.

In shoreline and hydrographic change analysis, empirical eigenfunction (EEF) analysis and one-line model theory were utilized. First of all, EEF was applied to

shoreline changes. The first spatial eigenfunction accounted for 90 % of the variance of shoreline data. Under normal incident wave, the spatial eigenfunction manifested a uniform recession and was very similar for natural beach and seawall backed beach. Under oblique wave, spatial eigenfunction exhibited a rhythmic features in addition to a uniform recession. With the presence of seawall, this rhythmic feature became more prominent on the updrift side. As the wave angle increased, the rhythmic features diminished in amplitude. The local effects of increased downdrift erosion and decreased updrift erosion were manifested in a rotational mode in the eigenfunction. The temporal eigenfunctions were very similar for natural beach and seawall backed beach irrespective of incident wave angles.

The spatial eigenfunctions of the hydrographic data were much more irregular than those of shoreline probably due to the three dimensional flow field. The contribution from the first eigenfunction became smaller, thus, the second mode of eigenfunction played a more important role. In erosional case, significant scouring in front of seawall was evident from the shape of the spatial eigenfunction. But in the recovery cases, it also revealed the rapid filling of these scoured troughs.

From the analysis of EEF, the empirical solution of Pelnard– Considere equation were presented. The alongshore diffusivity was calculated based on this solution. The alongshore diffusivity was compared with the conventional formula. It was found that both values agreed well for natural beach. Empirical formulas were derived to describe shoreline evolution. The ultimate mean shoreline change clearly showed downdrift erosion and updrift accretion for seawall backed beach.

Furthermore, the validity of the one-line model for seawall beach was examined. Comparisons between the measured shoreline and the calculated shoreline supported the validity of one-line model for natural beaches, but for seawalled beach especially at the initial stage of profile evolution while shoreline changes were dominated by on/offshore transport one-line model did not fare well.

One of the main contributions of this study was the verification of proper modeling laws. This permits conversion of the laboratory results to prototype applications. The empirical equation of equilibrium profile proposed by Dean was shown to be consistent with the modeling law based upon conservation of mass transport. The physical meaning of the scale parameter "A" appeared in the empirical equation was shown to be the scale of the sediment settling velocity. The experimental results were shown to properly portray the prototype conditions for erosional cases but not for the recovery case.

7.2 Recommendation for Future Study

In the present study, the effects of seawall were presented quantitatively. However, if the final goal is to develop a model which has the general ability to predict the effects of seawall, the cases tested in this study are not sufficient. The wave height, wave period and the location of seawall and the length of seawall and the angle of incident waves should be changed and tested. As mentioned earlier, the recovery condition could not be modeled properly due to scale effects. For the proper modeling, a larger scale model is necessary so that at least the flow regime can be properly modeled.

The modeling law for the bed-load dominated case should be tested. Finally, the question of proper modeling when both modes are important should be answered.

The proposed empirical solution for Pelnard-Considere equation also should be verified by more data sets with direct measurement of longshore transport rate and on/offshore transport rate.

APPENDIX A
CONTOUR MAPS

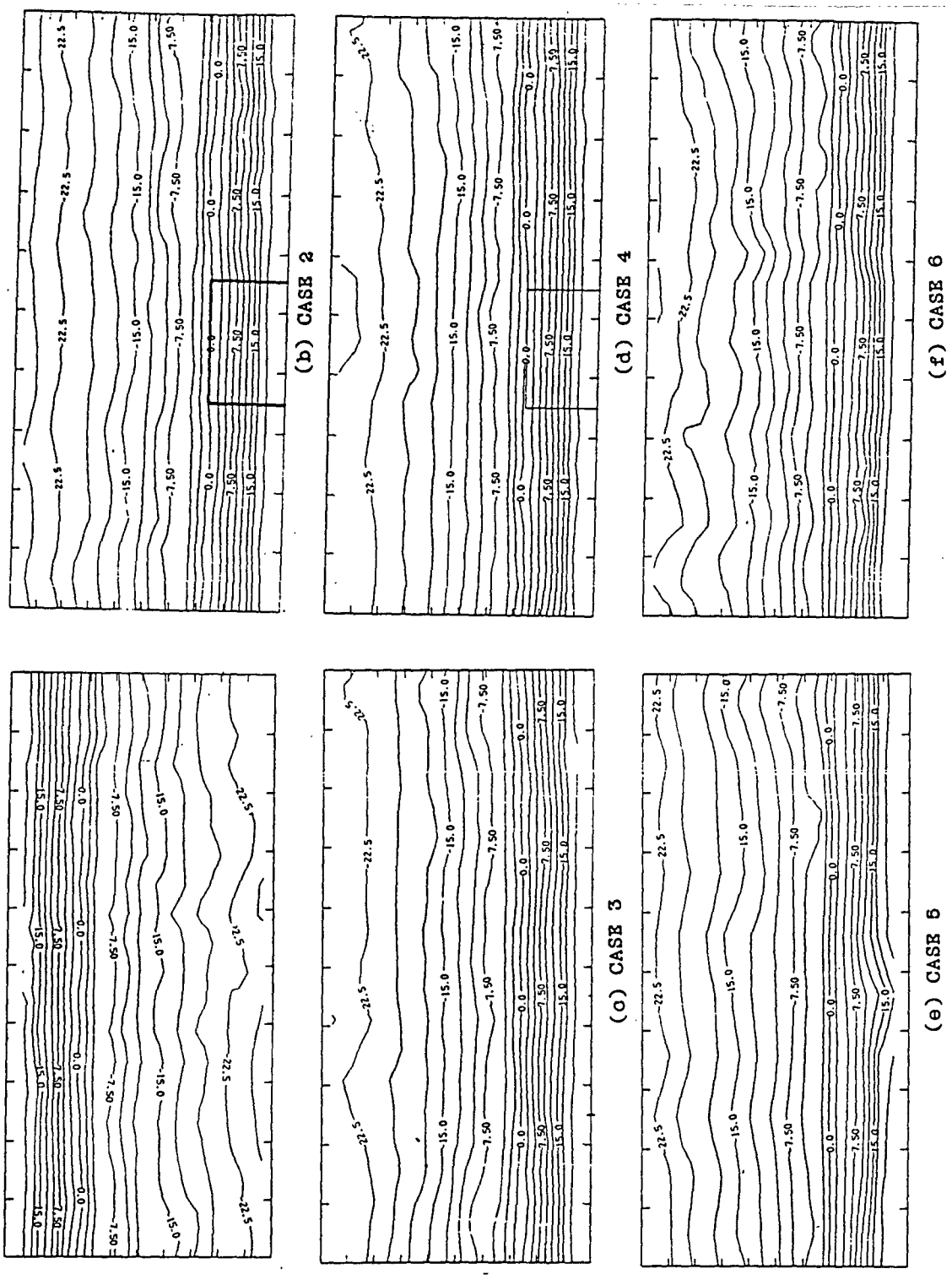

Figure A.1: Contour Map for Erosive condition t=0 hour

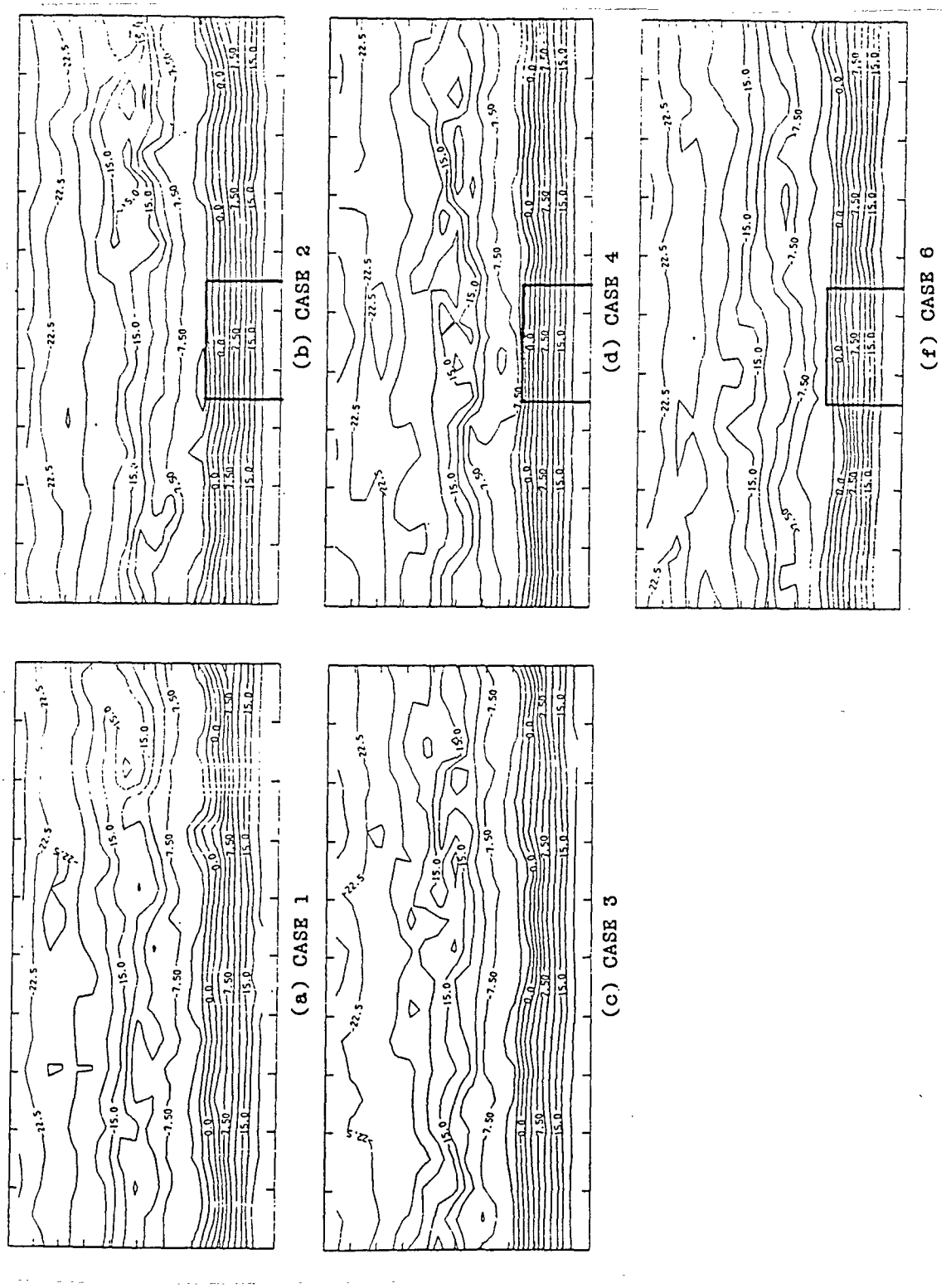

Figure A.2: Contour Map for Erosive condition t=1 hour

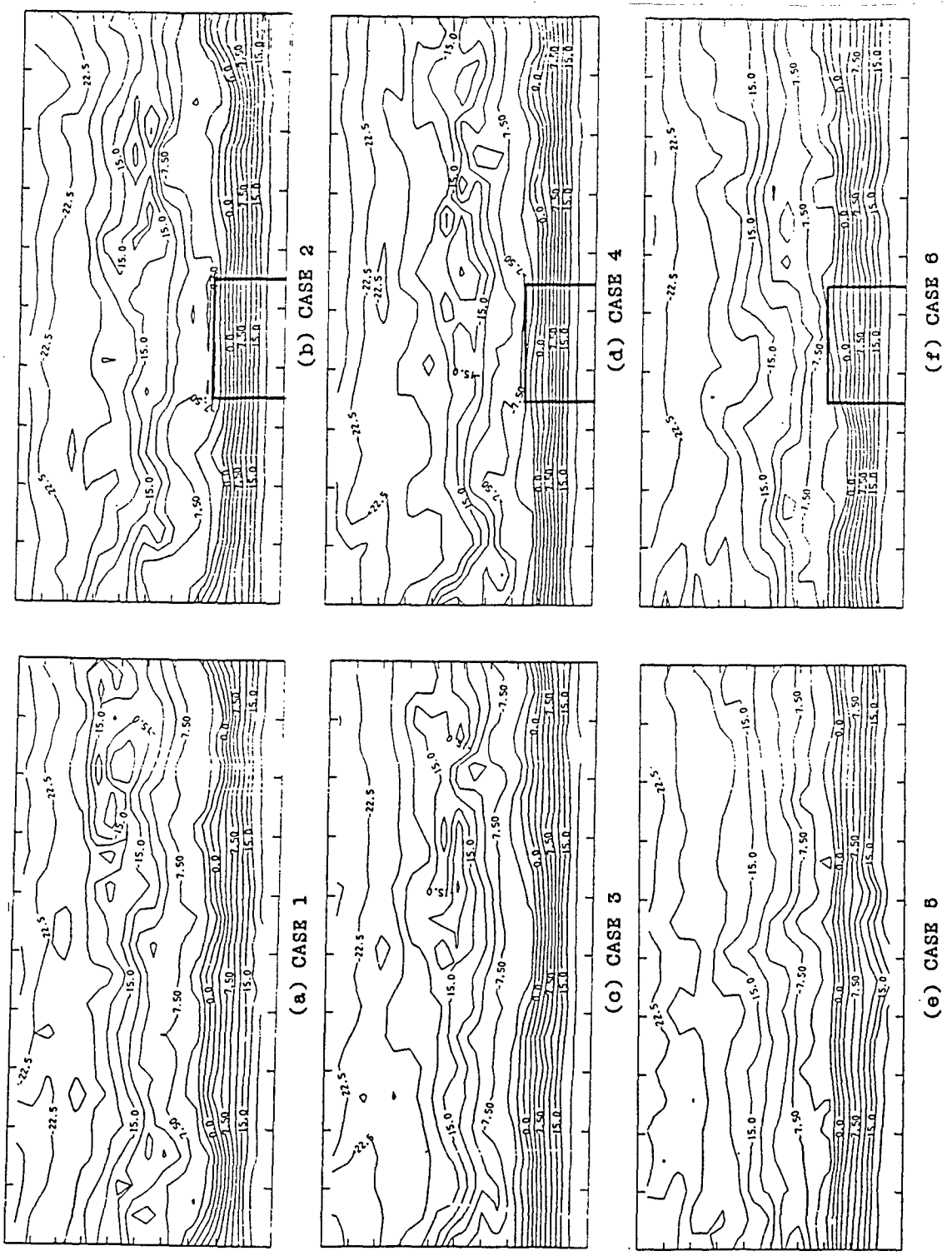

Figure A.3: Contour Map for Erosive condition t=2 hour

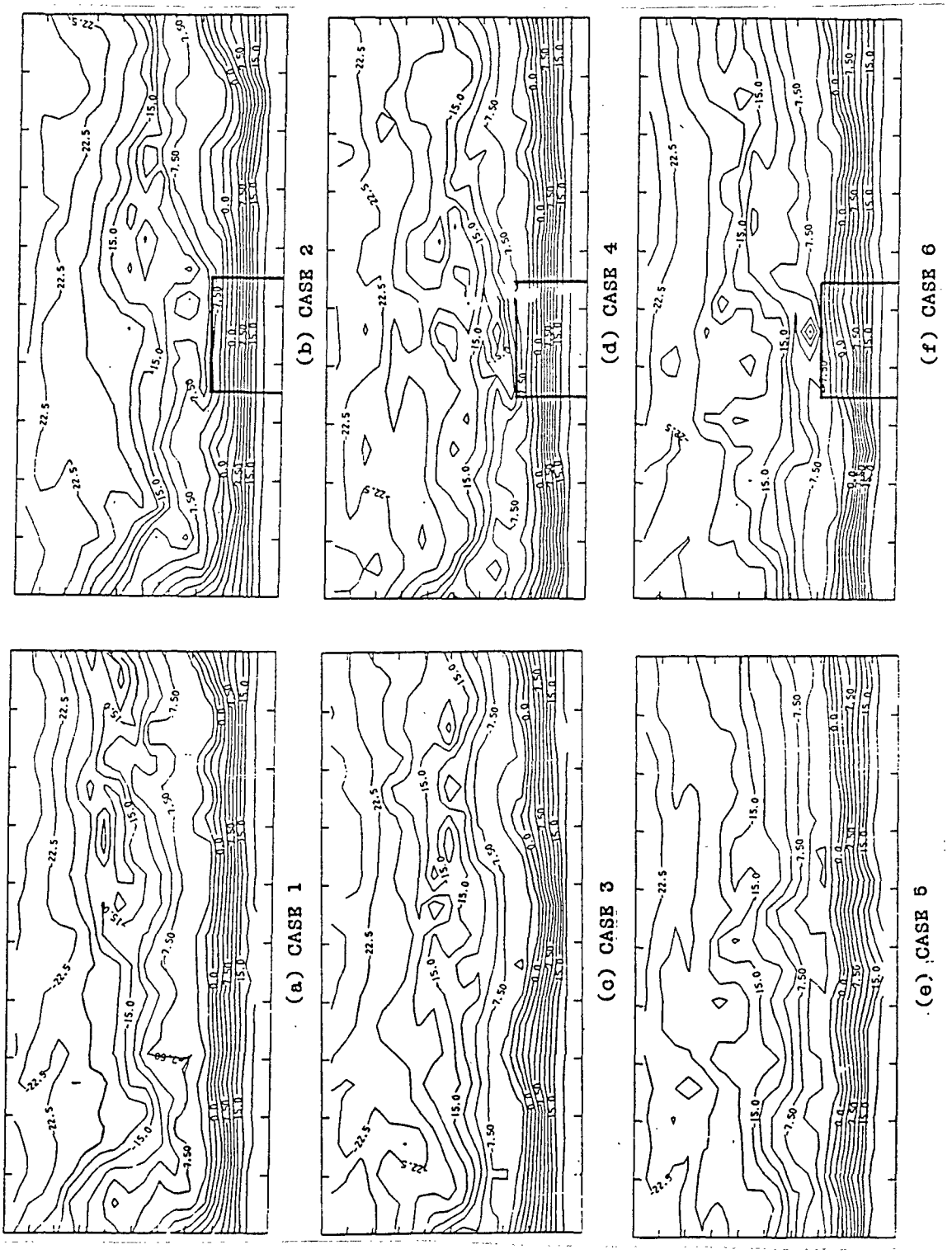

Figure A.4: Contour Map for Erosive condition t=4 hour

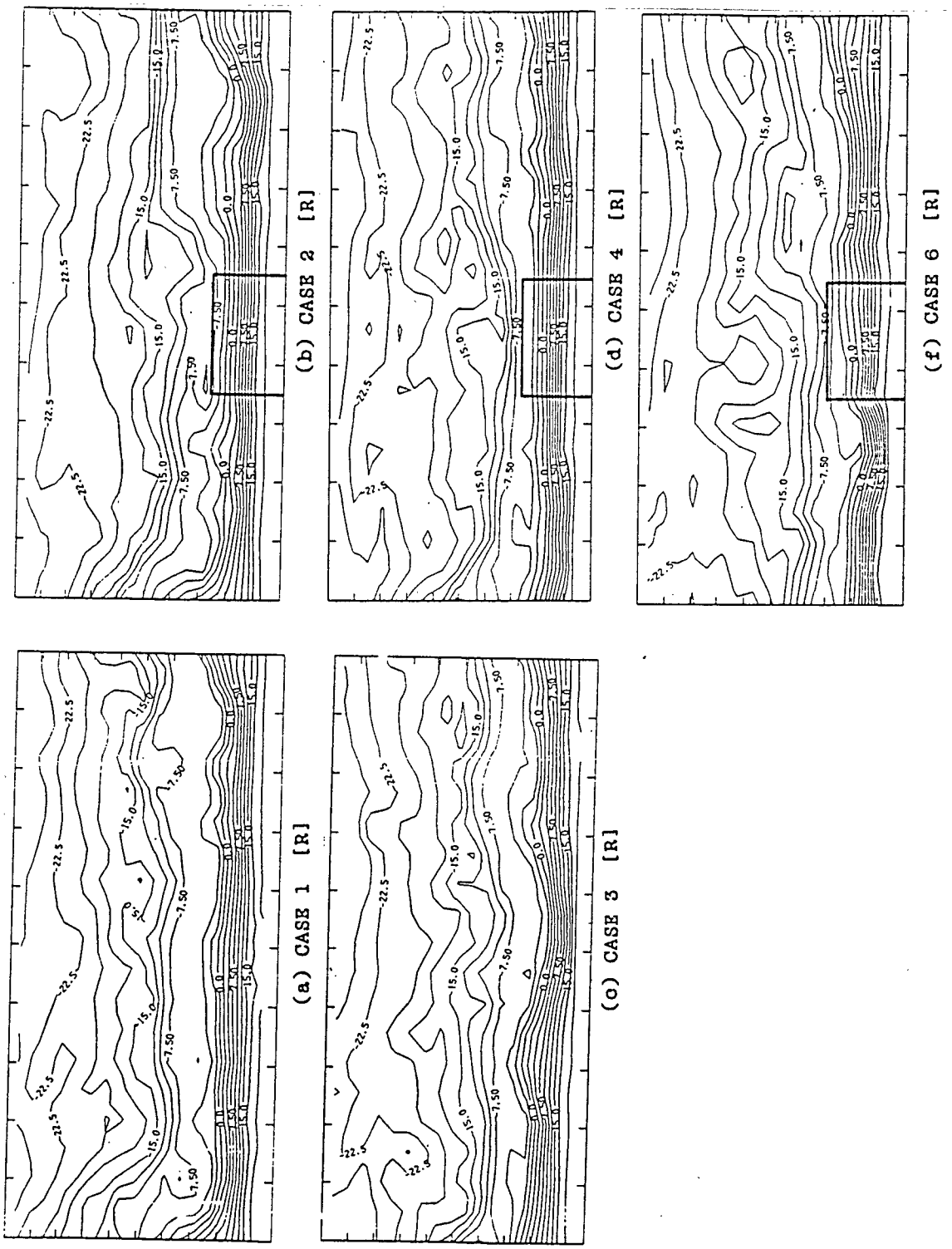

Figure A.5: Contour Map for Recovery condition t=1 hour

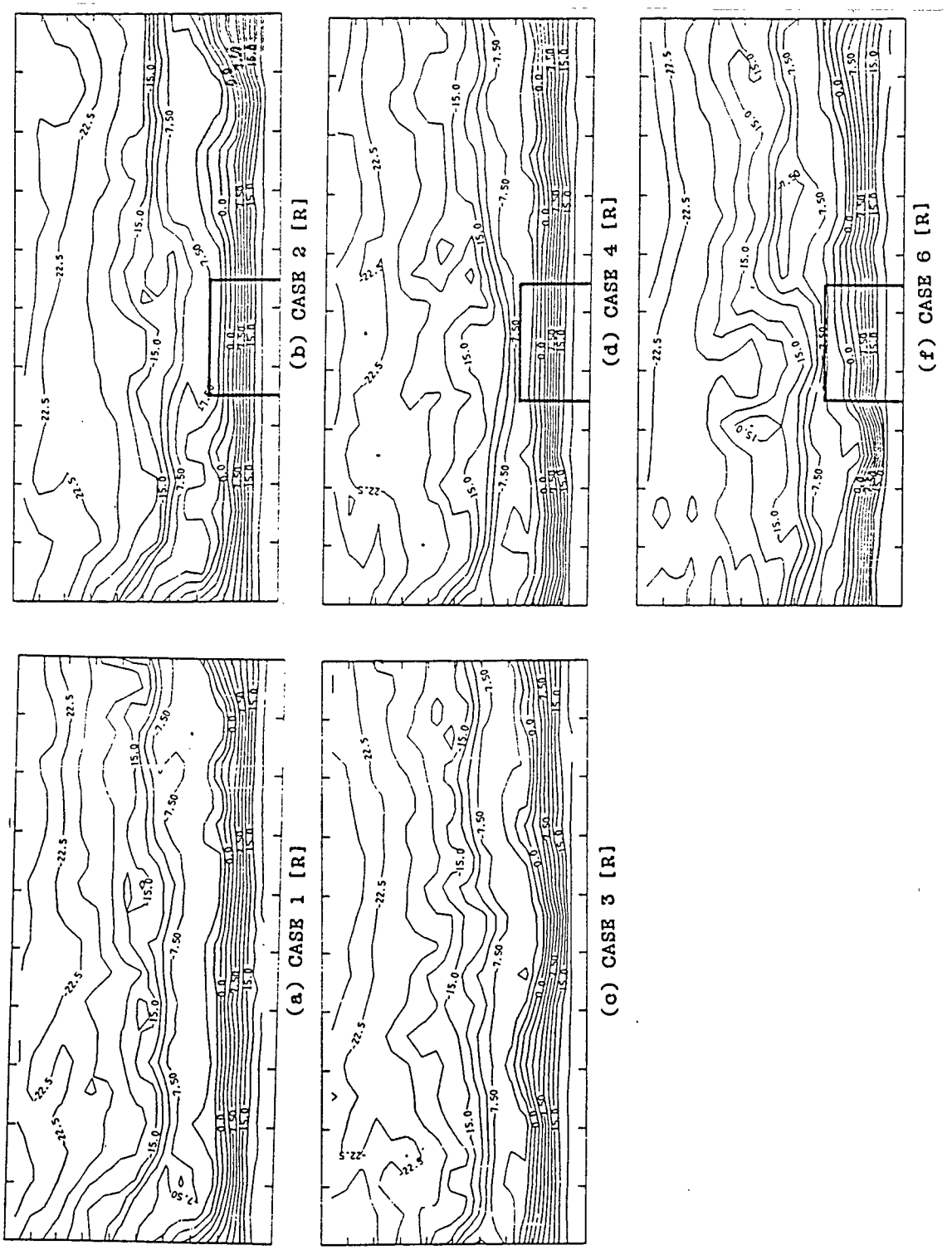

Figure A.6: Contour Map for Recovery condition t=2 hour

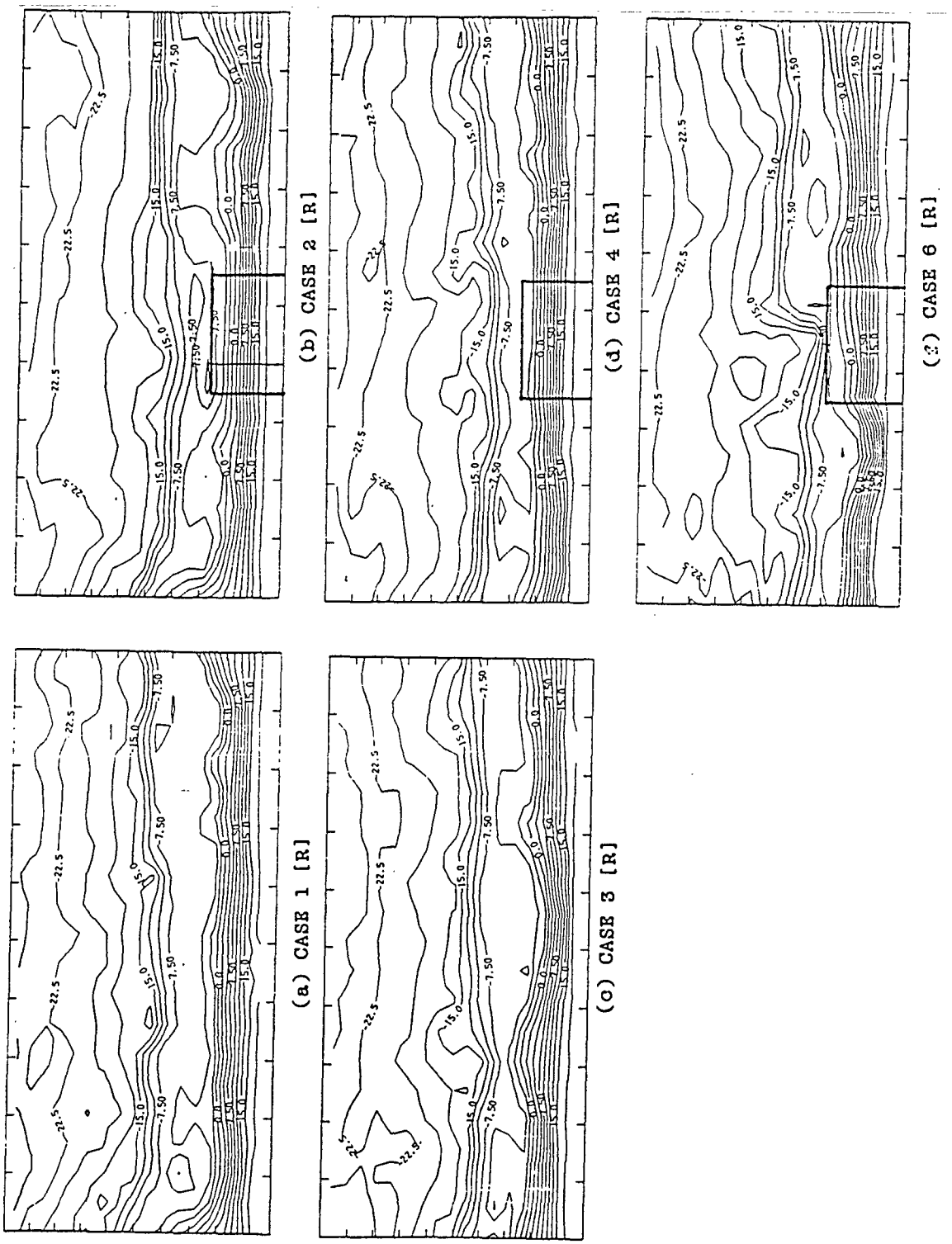

Figure A.7: Contour Map for Recovery condition t=4 hour

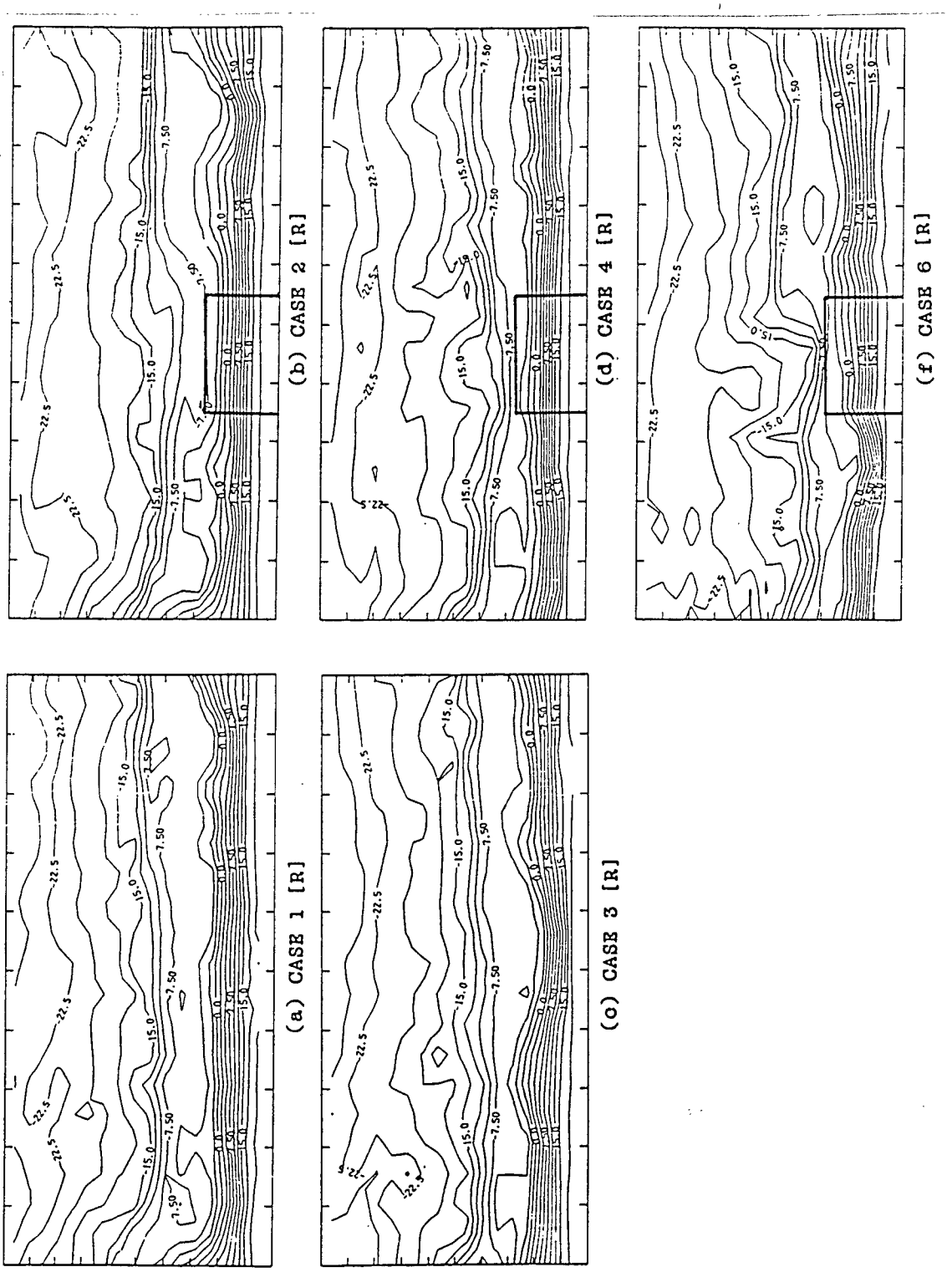

Figure A.8: Contour Map for Recovery condition t=8 hour

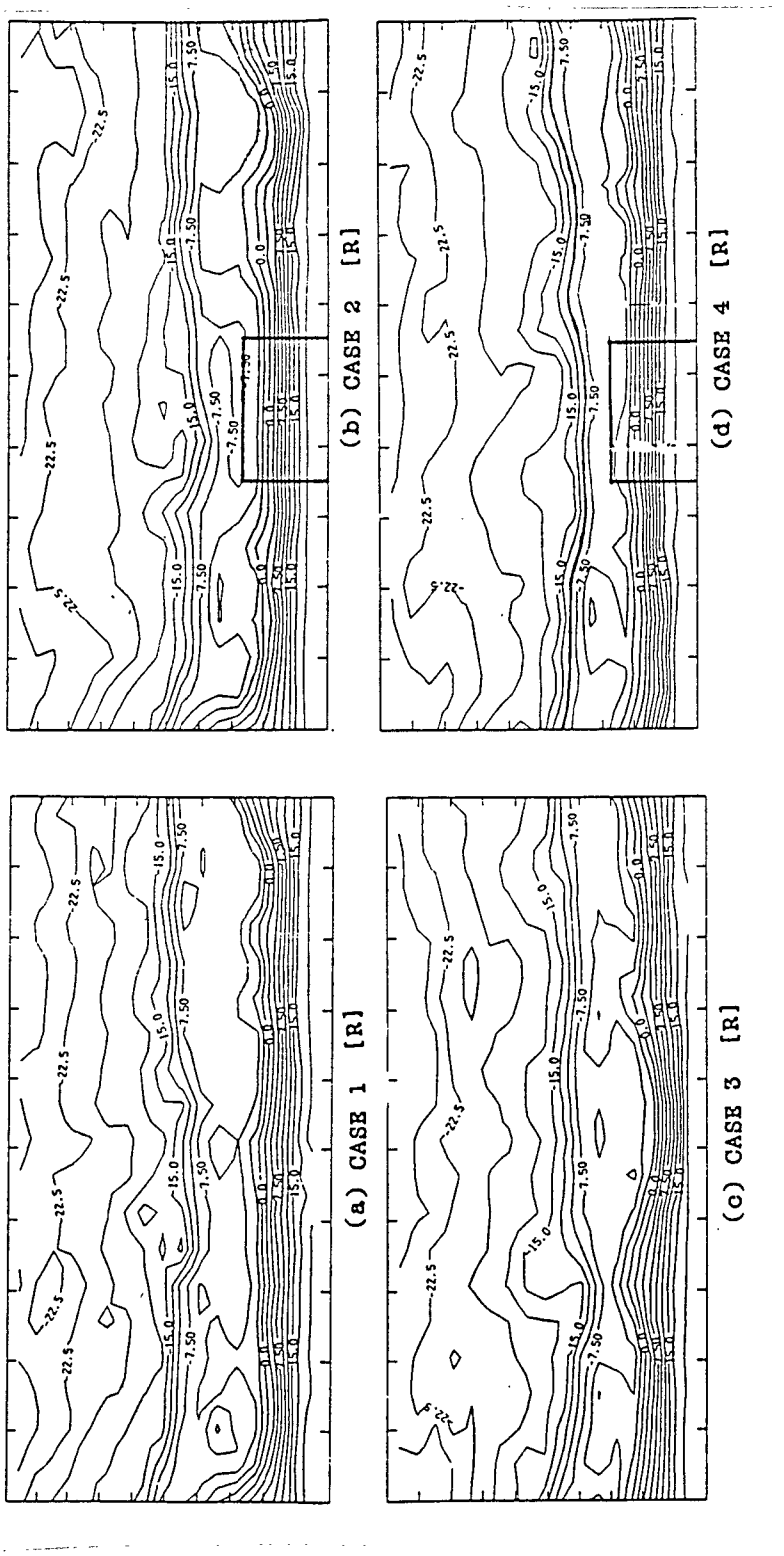

Figure A.9: Contour Map for Recovery condition t=12 hour

APPENDIX B
RESULTS OF EMPIRICAL EIGENFUNCTION ANALYSIS

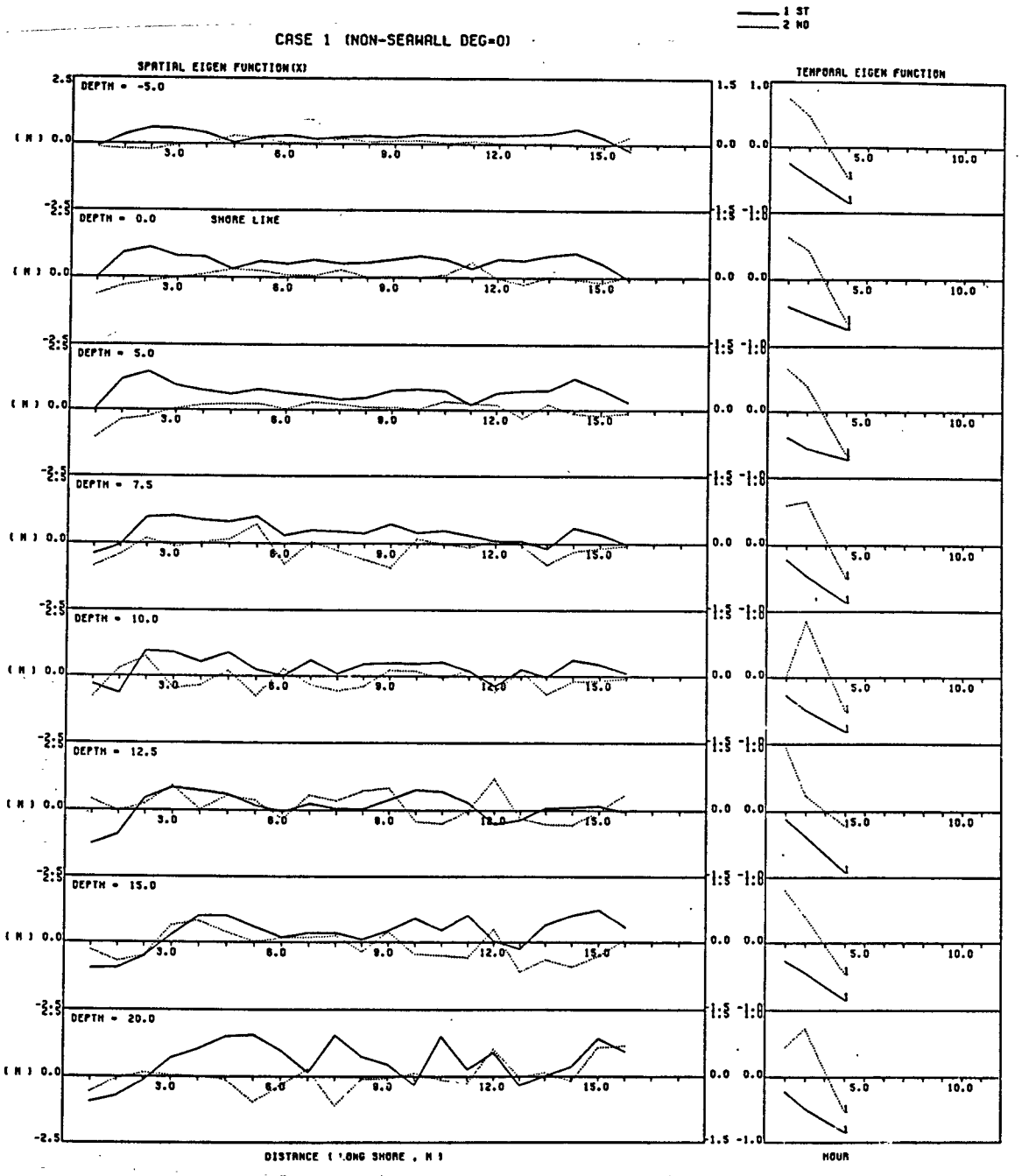

Figure B.1: Eigenfunction for Case 1

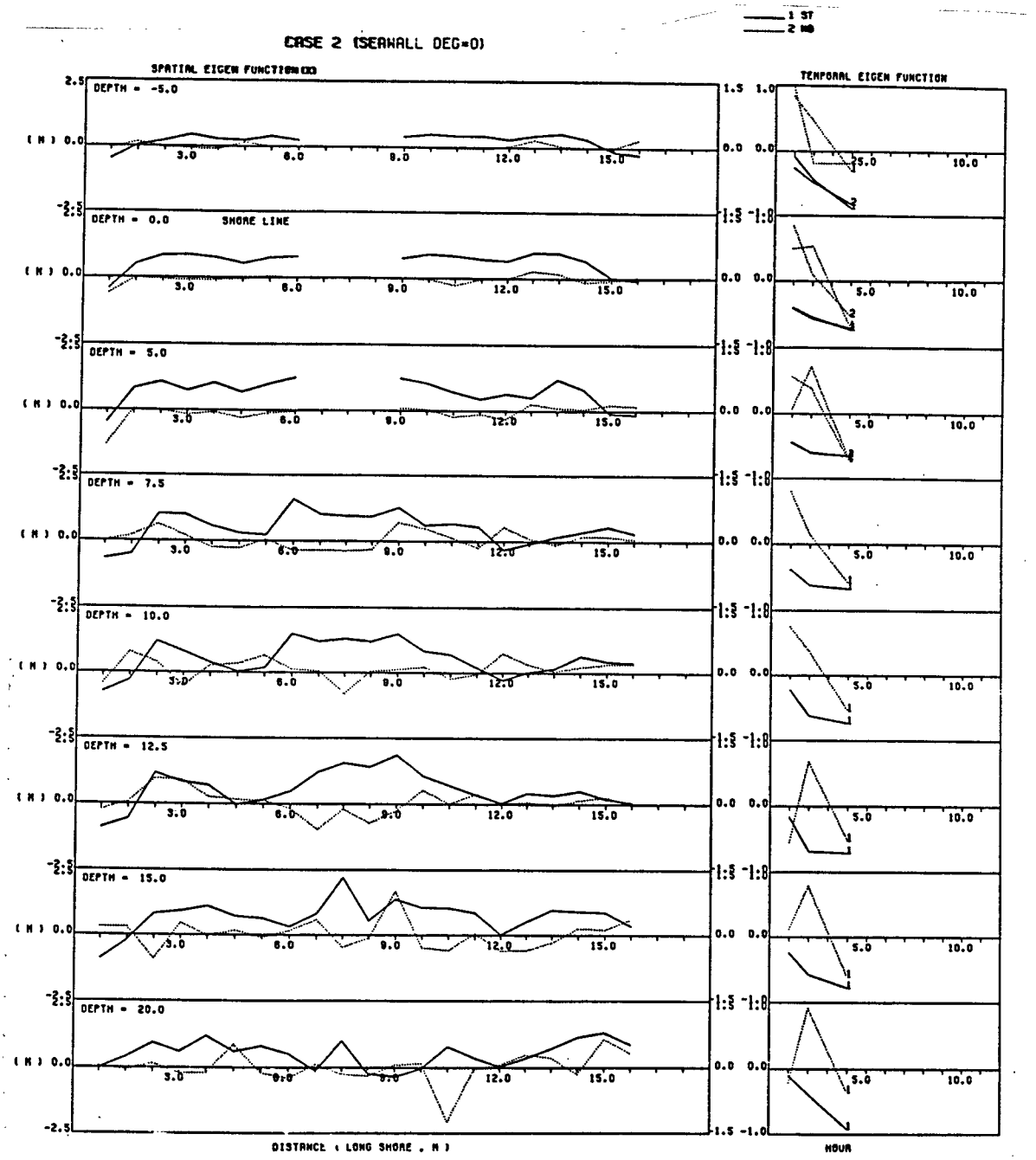

Figure B.2: Eigenfunction for Case 2

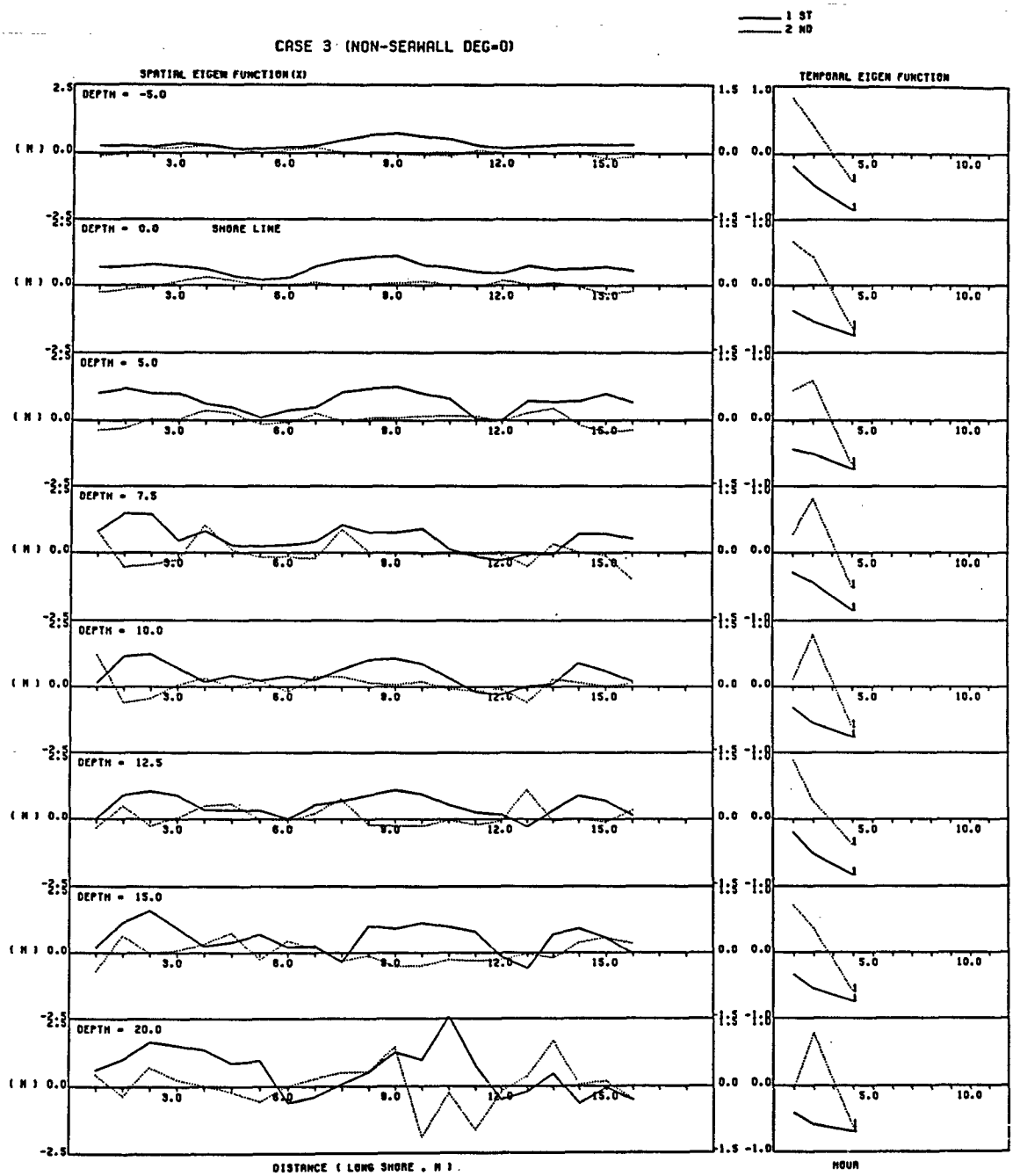

Figure B.3: Eigenfunction for Case 3

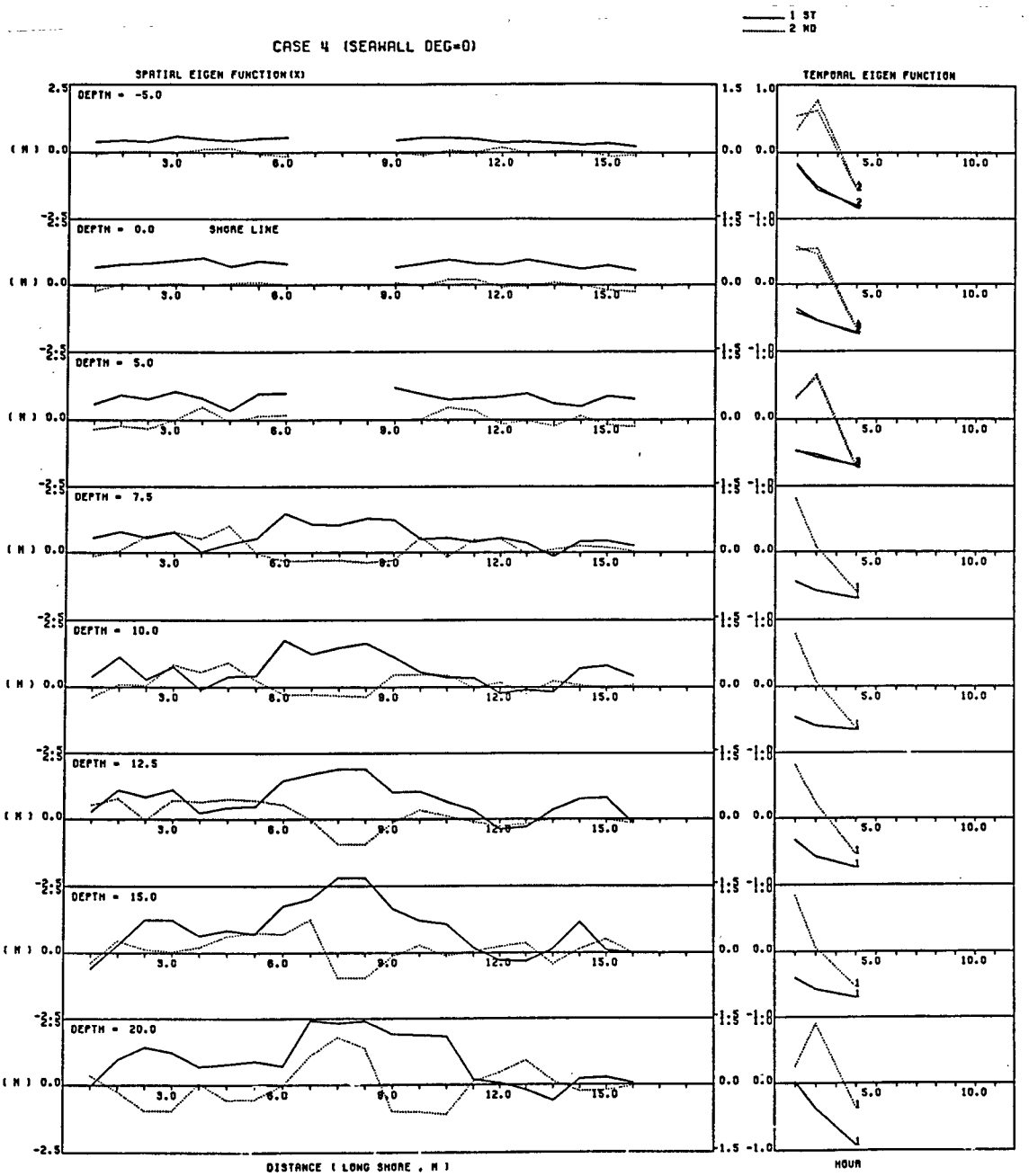

Figure B.4: Eigenfunction for Case 4

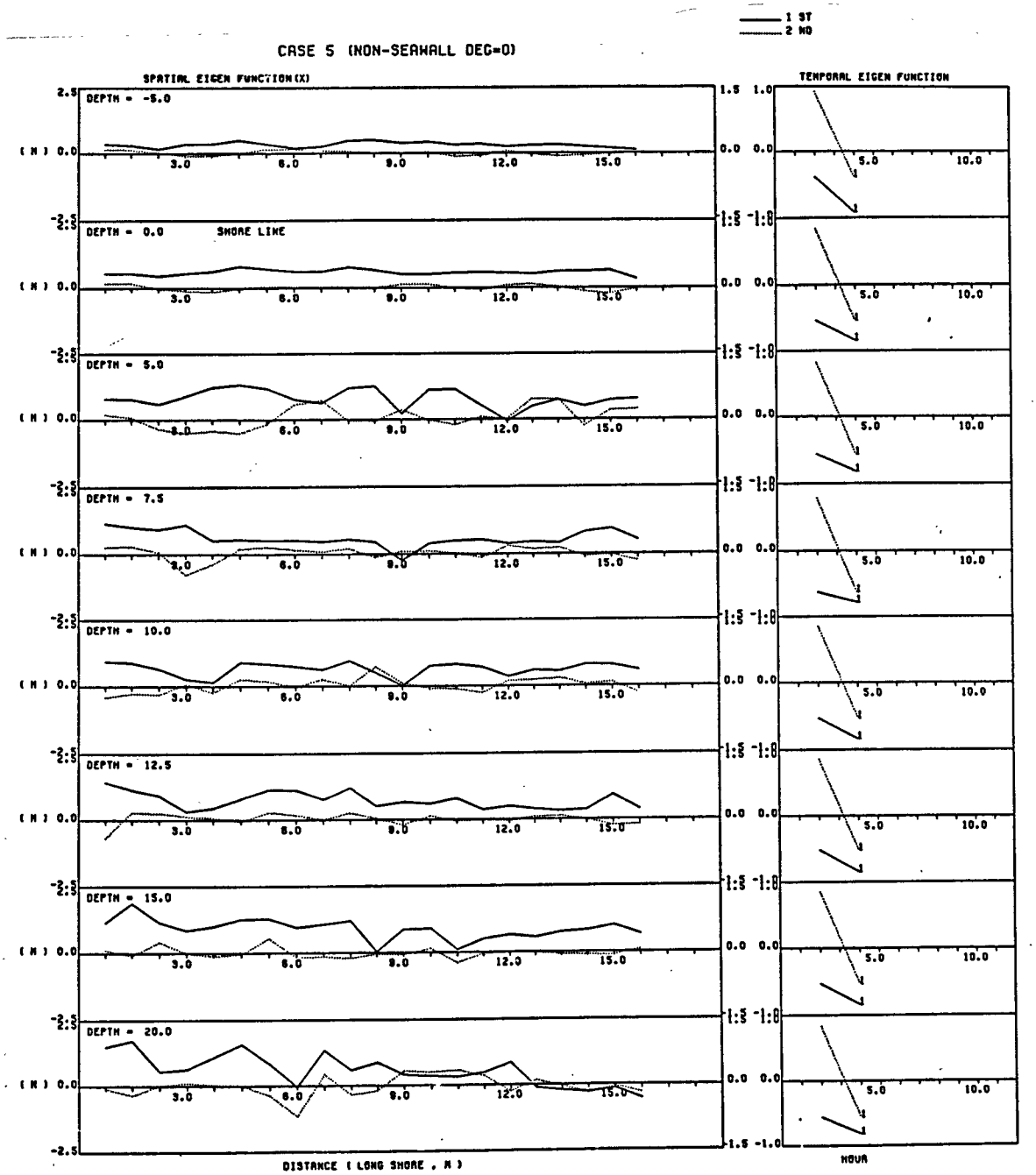

Figure B.5: Eigenfunction for Case 5

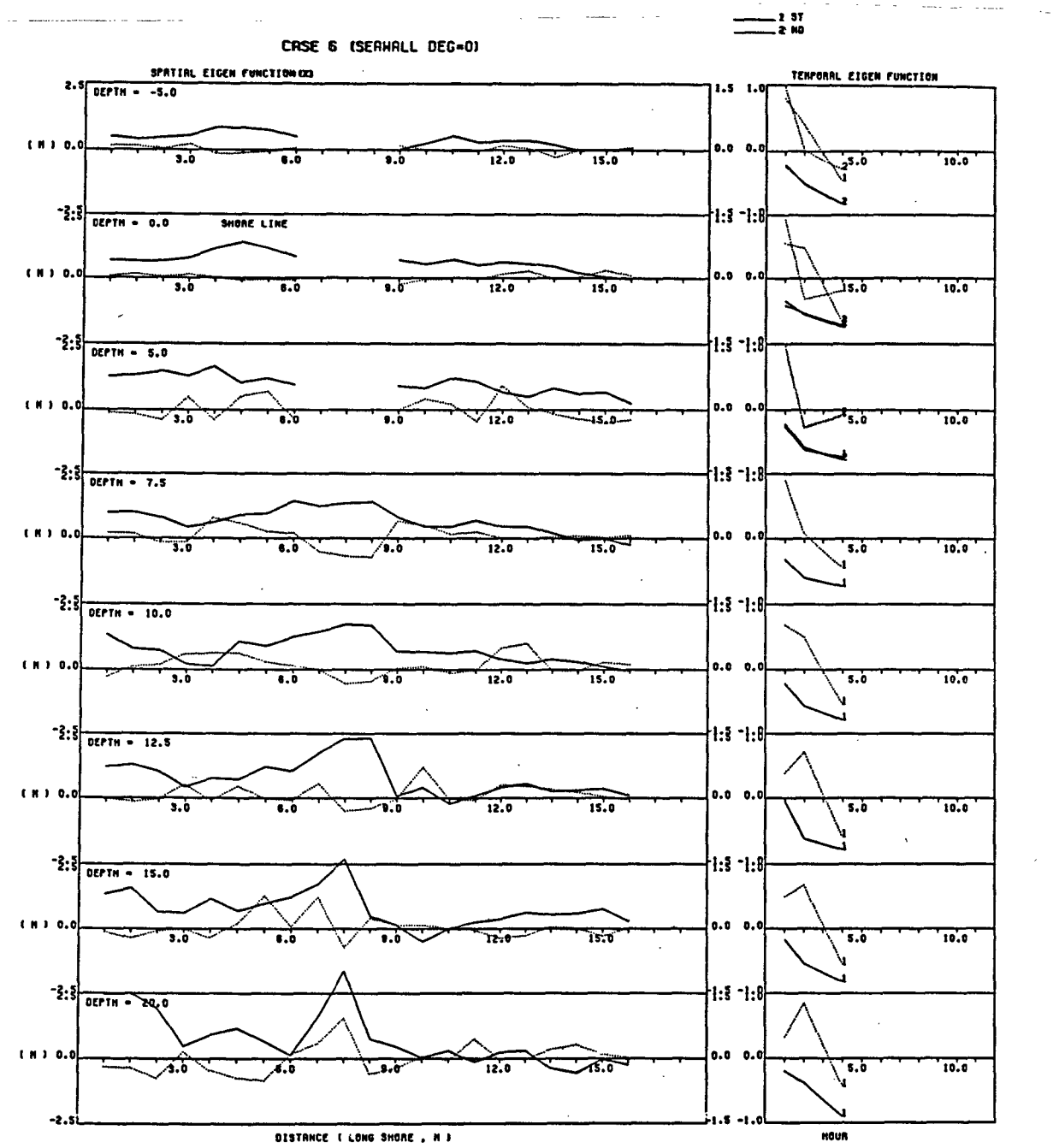

Figure B.6: Eigenfunction for Case 6

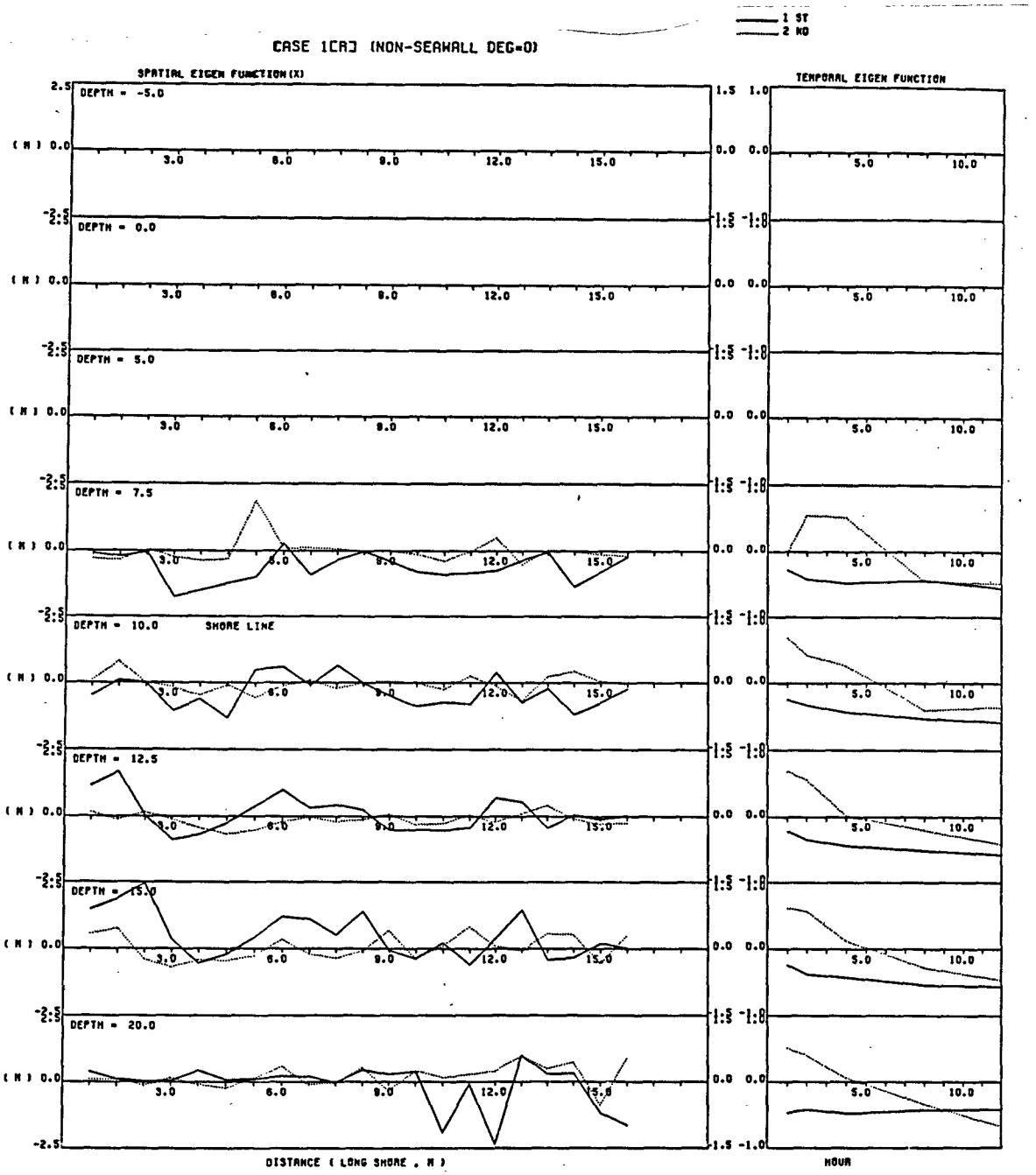

Figure B.7: Eigenfunction for Case 1 (recovery)

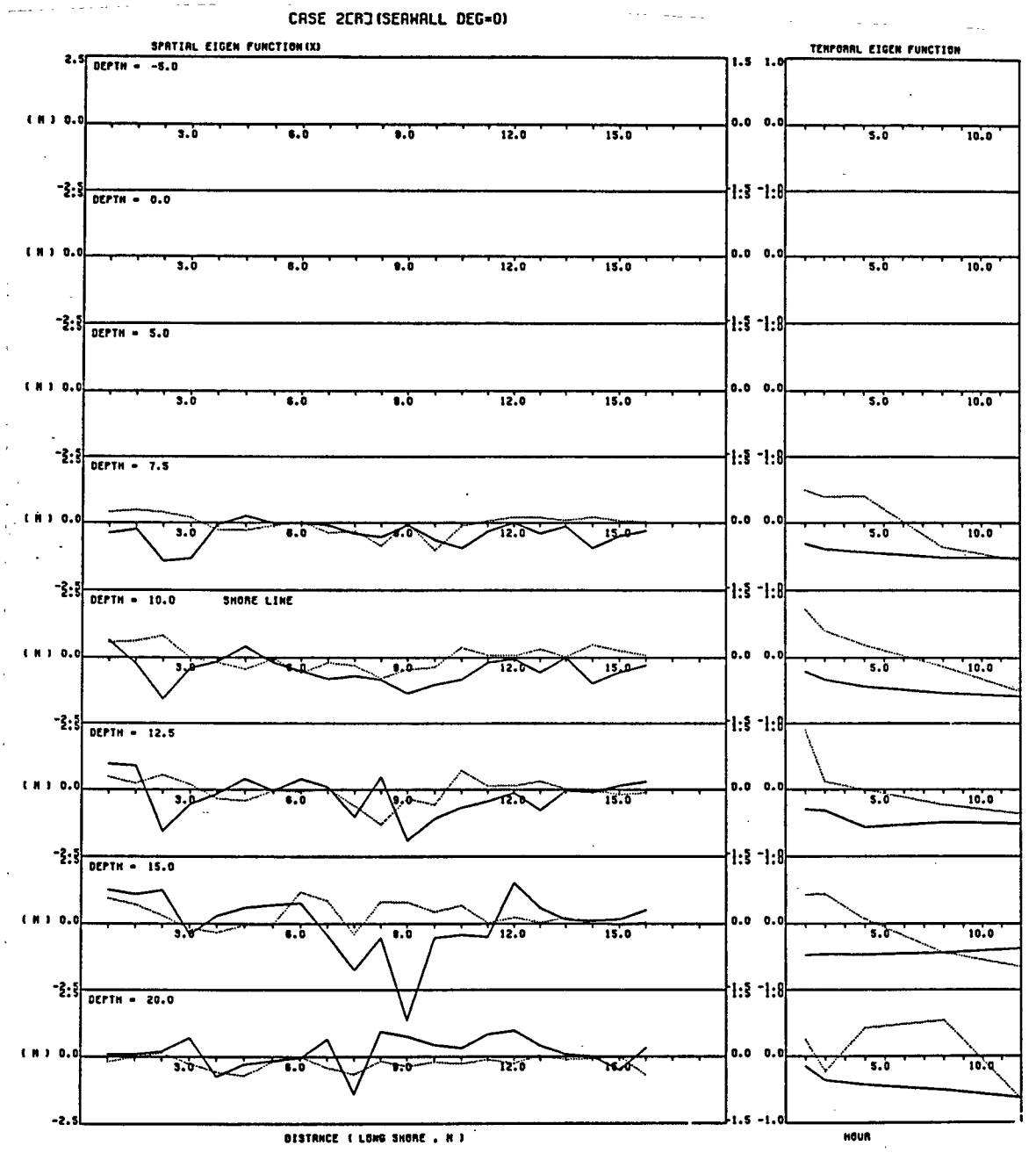

Figure B.8: Eigenfunction for Case 2 (recovery)

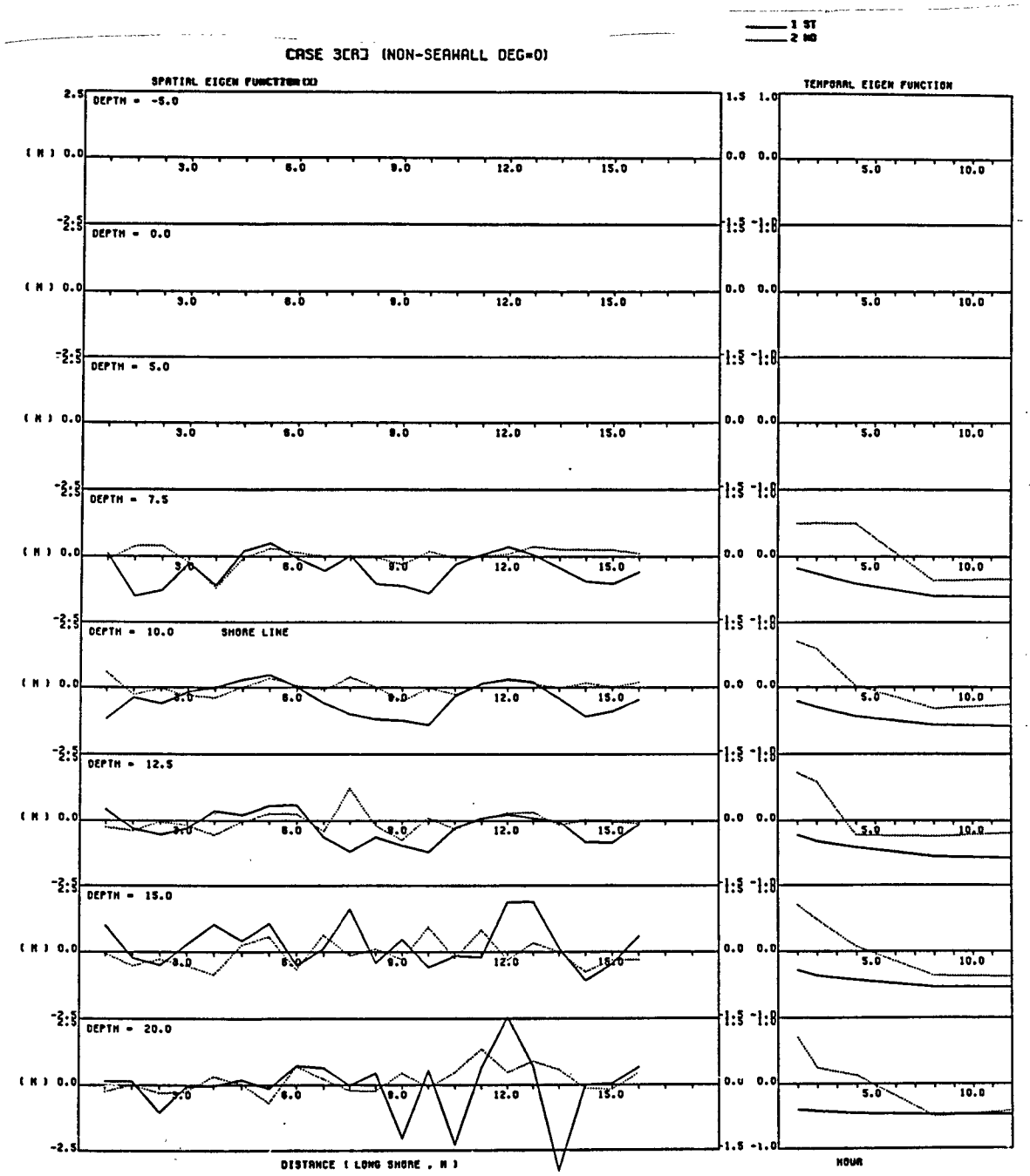

Figure B.9: Eigenfunction for Case 3 (recovery)

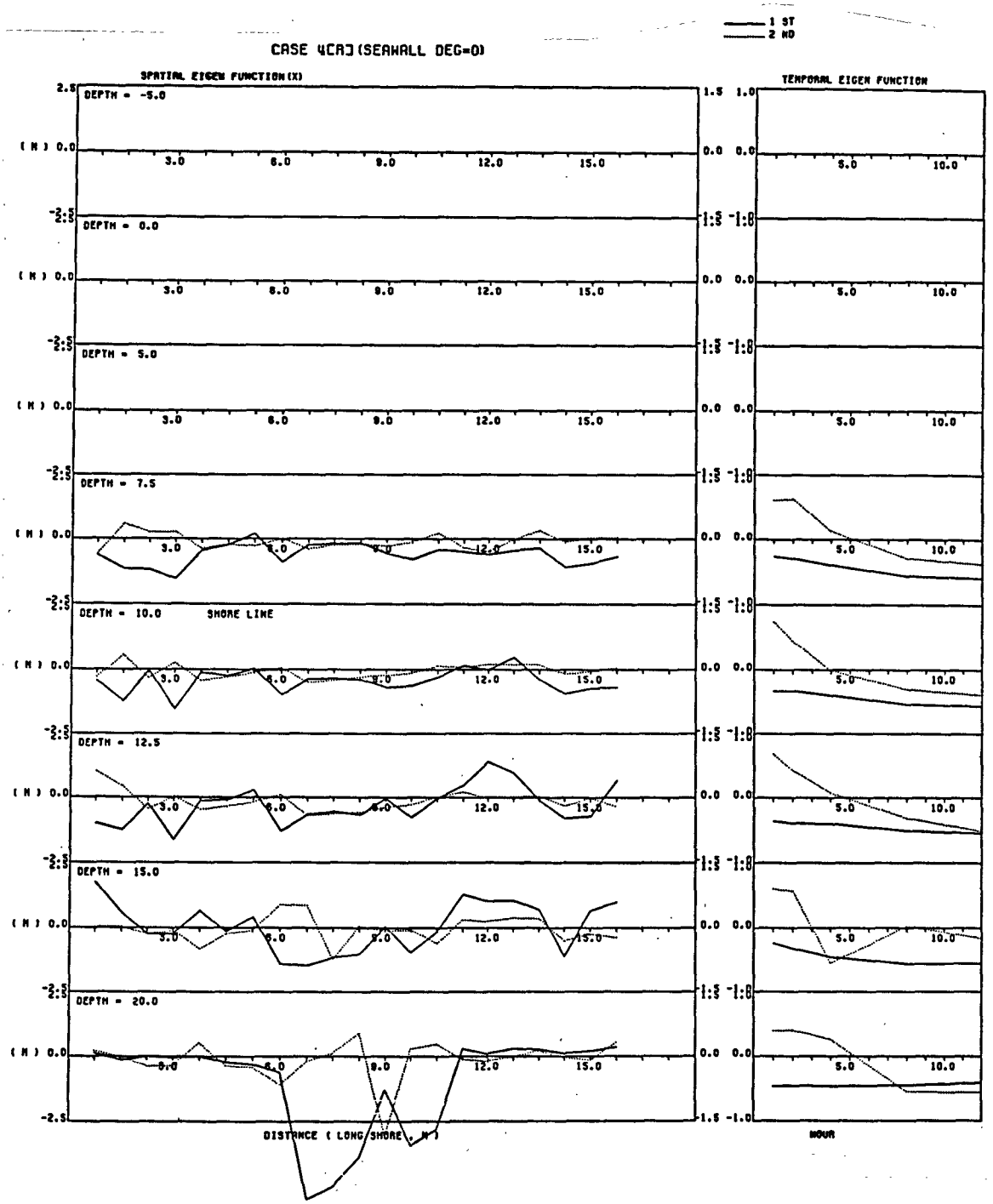

Figure B.10: Eigenfunction for Case 4 (recovery)

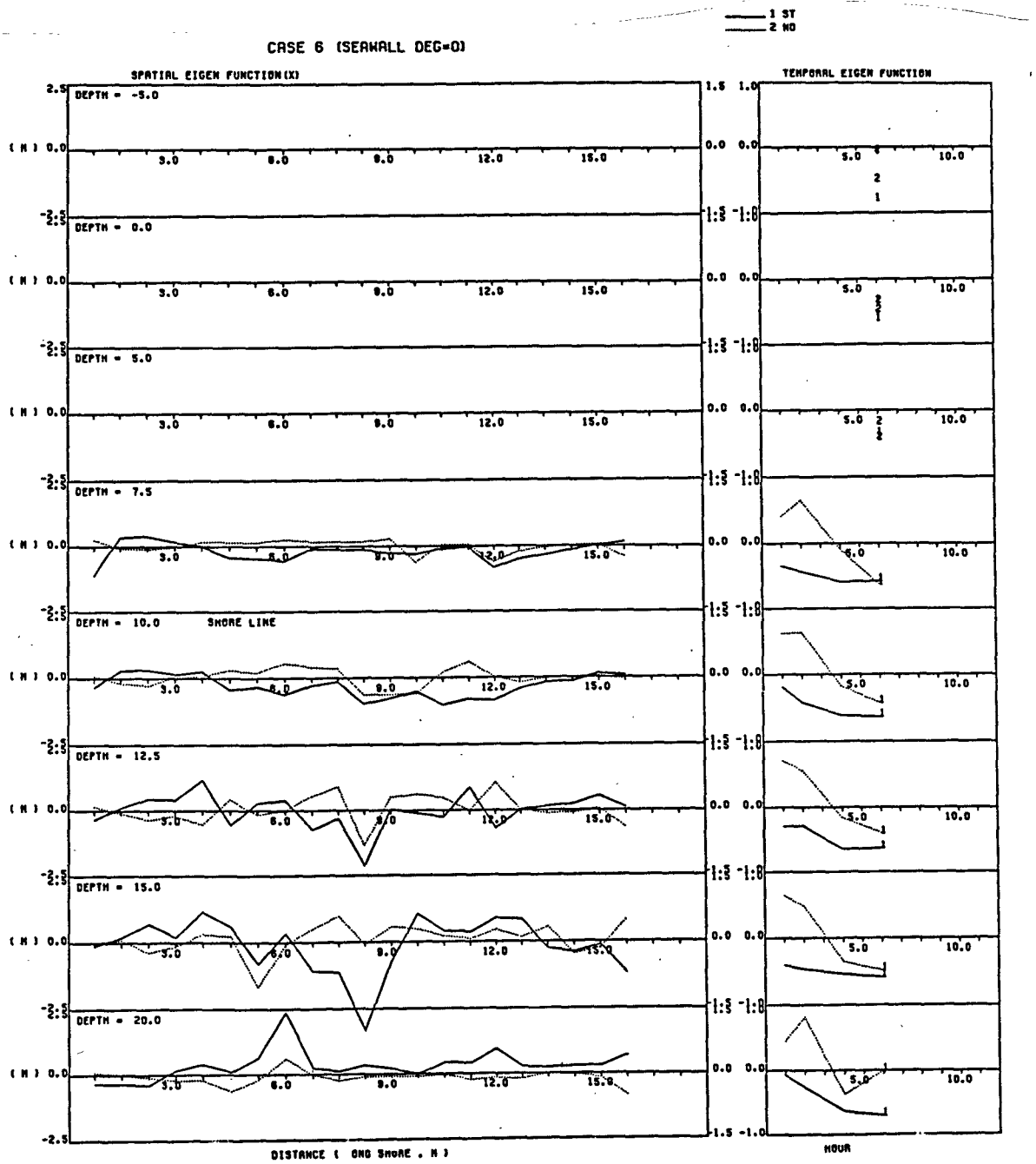

Figure B.11: Eigenfunction for Case 6 (recovery)

BIBLIOGRAPHY

Aubrey, D. G.,"Seasonal Pattern of Onshore/Offshore Movement," J. Geophys. Res., 84, 1979, pp. 6347-6354.

Barnett, M. R., "Laboratory Study of the Effects of a Vertical Seawall on Beach Profile Response," UFL/COEL-87/005, University of Florida, Gainesville, Florida, 1987.

Berigan, P. D., "The Travel Vertical Seawall," Shore & Beach, Vol. 53, No.1, 1985, pp. 2-7.

Berigan, P. D., "Seasonal Beach Changes at Traval Seawall," Shore & Beach, Vol. 53, No.2, 1985, pp. 9-15

Birkemeier, W. A., "The Effects of Structure and Lake Level on Bluff and Shore Erosion in Bernigen County, Michigan, 1970-74," Miscellaneous Report No. 80-2, Coastal Engineering Research Center, U.S. Army Corps of Engineers, Fort Belvoir, VA., 1980, 74pp.

Birkemeier, W. A. "Time Scale of Nearshore Profiles Changes," Proc. on 19th Conf. of Coastal Engineering, ASCE, New York, New York, 1984, pp. 1507-1521.

Bodge, R. K., "Short Term Impoundment of Longshore Sediment Transport," COEL/Tr-065, Coastal and Oceanographic Engineering, University of Florida, Gainesville, Florida, 1986.

Dean, R. G., "Heuristic Model of Sand Transport in the Surf Zone," Proc. of Conference of Engineering Dynamics in the Surf Zone, Sydney, Australia, May, 1973, pp. 208-214.

Dean, R. G., "Equilibrium Beach Profiles: U.S. Atlantic and Gulf Coast," Ocean Engineering, Report No.12, Department of Civil Engineering, University of Delaware, Newark, Delaware, 1977.

Dean, R. G., "Coastal Armoring Effects," Abstracts of the 20th Conf. of Coastal Engineering, Paper No. 175, Taipei, Taiwan, 1986, pp. 348-349.

Dean, R. G., "Damage Reduction Benefits by Restored Beaches," Abstracts of the 21st International Conf. on Coastal Engineering, No. 235, Malaya, Spain, 1988, pp. 461-462.

Deguchi, I., and Sawaragi, T., "Beach Fill at Two Coasts of Different Configurations," Proc on 20th Conf. of Coastal Engineering, ASCE, New York, New York, 1986, Vol. 3, pp. 1032-1046.

Dette, H. H., and Gartner, J., "Time History of Seawall on the Island of Sylt," Proc. of Coastal Sediment '87, ASCE, New York, New York, 1987, pp.1006-1022.

Dick, J. E., and Dalrymple, R. A., " Coastal Changes at Bethany Beach, Delaware," Proc. on 19th Conf. of Coastal Engineering, ASCE, New York, New York, 1984, Vol. 2, pp. 1650-1667.

Garrow H.C., "Quantification of Shoreline Rhythmicity," Proc. on 19th Conf. of Coastal Engineering, ASCE, New York, New York, 1984, Vol. 3, pp. 2165-2180.

Hanson, H., and Kraus, N. C. "Numerical Model for Studying Shoreline Changes in the Vicinity of Coastal Structure," Report No.3040, Department of Water Resource Engineering, Lund University, Sweden, 1980.

Hanson, H., and Kraus, N. C., "Seawall Boundary Condition in Numerical Models of Shoreline Evolution," Tr-86-3, Coastal Engineering Research Center, U.S. Army Corps of Engineers, U.S. Army, 1986.

Hashimoto, H., and Uda, T., "Field Investigation of Beach Profile Changes and the Analysis Using Empirical Eigenfunctions," Proc. on 18th Conf. of Coastal Engineering, ASCE, New York, New York, 1982, Vol. 2, pp. 1369-1384.

Hattori, M., and Kawamata, R., "Experiments on Restoration of Beaches Backed by Seawalls," Coastal Engineering in Japan, Vol. 20, Japan Society of Civil Engineering, Tokyo, Japan, 1977.

Hattori, M., and Kawamata, R., "Onshore-Offshore Transport and Beach Profile Changes," Proc of 17th Conference on Coastal Engineering, ASCE, New York, New York, Vol. 2, 1980, pp. 1175-1193.

Horikawa, K.(ed.), "Nearshore Dynamics and Coastal Process," University of Tokyo Press, Tokyo, Japan, 1988, pp. 522.

Hsu, J. R. C. and Silvester, R., "Model Test Results of Scour Along Breakwaters," ASCE, Vol. 1, No. WW 115, New York, New York, 1989, pp. 66-85.

Hughes, S. A., "Moveable-Bed Modeling Law for Coastal Dune Erosion," Journal WPCOE, ASCE, New York, New York, Vol. 109, No. 2, 1983, pp. 164-179.

Hwang, P., "Fall Velocity of Particles in Oscillating Flow," ASCE, New York, New York, J. Hydr. Eng., Vol. 111, No. 1, 1985, pp. 485-502.

Irie I., Nadaoka, K., Kondo, T. and, Terasaki, K., "Two Dimensional Sea Bed Scour in front of Breakwaters by Standing Waves," Report of Port and Harbor Research Institute, Vol. 23, No.1, 1984, pp. 3-52.

Jonsson, I. G., "Wave Boundary Layer and Friction Factors," Proc. on 10th Conf. of Coastal Engineering, ASCE, New York, New York, 1966, pp. 127-148.

Kamphuis, J. W., "The Coastal Mobile Bed Model," Civil Engineering, Rep. No. 75, Queen's University, Kingston, Ontario, Canada, 1975, pp. 113.

Kana, W. T., and Svetlichny, M., "Artificial Manipulation of Beach Profiles," Proc. on 18th Conf. of Coastal Engineering, ASCE, New York, New York, 1982, pp. 903-922.

Katsui, H., and Toue, T., "Inception of Sand Motion around a Large Obstacle," Proc. on 21st Conf. of Coastal Engineering, ASCE, New York, New York, 1988, pp. 1280-1294.

Keulegan, G. H., "An Experimental Study of Submarine Sand Bars," U.S. Army Corps of Engrs., B.E.B. Tech. Rep. No.3, Washtington, D.C., 1948, pp. 40.

Kraus, N. C., "The Effects of Seawalls on the Beach: A Literature Review," Proc. of Coastal Sediment '87, ASCE, New York, New York, 1987, pp. 945-960.

Kraus, N. C., and Larson, M., "Prediction of Initial Profile Adjustment of Nourished Beach to Wave Action," Proc. First Annual Conf. FSBPA, Gainesville, Florida, 1988, pp. 125-138.

Kriebel, D. L., Dally, W. R., and Dean, R. G., "Beach Profile Response Following Severe Erosion Events," UF/COEL-86/016, Coastal and Oceanographic Engineering Department, University of Florida, Gainesville, Florida, 1986.

Kutzback, J. E., "Empirical Eigenfunction of Sea Level Pressure, Surface Temperature and Precipitation Complexes over North American," Journal of Appl. Meteorol., Vol. 6, 1968, pp. 791-802.

Larson, M., "Quantification of Beach Profile Changes," Rep. No. 1008, Department of Water Resource Engineering, Lund University, Sweden, 1988.

Noda, E. K., "Equilibrium Beach Profile Scale–Model Relationship," ASCE, New York, New York, Journal of WHCE, Vol. 98, No. WW4, 1972, pp. 511-527.

McDougal, W. G., Sturtevant, M. A., and Kommer, D., "Fields and Laboratory Investigation of the Impact of Shoreline Stabilization," Proc. of Coastal Sediments '87, ASCE, New York, New York, Vol. 2, 1987, pp. 961-973.

Moore, B. D., "Beach Profile Evolution in Response to Changes in Water Level and Wave Height," unpublished M.S. Thesis, University of Delaware, Newark, Delaware, 1982.

Ozasa, H., and Brampton, A. H., "Mathematical Modeling of Beach Backed by Seawalls," Coastal Engineering Vol. 4, No. 1, 1980. pp. 47-64.

Shibayama, T., and Horikawa, K., "Sediment Suspension due to Breaking Waves," Coastal Engineering in Japan, Vol. 25, 1980, pp. 163-176.

Silvester, R., "The Influence of Oblique Reflection on Breakwaters," Proc. on 20th Conf. of Coastal Engineering, ASCE, New York, New York, 1987, pp. 2253-2267.

Sunamura, T., and Horikawa, K., "Two-Dimensional Beach Transformation due to Waves," Proc. on 14th Conf. of Coastal Engineering, ASCE, New York, New York, 1974, pp. 920-938.

Sunamura, T., "Predictive Relationships for Position and Size of Longshore Bars," Proc. of 32nd Japanese Conf. on Coastal Eng., JSCE, Tokyo, Japan, 1985, pp. 331-335. (in Japanese)

Uda, T., and Hashimoto, H., "Description of Beach Changes Using an Empirical Predictive Model of Beach Profile Changes," Proc. on 18th Conf. of Coastal Engineering, ASCE, New York, New York, 1982, pp. 1405-1418.

Vincent, C. C., and Resio, D. T., "An Eigenfunction Parameterization of a Time Sequence of Wave Spectra," Coastal Engineering, Vol.1, 1977, pp. 185-205.

Walton, T. C., and Sewsabaugh, W., "Seawall Design on the Open Coast," Report No. 29, Florida Sea Grant College, Gainesville, Florida, 1985, pp. 24.

Wang, H., "A Note on Beach Profile Scale Modeling," Leichtweiss-Institute fur Wasserbau, Technical University of Braunschweig, Germany, 1985.

Wang, H., and Yang, W.C., "A Similarity Model in the Surf Zone," Proc. on 17th Conf. of Coastal Engineering, ASCE, New York, New York, 1980, pp. 529-548.

Winant, C. D., Inman, D. L., and Nordstorm, C. E., "Description of Seasonal Beach Changes Using Empirical Eigenfunctions," Journal of Geophysical Research, Washington, D. C., Vol. 80, No. 15, 1975, pp. 1979-1984.

Wright, L. D., May, S. D., Short, S. D., and Greon, M.C., "Beach and Surfzone Equilibria and Response Times," Proc. on 19th Conf. of Coastal Engineering, ASCE, New York, New York, 1984, pp. 2150-2164.

Xie, S-L., "Scouring Pattern in Front of Vertical Breakwaters and Their Influence on the Stability of the Foundation of the Breakwaters," Technishe Hogesholl, Delft, 1981, pp. 61.